

The University of Maine

DigitalCommons@UMaine

Electronic Theses and Dissertations

Fogler Library

Fall 12-2020

Hydrogenation of 2-methylnaphthalene in a Trickle Bed Reactor Over Bifunctional Nickel Catalysts

Matthew J. Kline

University of Maine, matthew.kline@maine.edu

Follow this and additional works at: <https://digitalcommons.library.umaine.edu/etd>



Part of the [Catalysis and Reaction Engineering Commons](#), and the [Petroleum Engineering Commons](#)

Recommended Citation

Kline, Matthew J., "Hydrogenation of 2-methylnaphthalene in a Trickle Bed Reactor Over Bifunctional Nickel Catalysts" (2020). *Electronic Theses and Dissertations*. 3284.

<https://digitalcommons.library.umaine.edu/etd/3284>

This Open-Access Thesis is brought to you for free and open access by DigitalCommons@UMaine. It has been accepted for inclusion in Electronic Theses and Dissertations by an authorized administrator of DigitalCommons@UMaine. For more information, please contact um.library.technical.services@maine.edu.

**HYDROGENATION OF 2-METHYLNAPHTHALENE IN A TRICKLE BED REACTOR
OVER BIFUNCTIONAL NICKEL CATALYSTS**

By

Matthew J. Kline

B.S. Seton Hill University, 2018

A THESIS

Submitted in Partial Fulfillment of the

Requirements for the Degree of

Master of Science

(in Chemical Engineering)

The Graduate School

The University of Maine

December 2020

Advisory Committee:

M. Clayton Wheeler, Professor of Chemical Engineering, Advisor

Thomas J. Schwartz, Assistant Professor of Chemical Engineering

William J. DeSisto, Professor of Chemical Engineering

Brian G. Frederick, Professor of Chemistry

Douglas W. Bousfield, Professor of Chemical Engineering

Copyright 2020 Matthew J. Kline

All Rights Reserved

**HYDROGENATION OF 2-METHYLNAPHTHALENE IN A TRICKLE BED REACTOR
OVER BIFUNCTIONAL NICKEL CATALYSTS**

By Matthew J. Kline

Thesis Advisor: Dr. M. Clayton Wheeler

An Abstract of the Thesis Presented
in Partial Fulfillment of the Requirements for the
Degree of Master of Science
(in Chemical Engineering)
December 2020

Biomass thermal conversion processes, such as pyrolysis, tend to produce mixtures of mono- and poly-aromatic species. While the high aromatic content is desirable in gasoline fractions, middle-distillate cuts, particularly jet fuel and diesel, require upgrading via hydrogenation and ring opening to achieve better combustion characteristics. There have been many proposed methods for producing drop-in fuels from woody biomass, one of them being Thermal DeOxygenation (TDO). The TDO process converts organic acids from cellulose hydrolysis into a low-oxygen bio-oil containing large amounts of substituted naphthalene compounds.

Poly-aromatic molecules, such as those found in TDO oil, have low cetane numbers (CN), particularly due to their high aromatic content. Even after deep hydrogenation, certain combustion characteristics, such as specific volume, hydrogen content, and CN may still be below required specifications. Thus, naphthenic ring opening coupled with aromatic hydrogenation is the desired process to enhance the fuel characteristics.

This research focuses on the hydrogenation of 2-methylnaphthalene (2-MN) to increase the CN. These reactions are performed industrially using a precious metal catalyst (*e.g.*, based on palladium or platinum), but because of their intrinsically high cost and sensitivity to impurities, we focused on

supported nickel catalysts to perform the desired reactions. We hydrogenated 2-MN in a down-flow trickle-bed reactor at a variety of operating conditions.

In this research, we compared several Ni catalysts to a commercial Ni catalyst with respect to reaction rate and product selectivity. Impregnated Ni catalysts showed higher activation energies and lower reaction rates than the commercial catalysts, but coprecipitated Ni catalysts produced products with similar selectivities as the commercial catalyst. We found that higher amounts of Ni in the coprecipitated catalysts slightly increased the *cis/trans*-methyldecalin ratio, whereas higher temperatures decreased the same ratio. Impregnated coprecipitated catalysts with Ni and a precious metal also changed the *cis/trans*-methyldecalin ratio. Although bimetallic IrNi and PdNi catalysts barely altered the ratio, the PtNi catalyst was selective towards *trans*-methyldecalin, whereas RuNi was selective towards *cis*-methyldecalin. We provided a possible explanation for that observed selectivity as well as other trends throughout this research.

DEDICATION

I would like to dedicate this thesis to my family. I wish to thank my parents, George and Pam, for their unconditional love and for instilling in me an extremely strong work ethic. I would like to thank my siblings, Rachel, Adam, and Joshua, for being there for me every step of the way and for acting like you cared about my research. I appreciate all that my family has done to help me grow and succeed; without you guys, none of this would be possible.

ACKNOWLEDGEMENTS

This thesis is a culmination of two years of work, which would not have been possible without the help of many people. Firstly, I would like to acknowledge and thank my thesis advisor, Dr. Clay Wheeler. With your guidance, instruction, and mentorship, I have been able to learn an incredible amount of information not only from the laboratory work but also from our conversations. Your help and support were invaluable and have helped me grow as a researcher and as a person. I would also like to thank my graduate committee consisting of Dr. Thomas Schwartz, Dr. William DeSisto, Dr. Brian Frederick, and Dr. Douglas Bousfield for their guidance and contributions to this research.

Next I would like to thank Dr. Sampath Karunaratne. For the entirety of this research, I worked side-by-side with Sampath to design catalysts that would work not only for my reactions but also for TDO oil upgrading. Many of our conversations yielded valuable results that helped with our projects. I would also like to thank the members of the UMaine Catalysis group, led by Dr. Thomas Schwartz. In particular, I would like to thank Daniela Stück, Christopher Albert, Jalal Tavana, Hussein Abdulrazzaq, and Elnaz Jamalzade for their assistance and help on this research project.

I would like to thank the Department of Chemical and Biomedical Engineering as well as the Forest Bioproducts Research Institute (FBRI) for allowing me to use their laboratory space as well as their analytical instruments. I would like to thank Nick Hill for his technical assistance with my reactor as well as Amy Luce for her help in ensuring that my project went smoothly.

Lastly, this project would not have been possible without receiving funding. This research was funded by the Department of Transportation grant DTRT13-G-UTC43 through Maine Maritime Academy as well as the Department of Defense grant SP4701-18-C-0047.

TABLE OF CONTENTS

DEDICATION.....	III
ACKNOWLEDGEMENTS.....	IV
LIST OF TABLES	VIII
LIST OF FIGURES	IX
LIST OF ABBREVIATIONS	XII
Chapter	
1. INTRODUCTION.....	1
MOTIVATION	1
PETROLEUM REFINING	2
BACKGROUND.....	2
AROMATIC FRACTIONS OF PETROLEUM.....	5
PETROLEUM REFINING REACTIONS	7
CETANE NUMBER.....	9
THERMAL DEOXYGENATION (TDO) OIL	12
UPGRADING CHEMISTRY	16
HYDROGENATION	18
MODEL COMPOUNDS.....	18
THERMODYNAMIC LIMITATIONS	22
2. CATALYSTS IN OTHER HYDROGENATION STUDIES.....	25
CATALYST SUPPORTS	25
SILICA	26
ALUMINA	26

AMORPHOUS SILICA ALUMINA.....	27
ZEOLITES	28
OTHER SUPPORTS	29
METAL CATALYSTS	29
PRECIOUS METAL CATALYSTS	30
SULFIDED CATALYSTS.....	32
NON-PRECIOUS METAL CATALYSTS	34
CATALYST DEACTIVATION.....	35
3. SYNTHESIS AND DESIGN OF HYDROGENATION CATALYSTS.....	39
MATERIALS AND METHODS.....	39
CATALYST CHARACTERIZATION.....	39
NITROGEN ADSORPTION/DESORPTION	39
THERMOGRAVIMETRIC ANALYSIS (TGA)	40
X-RAY DIFFRACTION (XRD).....	42
TRANSMISSION ELECTRON MICROSCOPY (TEM).....	42
CATALYST SYNTHESIS	43
INCIPIENT WETNESS IMPREGNATION CATALYSTS.....	43
COPRECIPITATION CATALYSTS.....	44
MULTIPLE SYNTHESIS METHODS.....	46
COMMERCIAL CATALYST.....	47
RESULTS AND DISCUSSION	47
4. HYDROGENATION OF 2-METHYLNAPHTHALENE IN A TRICKLE BED REACTOR	51
INTRODUCTION	51
MATERIALS AND METHODS.....	54

FEEDSTOCK PURIFICATION	54
CATALYTIC REACTION TESTING.....	55
SAMPLE ANALYSIS.....	56
RESULTS AND DISCUSSION	58
DETERMINATION OF 2-MN ACTIVATION ENERGY	58
HYDROGENATION OVER COPRECIPITATED CATALYSTS	61
HYDROGENATION OVER IMPREGNATED COPRECIPITATION CATALYSTS	69
5. CONCLUSIONS AND RECOMMENDATIONS	73
CONCLUSIONS	73
RECOMMENDATIONS FOR FUTURE STUDIES	74
REFERENCES.....	77
APPENDIX A. SYNTHESIS METHODS OF SUPPORTED HYDROGENATION CATALYSTS	85
BIOGRAPHY OF THE AUTHOR	101

LIST OF TABLES

Table 1. Ultimate analysis of typical petroleum reserves.....	4
Table 2. Properties of crude and hydroprocessed TDO oil as reported by Eaton <i>et al.</i> (2015). ²¹	15
Table 3. Types of reactions discussed in this thesis.....	17
Table 4. Synthesis methods for producing each type of catalyst.	43
Table 5. Structure and melting points of 2-MN and impurities.....	55
Table 6. Nitrogen physisorption measurements of incipient wetness impregnation catalysts and a commercial Ni catalyst.....	59
Table 7. Cis/trans-MD selectivity of various monometallic and bimetallic coprecipitated catalysts.	61
Table 8. Nitrogen physisorption measurements of coprecipitated Ni catalysts synthesized at 25°C.	63
Table 9. Nitrogen physisorption measurements of coprecipitated Ni catalysts synthesized at 90°C.	64
Table 10. Conversion and selectivity of 80Ni and 100Ni catalysts (both synthesized at 90°C).	66
Table 11. Reference letters of each catalyst catalogued in Appendix A.....	69

LIST OF FIGURES

Figure 1. Viscosity, density, and specific gravity of some conventional and unconventional reserves.....	4
Figure 2. Refinery streams used to produce different petroleum fractions from light crude oil.	5
Figure 3. Cetane numbers of some hydrocarbon structures.	10
Figure 4. Cetane numbers for decalin ring opening.	11
Figure 5. Cetane number and density of some molecules formed by decalin ring opening.	12
Figure 6. TDO oil, showing phase separation between organic oil and water layers.	13
Figure 7. Molecular classes of components found in crude and hydroprocessed TDO oil at various carbon numbers.	15
Figure 8. GCMS chromatogram of TDO oil with major peaks displayed.....	16
Figure 9. Common model compounds used in hydrogenation reactions.....	19
Figure 10. Aromatic hydrogenation as a function of temperature and hydrogen pressure on Middle East heavy gas oil.....	23
Figure 11. Equilibrium between <i>cis</i> - and <i>trans</i> -decalin.	24
Figure 12. Price of several transition metals used in hydrogenation catalysts using 2006 (left) and 2019 prices (right).	30
Figure 13. ¹³ C solid-state NMR spectrum of used alumina-USY catalyst.	37
Figure 14. Micromeritics ASAP 2020 instrument used for nitrogen physisorption.	39
Figure 15. Nitrogen adsorption and desorption curves for Alfa Aesar catalyst.....	40

Figure 16. TGA Q500 used for this research.	41
Figure 17. TGA curve of uncalcined 100Ni catalyst.	41
Figure 18. Phillips CM-10 TEM.	42
Figure 19. TGA curve of uncalcined 60Ni catalyst.	48
Figure 20. XRD curves for Alfa Aesar catalyst as well as fresh and spent 60Ni catalyst.	49
Figure 21. Reaction network for hydrogenation and ring opening of 2-methylnaphthalene.	52
Figure 22. A more complete reaction mechanism for hydroconversion of methylnaphthalene showing hydrogenation, isomerization, ring contraction, and ring opening reactions.	53
Figure 23. Reactor schematic for hydroprocessing studies.	56
Figure 24. Arrhenius analysis to determine the activation energy of various supported Ni catalysts.	59
Figure 25. Apparent activation energies of the Ni catalysts in Figure 24.	59
Figure 26. BET surface area and pore volume measurements of coprecipitated Ni/Al ₂ O ₃ catalysts at various Ni content.	64
Figure 27. <i>Cis</i> -MD selectivity of coprecipitated Ni catalysts and a commercial Ni catalyst.	67
Figure 28. TEM images of coprecipitated 60Ni catalyst (left) and Alfa Aesar commercial Ni catalyst (right).	68
Figure 29. <i>Cis</i> -MD selectivity of various bimetallic coprecipitated Ni catalysts.	70
Figure 30. Possible reaction network for hydrogenation of tetralin through an octalin intermediate proposed by Weitkamp (1968). ²⁹	71
Figure 31. Stages of incipient wetness impregnation for a 20 wt% Ni/SiO ₂ catalyst.	85
Figure 32. Stages of synthesis of ASA support.	87

Figure 33. Various stages of incipient wetness impregnation using nickel on amorphous silica-alumina (ASA).....	87
Figure 34. Comparison of dried ASA support, calcined support, and synthesized 20 wt% Ni/ASA catalyst.	88
Figure 35. Images of coprecipitated 60Ni catalyst.	88
Figure 36. Images of coprecipitated 60Co catalyst.....	89
Figure 37. Images of coprecipitated NiCr catalyst.....	90
Figure 38. Images of coprecipitated NiMn catalyst.	90
Figure 39. Images of coprecipitated NiFe catalyst.....	91
Figure 40. Images of coprecipitated NiCo catalyst.	92
Figure 41. Images of coprecipitated NiCu catalyst.	92
Figure 42. Images of coprecipitated NiZn catalyst.....	93
Figure 43. A TEM image of the Alfa Aesar catalyst showing a diatomite littered with Ni particles.....	100

LIST OF ABBREVIATIONS

°API – American Petroleum Institute gravity	HDS – Hydrodesulfurization
1-MN – 1-methylnaphthalene	HMW – High Molecular Weight
2-MN – 2-methylnaphthalene	HHV – Higher Heating Value
AGO – Atmospheric Gas Oil	HYD – Hydrogenation
ASA – Amorphous Silica Alumina	IWI – Incipient Wetness Impregnation
ASAT – Aromatic Saturation	LCO – Light Cycle Oil
ASTM – American Society for Testing and Materials	LMW – Low Molecular Weight
BET – Brunaner-Emmett-Teller	MD – Methyldecalin
BTX – Benzene, Toluene, Xylene	MN – Methylnaphthalene
CGO – Coker Gas Oil	MT – Methyltetralin
CN – Cetane Number	NIST – National Institute of Standards and Technology
DAP – Dealkylated Products	NMR – Nuclear Magnetic Resonance
DI - Deionized	ROP – Ring Opening Product
FCC – Fluid Catalytic Cracker	SiAl – Mixture of Silica and Alumina
GCMS – Gas Chromatograph-Mass Spectrometer	SRO – Selective Ring Opening
HDA – Hydrodearomatization	TDO – Thermal DeOxygenation
HDM – Hydrodemetallization	TEM – Transmission Electron Microscopy
HDN – Hydrodenitrogenation	TGA – Thermogravimetric Analysis
HDO – Hydrodeoxygenation	TMS – Transition Metal Sulfide
	TOF – Turnover Frequency

TPR – Temperature Programmed Reduction

ULSD – Ultra-Low Sulfur Diesel/Distillate

VGO – Vacuum Gas Oil

VR – Vacuum Residue

WHSV – Weight Hourly Space Velocity

XRD – X-Ray Diffraction

CHAPTER 1

INTRODUCTION

MOTIVATION

Fossil fuels play a crucial role in our everyday lives, allowing us to maintain a high standard of living and forming a foundation for modern society. In the last handful of decades, the United States has been a net importer of petroleum products, recent events have allowed the United States to be a net exporter and one of the largest oil producers in the world. Crude oil production is projected to reach 14 million barrels per day by the year 2022 and remain at this level through 2040.¹ And of the products obtained from oil, transportation fuels, such as diesel and jet fuel, are projected to have increased demand in the United States at least through 2050.

Most commercially available transportation fuels are petroleum-based, despite their detrimental environmental effects and status as a nonrenewable energy source. Over the last two decades, there has been a push towards the use of renewable and sustainable fuels from feedstocks like ethanol and cellulose. These renewable fuels are a sustainable alternative to traditional fossil fuels and comprised approximately 7.3% of the fuel blending pool in 2019.¹ By 2050, that market share is expected to grow to about 9.0% with moderate fuel prices, but models with higher crude oil prices predict the biofuel market share to rise to about 13.5%.

Cellulosic fuels could be an important source of biofuel in many parts of the United States. Cellulose comprises approximately 40 to 50% of wood content, and it can easily be obtained from woody biomass using existing techniques and infrastructure. Additionally, sources of cellulose are numerous and include forest residues, agricultural residues, and municipal solid waste, just to name a few. Efforts have

been made to develop processes that economically convert these waste materials into usable transportation fuels, which can reduce our reliance on fossil fuels.

In this thesis, we discuss a process coined Thermal DeOxygenation (TDO) that produces an aromatic-rich oil from cellulose hydrolysate. We evaluate methods of upgrading the material into diesel and jet fuels by use of model compounds to study hydrogenation reactions over a variety of catalysts. The conversion and selectivity data were compared to those obtained using a commercial hydrogenation catalyst. We also discuss future upgrading steps that could be employed to use TDO oil as a blending agent in diesel fuel.

To understand how cellulosic fuels might fit into the existing transportation fuel infrastructure, it is helpful to understand the process of refining petroleum as well as similarities that exist between renewable fuels and refinery intermediates.

PETROLEUM REFINING

BACKGROUND

Since the start of the Industrial Revolution, fossil fuels have played an increasingly important role in advancing society and increasing our quality of life. In the 18th century, the mining and burning of coal was essential for the production of iron, which helped spur economic growth throughout Europe and the United States. Most power generated today in the United States and around the world comes from burning coal, petroleum (oil), and natural gas. Additionally, most plastics are derived from petroleum, which are used for a large array of consumer goods from food storage to furniture. However, the largest use of petroleum is for liquid transportation fuels. Although small seeps of oil had been used since ancient times, large-scale oil production started in the late-1850's after the discovery of oil by Edwin Drake in Titusville, PA. A few years later in nearby Findlay, OH, the first commercial natural gas well was drilled.

Although the fossil fuel industry has dramatically increased production and designed vast new technologies since the first wells and mines were constructed, the demand for these materials has also grown.

Transportation fuel demand is expected to increase worldwide in the future, and the demand for cleaner-burning diesel fuel is projected to increase much faster than gasoline. This growth in demand is largely driven by the Asia-Pacific region, where diesel fuel is more commonplace.² This is in contrast to North America, where gasoline demand is higher. And while gasoline demand is projected to increase by 2 million barrels per day, the increase in diesel is projected to be about 5 million barrels per day.³

Although there is increased demand for transportation fuels, there has also been a notable decrease in the availability of conventional reserves throughout the world because those were preferentially extracted due to their lower boiling points and number of impurities. Unfortunately for refiners, unconventional reserves (*e.g.*, shale gas, heavy oil, bitumen, etc.) are becoming more commonly extracted. These are unwelcome changes because these residues contain larger quantities of nonvolatile (*i.e.*, asphaltene) components and heavier molecules. In turn, these are more difficult to refine and contain higher quantities of heteroatoms.⁴ This trend is evidenced by the decrease in average crude oil specific gravity by 0.12 °API/yr and an increase in the average sulfur content by 0.057 wt%/yr between 1997 and 2001.⁵ Figure 1 shows characteristics of conventional and unconventional reserves of crude oil, while Table 1 shows the composition of a typical barrel of petroleum.

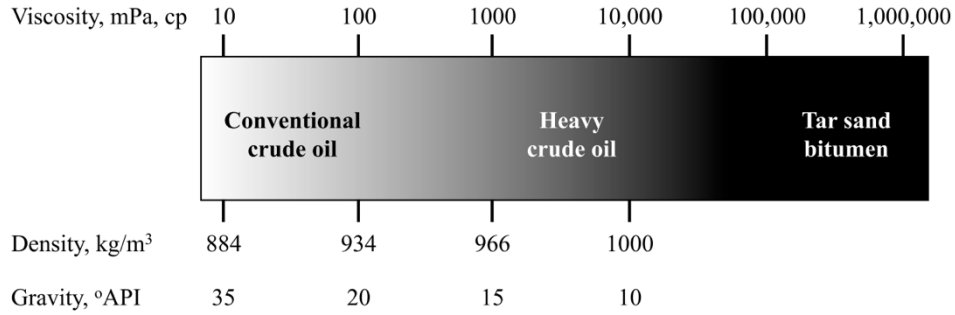


Figure 1. Viscosity, density, and specific gravity of some conventional and unconventional reserves. Reproduced from Speight (2007).⁴

Table 1. Ultimate analysis of typical petroleum reserves. Adapted from Speight (2007).⁴

Element	Composition
Carbon	83 – 87%
Hydrogen	10 – 14%
Oxygen	0.05 – 1.5%
Nitrogen	0.1 – 2%
Sulfur	0.05 – 6%
Metals (Ni and V)	<1000 ppm

Petroleum refineries are highly complex and systematic processing facilities that can produce vast quantities of fuel and petrochemicals from crude oil feedstocks. Although crude oil is distilled into different fractions, each fraction usually requires a series of upgrading steps before reaching the desired product. A schematic of a refinery is displayed in Figure 2, which shows several intermediate steps that are used to produce gasoline (motor gasoline blending) and diesel fractions (distillate fuel blending).

that require upgrading (via hydrogenation or hydrocracking) to be blended into fuel or converted to BTX molecules. These feedstocks are all similar in the fact that they contain large quantities of unsaturated (aromatic) molecules.

Light Cycle Oil (LCO) is the best-known petroleum stream that contains aromatic molecules. It is a middle distillate fraction (170° – 370°C) produced from a fluid catalytic cracking (FCC) unit. LCO is known for its high sulfur, nitrogen, and aromatic (diaromatics in particular) content. In the past, it was added to heavy fuel oil (for use on ships) to change the viscosity, but with decreasing demand for those heavy oils, it is an ideal candidate to upgrade to more valuable products.⁹ In a refinery, LCO is typically processed in one of two ways: 1- complete hydrotreating and heteroatom removal then blending in diesel fuel or 2- partial aromatic saturation and heteroatom removal, then hydrocracking to produce a BTX fraction.¹⁰

Atmospheric gas oil (AGO) is an aromatic stream that is sometimes present near the bottom of the atmospheric distillation column, with a boiling point range of 250 – 350°C.³ It has similar characteristics to heavy fuel oil, and depending on the refinery, the terms are somewhat interchangeable.⁴ Vacuum gas oil (VGO) is another important source of aromatic molecules that are used in the diesel blending pool. These materials are fractionated from the vacuum distillation unit and are sent to either a hydrocracking unit or to the FCC to produce middle distillates. Coker gas oil (CGO) also contains a high quantity of aromatic materials and is sent to the same units as VGO, but it differs from VGO because it is formed in the coker.

Vacuum residue (VR) is the heaviest fraction produced from the vacuum distillation of atmospheric bottoms, as Figure 2 shows. The VR fraction contains hydrocarbons with atmospheric equivalent boiling points higher than 565°C, roughly 3% sulfur and 0.5% nitrogen, and upwards of 10 wt% asphaltenes (depending on the material source).⁴ With the increasing use of unconventional feedstocks

(such as heavy crude oil and bitumen), on average about 25 wt% of crude oil feed contains VR.¹¹ By the use of coking, visbreaking, cracking, and hydrocracking, this heavy VR material can be converted into lower-boiling point components. VR hydrocracking is usually performed in two reactors, with different catalysts operating at different temperatures.

PETROLEUM REFINING REACTIONS

During the refining process, there are multiple reactions that occur, which are useful in meeting fuel and industry standards for final products. Heteroatoms (oxygen, nitrogen, sulfur, and metals) are found in crude oil throughout the world, regardless of the deposit or geology as Table 1 shows. These atoms need to be selectively removed to avoid destroying or poisoning catalysts in downstream refining reactors and to avoid the formation of harmful compounds during combustion in an engine (*e.g.*, nitrogen oxides, NO_x, and sulfur oxides, SO_x).

Hydrogenation (HYD) is the process of adding hydrogen to unsaturated molecules. In this thesis, HYD reactions involve adding hydrogen to both olefins and aromatic molecules, but more often the latter. HYD is a common refinery process, and hydrogen is used to remove heteroatoms or functional groups from different fractions of crude oil.

Hydrodearomatization (HDA), or aromatic saturation (ASAT), is the process of removing aromatic groups from crude oil. Although light fractions have very little aromatic content, polyaromatic molecules comprise a majority of heavier fractions. The amounts of aromatic molecules are limited in transportation fuels because they lead to the formation of particulate matter when burned. There are regulations in place that specify the maximum aromatic content of diesel fuel, which is currently capped at 35% in the United States.¹² To address this issue, HDA reactions strive for partial or complete aromatic saturation, depending on the desired product. Typical HDA catalysts are also very active for HYD reactions as well.

Although Table 1 shows that the oxygen content of crude oil is very low, it is nonetheless found in a variety of functional groups. Lighter fractions contain few oxygen compounds, but heavier fractions of crude oil contain as much as 8 wt% oxygen, mostly found in phenolic-like groups.⁴ To remove these compounds, hydrodeoxygenation (HDO) is employed, and because oxygen is found in different functional groups, upgrading strategies vary depending on the molecules present in the specific fraction. However, when looking at all the reactions employed, HDO reactions are not critical upgrading steps for a petroleum refinery because oxygen is typically removed with other heteroatoms, such as sulfur and nitrogen.

Hydrodesulfurization (HDS) is arguably the most important process in a refinery. Not only is the amount of sulfur in final products regulated (15 ppm S in diesel fuel), but sulfur also poisons many catalysts used in downstream operations. Most catalysts that facilitate HYD reactions also catalyze HDS reactions, though they can be limited because of sulfur poisoning and their activity level.⁴ Sulfur compounds in crude oil commonly take the form of thiophenes or benzothiophenes, both heterocyclic aromatic molecules.¹³ The sulfur compounds are usually termed reactive or refractive species, which differ in their reactivity. Reactive sulfur species are reacted quickly when they reach the catalytic surface, but refractory sulfur species require longer residence times to reach the same level of HDS as reactive species.¹⁴ Sulfur is removed from HDS reactions as H₂S, a deadly gas that is further converted to elemental sulfur using the Claus process. Because of the crucial importance of HDS reactions, there has been plenty of research in developing catalysts with higher sulfur tolerance and better ability to perform HYD and HDS reactions.

Hydrodenitrogenation (HDN) is another reaction that takes place in petrochemical reactors because nitrogen is also heavily regulated. Most nitrogen-containing compounds are aromatic with nitrogen incorporated into a cyclic structure (such as pyrrole, pyridine, indole, and other derivatives).¹⁵ Nitrogen is removed from the reactor in the form of NH₃, which can temporarily poison many catalysts,

despite catalytic advances meant to tolerate higher amounts of ammonia. HDN is generally more difficult to accomplish than HDS because C-N bonds are more difficult to break than C-S bonds. However, since nitrogen comprises a smaller fraction of crude oil (as Table 1 shows), most catalysts are optimized for HDS, although there has been some recent interest in designing HDN catalysts as the nitrogen content of crude oil increases.⁴

A vast majority of the metals found in crude oil are nickel and vanadium, with trace amounts of others, depending on the original source.⁴ The metals are not freely floating around in the oil; they are usually chelated in porphyrins. When passed over an HDS catalyst, hydrodemetallization (HDM) reactions take place. The metal is broken from its structure and is deposited on the catalyst surface, which in turn poisons the catalyst. For this reason, there are sometimes extra steps required to improve the catalyst lifespan. When there are high concentrations (>300 ppm) of metals, a guard reactor is sometimes used. The guard reactor uses a cheaper catalyst to remove metal heteroatoms without poisoning a more expensive HDS catalyst.⁴ However, to ensure continuous HDM, fresh catalyst is continuously added.

Various catalysts have been developed for each of these petroleum refining reactions, and an example of an HYD/HDS catalyst is discussed in further detail in a later section (*c.f.*,

Sulfided Catalysts). Although removing heteroatoms does not dramatically change the fuel combustion characteristics, the removal or saturation of aromatic molecules is crucial in producing diesel fuel with enhanced characteristics, like cetane number.

CETANE NUMBER

Cetane number (CN) is an important factor in determining the ignition quality of diesel fuel. Fuels with high cetane numbers have short ignition delay times and are more beneficial in an engine. Just as octane number is important for gasoline, cetane number is probably the most important factor that

affects the combustion of diesel fuel. Cetane numbers are typically between 0 and 100, and the scale is based on two chemicals, 1-methylnaphthalene and *n*-hexadecane.

The linear hydrocarbon *n*-hexadecane (also known as *n*-cetane) is assigned a cetane number of 100, whereas the polyaromatic molecule 1-methylnaphthalene is assigned to the number 0. Figure 3 shows the cetane numbers of various classes of molecules. The graph shows that molecules with the best cetane numbers are paraffins and olefins, with isoparaffins and aromatics lagging behind. The graph also shows that the cetane number tends to increase with the number of carbons, although the molecular structure turns out to be more important than the number of carbon atoms in a hydrocarbon.

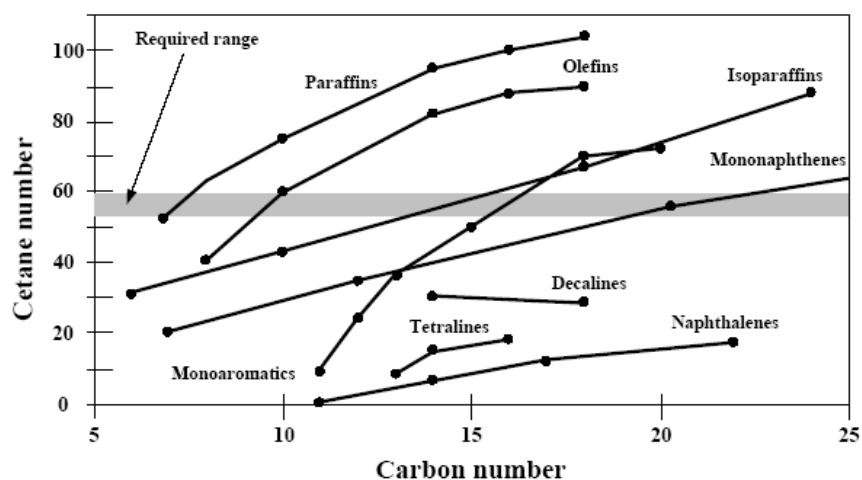


Figure 3. Cetane numbers of some hydrocarbon structures. Reproduced from Rédey *et al.* (2011).¹⁶

Cetane number is highly dependent on the arrangement of carbon atoms in a molecule.¹⁷ Linear molecules (*i.e.*, paraffins) have higher cetane numbers than branched ones (*i.e.*, isoparaffins), as Figure 3 shows. In fact, the more branching that occurs in a molecule, the lower the cetane number, and molecules that have multiple branches lead to little-to-no cetane improvement from a molecule like decalin. Figure 4 shows some products that can be obtained from decalin ring opening, a reaction that can occur on some hydrogenation catalysts. The first ring opening reaction produces chemicals that slightly increase the

cetane number, but the second ring opening is more important in the determination of the cetane number.¹⁸ The final products obtained from decalin can capture a wide range of cetane numbers, even beyond the ones shown in Figure 4.

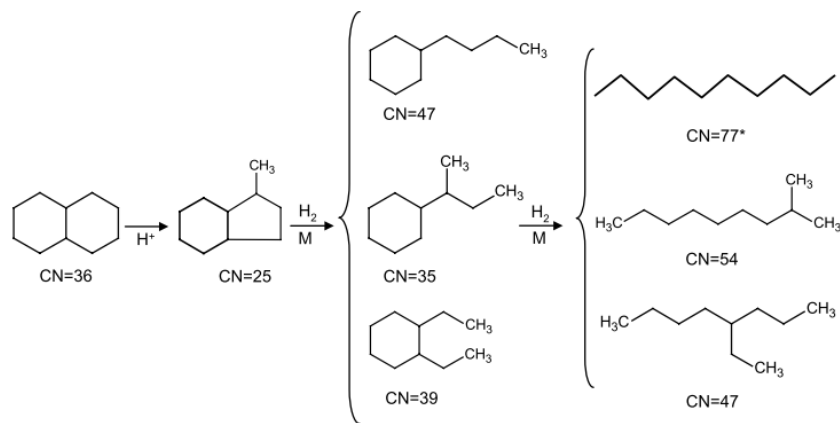


Figure 4. Cetane numbers for decalin ring opening. Reproduced from Santana *et al.* (2006).¹⁸

The current fuel standard in most of the European Union is EN 590, which sets the minimum cetane number at 51. That is in contrast with most areas in the United States, which base their cetane number off ASTM D975 and have a minimum cetane number of 40, with values typically ranging between 42 and 44.¹² However, states have the opportunity to pass legislation that exceeds federal regulations, and California, which is known for having strict regulations, requires a cetane number of 53, much higher than the national average of 42.¹⁹

As was mentioned before, aromatic molecules have the lowest cetane numbers of any hydrocarbon class. And of the aromatic molecules, polyaromatic compounds have lower cetane numbers than monoaromatic ones. From a refiner's perspective, to increase the cetane number of a feedstock like LCO that has plentiful aromatic molecules, there should be hydrogenation followed by ring opening reactions.²⁰

Naphthalene, a diaromatic molecule found in the diesel range, has a cetane number of only 5, and a density around 1 g/mL. The requirement for diesel fuel is to have a minimum cetane number of 40 and a maximum density (specific gravity) of 0.878 g/mL.²¹ Figure 5 shows that the hydrogenation of naphthalene to decalin dramatically improves the cetane number and density, but the two characteristics still remain below the required specifications. Ring opening can be used to increase the cetane number. However, it is important to use selective ring opening (SRO), which minimizes the branching in a molecule favoring products with higher cetane numbers.

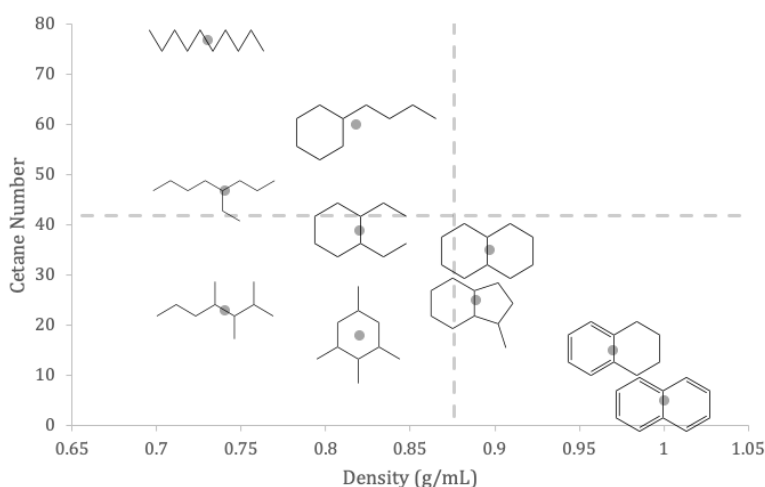


Figure 5. Cetane number and density of some molecules formed by decalin ring opening. Modified from Santana *et al.* (2006).¹⁸

THERMAL DEOXYGENATION (TDO) OIL

There have been many processes developed to produce diesel and other renewable fuels from cellulosic sources. The most common process uses pyrolysis, which involves heating biomass to produce a mixture of aromatic hydrocarbons. However, one of the issues with this process is that the oily mixture contains large amounts of oxygen, which makes it unstable and difficult to upgrade. It is also difficult to store and transport because it forms gums that clog pipes and other infrastructure. For these reasons and others, there have been other processes to produce renewable fuels.

Another process that has been developed to produce renewable diesel fuel is through a process called Thermal DeOxygenation (TDO). Schwartz *et al.* (2010) found that when calcium levulinate was heated to 450°C, it produced a vast array of substituted, cyclic hydrocarbons that had a potential higher heating value (HHV) of 35 MJ/kg.²² Case *et al.* (2012) further advanced the work by testing various mixtures of calcium formate and levulinate salts to further increase the HHV.²³ They found that an equimolar mixture of levulinic and formic acids produced a bio-oil, shown in Figure 6, that had a very low oxygen content and a HHV of 40.7 MJ/kg.²⁴



Figure 6. TDO oil, showing phase separation between organic oil and water layers. Reproduced from Case *et al.* (2012).²³

Production of TDO oil requires both levulinic and formic acids, and the Biofine process can produce both acids from cellulose using a dual-reactor setup.^{25,26} The first reactor operates in plug flow mode and converts hexosan into a mixture of 5-hydroxymethylfurfural and hexose sugars. The second reactor, a continuous stirred tank reactor, converts hydroxymethylfurfural and the hexose sugars into levulinic and formic acid in a 1:1 molar ratio as Equation 1 shows:



Eaton *et al.* (2013) further studied the TDO oil by analyzing its combustion characteristics and increasing the reactor scale from a 300 mL Parr reactor to a 3 L semibatch reactor.²⁷ They found that the oil had a broad boiling point distribution (75 – 550°C) and low total acid number, making it a candidate for different types of fuel. However, the high aromatic content causes the specific gravity, hydrogen content, and cetane number to be off from the required specifications for diesel fractions. Further evaluations of the distilled fractions indicated that about 15 wt% of the crude TDO oil was in the naphtha fraction (<200°C) with an octane rating of 81 – 87 and had potential for blending in gasoline.²⁷ Further distillation yielded about 70 wt% of the fuel in the middle distillates region, with the remaining 15 wt% fraction present as heavy gas oils.

In another study, Eaton *et al.* (2015) further increased production of crude TDO oil by increasing the scale to a 50 L semibatch reactor.²¹ The crude oil was found to have similar characteristics as the oil from the 3 L reactor, and several of those properties are displayed in Table 2. Unlike pyrolysis oil which contains a high percentage (~20 wt%) of oxygen, TDO oil is noted for its low oxygen content (<6 wt%). Additionally, the oxygen atoms are mostly present in ketone and alcohol functional groups, which are easily removed by catalysts. However, the hydrogen content and cetane number were found to be well below specifications due to the high aromatic content of the middle distillate fraction. The crude TDO oil needed further upgrading to be used in diesel or jet fuel fractions.

Table 2. Properties of crude and hydroprocessed TDO oil as reported by Eaton *et al.* (2015).²¹

Fuel Characteristic	ASTM Method	Requirement ^a	Crude	Hydroprocessed
Density (kg/dm ³)	D1298	0.876 (max)	1.003	0.89
Carbon (wt%)	D5291		86.3	87.4
Hydrogen (wt%)	D5291	13.5 (min)	8.3	12.7
Oxygen (wt%) ^b	D5291-Diff		5.7	-
Cetane Number	D976	40 (min)	- ^c	26.3

^a Requirements for ASTM D975 No. 2 Distillates

^b Oxygen content measured by difference.

^c Cetane number was not tested for crude TDO oil, but it was estimated to be <10.

In the same study, Eaton *et al.* (2015) further hydroprocessed the TDO oil using a silica-alumina-supported nickel catalyst purchased from Alfa Aesar.²¹ They obtained a 94% mass recovery of hydrotreated TDO oil after processing for 700 hours of time-on-stream, and the upgraded TDO oil had a better density, hydrogen content, and cetane number values than the crude oil. The oxygenate species had also been completely removed from the hydroprocessed oil, but the cetane number of the fuel was still only found to be 26.3. Analysis of the molecules found in the naphtha fraction of crude and hydroprocessed TDO oil are found in Figure 7.

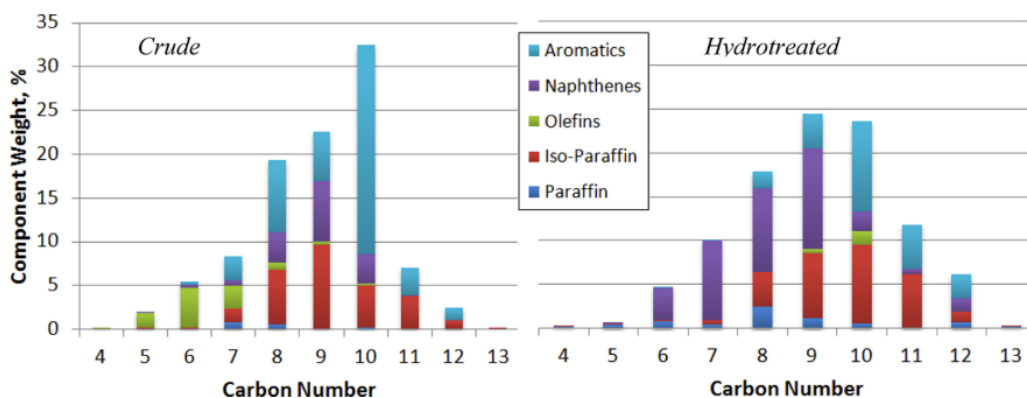


Figure 7. Molecular classes of components found in crude and hydroprocessed TDO oil at various carbon numbers. Reproduced from Eaton *et al.* (2015).²¹

Although hydroprocessing the fuel with the Alfa Aesar catalyst increased the values of the crude TDO oil, it still did not reach specifications. This problem was caused because the catalyst did not completely hydrogenate the molecules and because the cycloparaffin content was still too low.

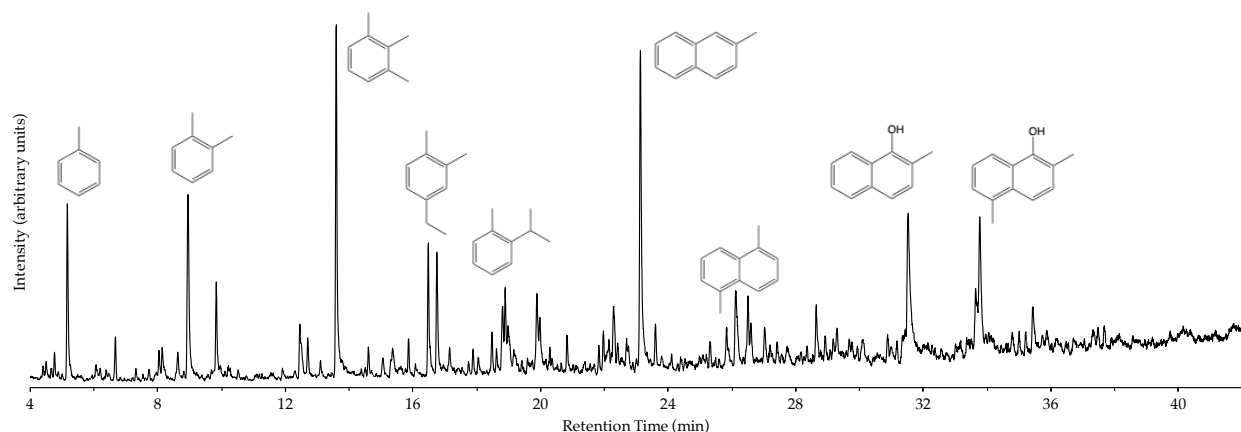


Figure 8. GCMS chromatogram of TDO oil with major peaks displayed. *Labeled molecules are not necessarily the correct isomer present in TDO oil but are meant to give the reader an illustration of a possible isomer.

The major components of TDO oil are mono- and diaromatic molecules, as Figure 8 shows, with the most common molecule being 2-methylnaphthalene (2-MN), a diaromatic compound. Because of its prevalence in TDO oil and the relative difficulty of hydrogenating and ring opening polycyclic molecules, 2-MN would make a good model compound to study. If a catalyst was designed that had good hydrogenation ability, we could potentially increase the cetane number of the fuel beyond the values reported by Eaton *et al.* (2015). Then, the TDO oil could potentially be used as a renewable blending component for diesel or jet fuels.

UPGRADING CHEMISTRY

Like petroleum, TDO oil is a complex mixture of molecules, comprising many hydrocarbon classes, as Figure 7 shows. The hydroprocessing experiments performed by Eaton *et al.* (2015) did not completely

hydrogenate the aromatic molecules found in crude oil, and although there was an increase in the cycloparaffin (naphthene) content, it was not enough to increase the cetane number of the fuel, owing to the low amount of paraffins and olefins.

To convert the aromatic and naphthenic molecules into ones that have better combustion characteristics, there are a variety of chemical reactions that can occur. The reactions occur on the surface of a catalyst, which ideally can be tailored to promote certain reactions for improving the combustion characteristics of fuel and avoiding unwanted side reactions.

Table 3. Types of reactions discussed in this thesis.

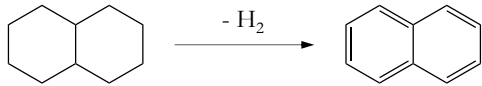
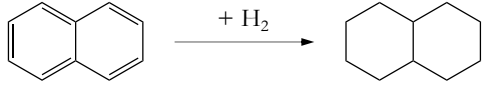
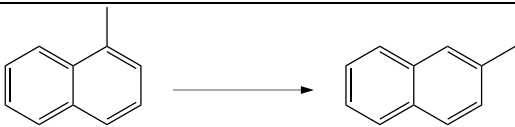
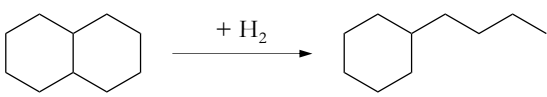
Reaction Type:	Sample Reaction:	
Dehydrogenation		(Reaction 1)
Hydrogenation		(Reaction 2)
Isomerization		(Reaction 3)
Ring Contraction		(Reaction 4)
Ring Opening / Hydrocracking		(Reaction 5)

Table 3 showcases examples of most of the reactions that are discussed in this report. Reaction 1 is a dehydrogenation reaction that converts decalin ($C_{10}H_{18}$, decahydronaphthalene) to naphthalene ($C_{10}H_8$). Dehydrogenation reactions are thermodynamically favored at high temperatures ($>400^{\circ}C$) and are one of a limited number of reactions that generate hydrogen (as opposed to consuming it) in a

petroleum refinery. Reaction 2 is a hydrogenation reaction, which proceeds in the opposite direction as reaction 1. This process consumes hydrogen and is thermodynamically favored at low temperatures. Because this thesis focuses on hydrogenation reactions, these are treated in more detail in another section (*c.f.*, Hydrogenation).

Reaction 3 is an isomerization from 1-methylnaphthalene (α -methylnaphthalene) to 2-methylnaphthalene (β -methylnaphthalene). Both molecules have the same molecular formula, $C_{11}H_{10}$, and they only differ by the position of the methyl- group on the naphthalene ring. Isomerization reactions tend to occur at higher temperatures and on acidic sites of a catalyst.

Reaction 4 is a ring contraction reaction forming methylperhydroindan from decalin. This reaction also does not require hydrogen and both molecules have identical molecular formulas of $C_{10}H_{18}$. The only difference is that a cyclohexane-like molecule (6-membered ring) in the structure is converted to a cyclopentane-like ring (5-membered ring). This process is only possible over a Brønsted acid site and is usually paired with a ring opening or hydrocracking reaction (reaction 5).²⁸ In this last reaction, the addition of diatomic hydrogen to decalin opens one of the 6-membered rings. Ring opening reactions usually occur alongside ring contraction reactions, and these high-temperature processes are useful in creating molecules with high cetane numbers.

HYDROGENATION

Hydrogenation (HYD), also known as hydrotreating, is the process of adding hydrogen to unsaturated molecules or to remove heteroatoms. However, in the scope of this thesis, hydrogenation reactions occur when hydrogen is added to saturate aromatic molecules, similar to reaction 2 in Table 3.

MODEL COMPOUNDS

Although reaction 2 shows the hydrogenation of naphthalene, a diaromatic compound, researchers have analyzed the hydrogenation of a variety of aromatic compounds. These molecules are good representations of aromatic streams present in LCO and other aromatic-rich petroleum streams. In general, the last aromatic ring in a molecule is the most difficult to saturate because the ring contains resonance stabilization.²⁹ Additionally, hydrogenating the first ring in naphthalene only requires the addition of two H₂, whereas three are required for the final ring. Moreau *et al.* (1988) claimed that the hydrogenation of naphthalene behaved similarly to the hydrogenation of butadiene (an olefin), whereas the hydrogenation of the final ring in tetralin behaved like benzene (an aromatic molecule).¹⁵

The reactivity of aromatic molecules follows the trend polyaromatics \geq diaromatics $>$ monoaromatics because larger molecules have an easier first hydrogenation step. In a study of tetralin (monoaromatic), naphthalene (diaromatic), and phenanthrene (polyaromatic) hydrogenation, Beltramone *et al.* (2008) found that the conversion was $>90\%$ for phenanthrene and naphthalene, but at identical conditions, the tetralin conversion was only 45% .³⁰

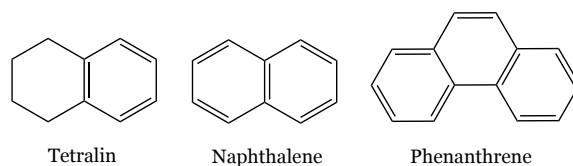


Figure 9. Common model compounds used in hydrogenation reactions.

It has also been postulated that the hydrogenation of tetralin (monoaromatic) and naphthalene (diaromatic) take place via different reaction mechanisms or on different adsorption sites.³¹ Rautanen *et al.* (2002) showed that the deactivation order for the hydrogenation of naphthalene and tetralin was significantly different and did not follow a sequential model of hydrogen addition, which was assumed to occur at the time.

In hydrogenation studies, the concentration of the model aromatic species is generally not very high. The first reason is because aromatic species like naphthalene and phenanthrene (shown in Figure 9) are solids at room temperature, so it would be challenging to test in a flow reactor unless they were dissolved. Secondly, with such a high concentration of aromatic species, there must also be an increase in catalyst mass to reach an appreciable weight hourly space velocity (WHSV). This is also a challenge because aromatic molecules can deactivate catalysts quickly, so having a lower aromatic concentration usually means a lower deactivation rate. In most catalytic studies, there is usually between 5 and 20 wt% of aromatics in the feed, which is dissolved in a nonpolar solvent that cannot undergo hydrogenation reactions. For these reasons, toluene or cyclohexane are not appropriate solvents because they could undergo hydrogenation and ring opening reactions respectively. As a result, the solvent for these reactions is usually a paraffin, like *n*-decane.

MONOAROMATICS. The hydrogenation of monoaromatic molecules has been heavily researched. Most studies focus on hydrogenation of benzene or tetralin, but phenol has also been a common starting point for hydrodeoxygenation reactions.²⁰ One of the most important studies on benzene hydrogenation was performed by van Meerten *et al.* (1976), who found that there are three different ways that benzene can adsorb on a catalytic surface.³² Two of the forms are reactive, but the last form of adsorption occurs dissociatively and acts as an inhibitor to the hydrogenation reaction. Lin and Vannice (1993) also found that the strength of benzene adsorption onto Lewis acid sites increased as the number of sites increased.³³

However, since benzene and toluene are found in the gasoline fraction of crude oil, our interest in their hydrogenation is limited. However, tetralin (the first compound shown in Figure 9) is considered a monoaromatic molecule even though it is formed from the partial hydrogenation of naphthalene (a diaromatic) and is found in diesel fractions of crude oil. Tetralin hydrogenation was found to take place

on both metal sites and with metal-assisted acid spillover sites, indicating that bifunctional catalysts are ideal for this process.³⁴ Additionally, Rautanen *et al.* (2002) also found that the hydrogenation of tetralin was irreversible, as decalin did not dehydrogenate back to tetralin, especially if there was still tetralin in the feed.

DIAROMATICS. Naphthalene, the simplest diaromatic compound, has been studied extensively, and a review and study of naphthalene hydrogenation was published by Weitkamp (1968).²⁹ In it, he discussed the likelihood that naphthalene adsorbed differently on different metals (Pt, Pd, Ru, and Rh), which was confirmed in later studies. Jacquin *et al.* (2003) found that on rhodium and ruthenium, naphthalene adsorbed similar to an olefin, whereas on platinum, naphthalene adsorbed like an aromatic molecule.³⁵ They also postulated that the adsorption caused the final product distribution to change, and for rhodium and ruthenium, the major product was mostly tetralin, whereas fully hydrogenated decalin was the predominate product for platinum.

Methylnaphthalenes have also been studied for hydrogenation reactions, though most studies focus on their hydrocracking ability. Miki and Sugimoto (1995) looked at hydrocracking reactions with 1-methylnaphthalene (1-MN) and 2-methylnaphthalene (2-MN).³⁶ They found that the hydrogenation of 1-MN and 2-MN both favor saturation of the ring without the methyl group, although the ratio of methyltetralins was found to be independent of temperature for 1-MN and slightly dependent on temperature for 2-MN. They also noted that 1-MN tended to crack into lower molecular weight (LMW) fragments, whereas 2-MN tended to ring open instead of crack, which yielded higher molecular weight (HMW) fragments. Karakhanov *et al.* (2018) found the same ring opening result using a similar catalyst.³⁷ And although ring opening of 2-MN had a higher selectivity towards ring opening than 1-MN, the ring opening was still more difficult for the β -isomer (2-MN) relative to the α -isomer (1-MN).

POLYAROMATICS. Polyaromatic molecules like phenanthrene (see Figure 9), anthracene, and larger ring structures are not typically used as model compounds for hydrogenation reactions. These molecules have higher boiling points and, in a refinery, would be sent to a hydrocracker to break the molecules into smaller components rather than hydrogenating them. Additionally, the reactivity of polyaromatics is fairly similar to that of diaromatics, but in general, the trend is that the reactions are 1st order in the aromatic species and each successive ring saturation becomes more difficult for polyaromatics.²⁰

THERMODYNAMIC LIMITATIONS

Hydrogenation is an exothermic reaction favored at low temperatures.³⁸ Additionally, hydrogenation is a reversible reaction, and there are times where it may not be possible to achieve complete conversion. Cooper and Donnison (1996) showed the equilibrium concentration of an aromatic species, A, is given by Equation 2:

$$\frac{Y_A}{Y_A + Y_H} = \frac{1}{1 + K_a \cdot P_{H_2}^n} \quad (2)$$

where Y_A and Y_H are the mole fractions of an aromatic species A and the hydrogenated product H, respectively, K_a is the equilibrium constant, P_{H_2} is the hydrogen pressure and n is the number of moles of hydrogen required for saturation.²⁰ Increasing the reaction temperature decreases the K_a which favors the aromatics, but high partial pressures of hydrogen, P_{H_2} , favor formation of the hydrogenated product.

However, as discussed in the next chapter, most catalysts that are active for hydrogenation are more efficient at high temperatures, where the reverse (dehydrogenation) reaction is favored. This is especially true for sulfided catalysts, which require severe operating conditions to hydrogenate aromatic compounds. These catalysts require high temperatures and high pressures as well as low space velocities to favor the hydrogenation reaction and achieve acceptable aromatic saturation. Figure 10 shows

aromatic saturation of a heavy gas oil stream over a sulfided catalyst as a function of reactor temperature and pressure.

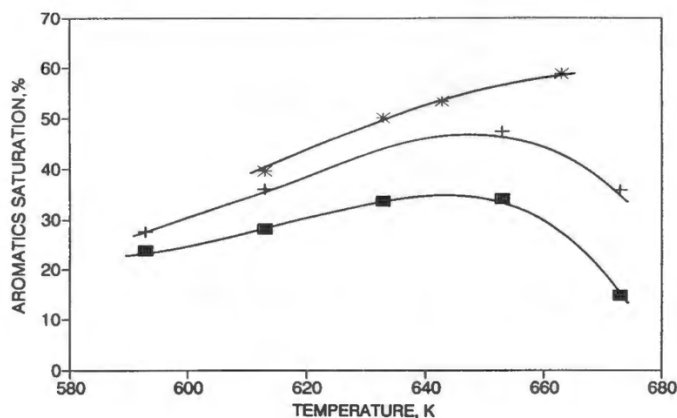


Figure 10. Aromatic hydrogenation as a function of temperature and hydrogen pressure on Middle East heavy gas oil: ■, 4.5 MPa; +, 6.5 MPa; *, 12.5 MPa. Reproduced from Cooper *et al.* (1992).³⁹

As Figure 10 shows, aromatic saturation is dependent on both the temperature and hydrogen pressure. At low pressures, there appears to be a point of maximum saturation, which occurs around 650 K (375°C). However, increasing the hydrogen partial pressure dramatically increased the amount of saturation that occurs.

Jacquin *et al.* (2003) also showed that naphthalene hydrogenation is thermodynamically limited at atmospheric pressure, and incomplete conversion (14-90%) was reached with a variety of metals, compared with almost complete conversion (>95%) when the reactions were conducted at 6 MPa.³⁵ The high pressure requirement of hydrogen in these reactions is consistent with collision theory and Le Chatelier's principle of forcing the reaction forward by adding more reactant.⁴⁰

Thermodynamic limitations also exist within the reaction products. Figure 11 shows the equilibrium that exists between *cis*- and *trans*-decalin, the fully hydrogenated derivatives of naphthalene. Rautanen *et al.* (2001) performed Gibb's free energy calculations and found that *trans*-decalin is

thermodynamically favored by more than 90% at typical reaction temperatures.⁴¹ However, they showed that each catalyst had different selectivity and *cis/trans* ratios, which led them to conclude that the *cis/trans* ratio of decalin was governed solely by kinetics and was not thermodynamically limited. Furthermore, Schmitz *et al.* (1996) showed that the *cis/trans* ratio was highly dependent on the metal and support used for hydrogenation.⁴² The importance of forming each decalin isomer is discussed in further detail in the introduction of Chapter 4.

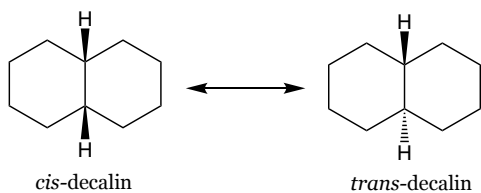


Figure 11. Equilibrium between *cis*- and *trans*-decalin.

CHAPTER 2

CATALYSTS IN OTHER HYDROGENATION STUDIES

CATALYST SUPPORTS

The majority of metallic catalysts are synthesized as metal nanoparticles dispersed on a support. Unsupported catalysts are uncommon, but there are some reactions that use them.⁴³ While there are many reasons to use supported catalysts, perhaps the most important reason is the price of the metal being used. Reactions only occur on the surface of a catalyst, and any metal inside the bulk of a catalyst is essentially wasted, because it cannot participate in reactions. Some metals used for hydrogenation, like platinum and palladium, are very expensive (as Figure 12 shows), so limiting their use in a catalyst by supporting a small amount of metal (*e.g.*, 1 wt%) on an inexpensive support makes more financial sense when dealing with large amounts of catalyst.

Another important factor in determining a good support is finding a catalyst with a large surface area. Since reactions only occur at the catalyst surface, doubling the surface area of a catalyst could potentially mean doubling the number of reactions that can simultaneously occur (assuming there were no diffusion limitations and the metal was dispersed equally across both catalysts).

It is generally assumed that at low metal loadings, metal nanoparticles become highly dispersed across the surface of a catalyst and act like nanoparticles (isolated from other metal clusters), but this is not always true. Some metal-catalyzed reactions can be assisted by or occur on the surface of a support. Hydrogenation reactions can be assisted by acid sites via several methods.

Bifunctional catalysts (as discussed in this research) are catalysts that contain both metal and acid sites. The hydrogenation ability of metals will be discussed later (*c.f.*, Metal Catalysts), but in general supports with a moderate acidity are most efficient at hydrogenating aromatic molecules. Supports with

no acidity are not able to assist the reaction, but supports that are too acidic will catalyze coking reactions that deactivate catalytic sites and excessively crack components.⁴⁴ The acidic strength of catalytic supports follows the order: $\text{SiO}_2 < \text{Al}_2\text{O}_3 < \text{amorphous silica alumina} < \text{zeolites}$, which encapsulates supports with no acidity (silica) and supports with very high acidities (zeolites).⁴⁵

SILICA

Silica (SiO_2) is a commonly used support because of its abundance and very large surface area that can be attained ($>1000 \text{ m}^2 \text{ g}^{-1}$). Silica is also neutral in acidity because it lacks both Brønsted and Lewis acid sites. Thus, a hydrogenation catalyst supported on silica would only have metal sites. This is disadvantageous for hydrogenation reactions, because the support does not assist in the reaction. However, it can be beneficial to help avoid any reactions that are caused by acidity, like isomerization, ring contraction, and ring opening reactions.

Despite a lack of acid sites, silica is thermally stable and can easily be formed into mesostructures like SBA-15, HMS, and MCM-41. Of these, SBA-15 has been demonstrated to have better characteristics for hydrogenation of polyaromatic molecules.⁴⁶ Additionally, incorporating aluminum into the framework of SBA-15 has been shown to greatly increase the acidity, which increases the catalyst's ability to perform hydrogenation and ring opening reactions.⁴⁷

ALUMINA

Alumina (Al_2O_3) is the most common support for hydrogenation reactions, mainly due to its high surface area, stability, and low cost.⁴⁸ Of the different phases of alumina that can be synthesized, gamma-alumina ($\gamma\text{-Al}_2\text{O}_3$) has the best catalytic properties for most reactions owing to its higher surface area, presence of Lewis acid sites, and decent thermal stability. For the remainder of this thesis, gamma-alumina will be referred to as alumina for simplicity.

Alumina possesses mainly Lewis acid sites, although there are a few weak Brønsted acid sites that can be found on the support. Those sites exist as isolated surface hydroxyl groups, but they comprise a very small number of the acid sites on the support.⁴⁹

Because most of the acid sites on alumina are Lewis acids, alumina is not a good fit for reactions that require Brønsted acid sites. For instance, the Brønsted acid sites on alumina were not abundant enough to isomerize or promote ring-opening reactions of aromatic compounds when tested.⁵⁰ However, modifying an alumina support with halogens has been reported to increase their acidity and activity. The addition of Cl⁻ was shown to increase the number of Brønsted acid sites on an alumina catalyst, which in turn increased the catalytic activity for methylnaphthalene hydrogenation.⁴⁷

AMORPHOUS SILICA ALUMINA

Amorphous silica alumina (ASA) supports are comprised of a mixture of Si and Al atoms arranged on a molecular level (*i.e.*, not a physical mixture of silica and alumina). ASA supports are usually comprised of more Si than Al, but they each can range from 0-100% of each element. Because the ASA support contains both Si and Al, it possesses both Lewis and Brønsted acid sites, which are relative to the Si/Al molar ratio. Catalysts with high amounts of Si have low Brønsted acidity, and in those catalysts, the Lewis acidity dominates over the Brønsted acidity.⁵¹

Catalysts with atomic Si/Al ratios approximately equal to unity have ideal characteristics for hydrogenation experiments, with the range 0.75 to 1.5 being the best.⁵² In a study with catalysts of various amounts of silica and alumina, it was found that the SIRAL support (a type of ASA) with 40 wt% silica displayed the highest strength and quantity of acid sites.⁴⁹ With higher silica content, the activity dramatically dropped as the support surface became coated with silica.

ASA catalysts also have other advantages over some supports. For instance, it was found that the acidity in an ASA support increased the sulfur tolerance of a precious metal catalyst supported on silica from a few ppm to 10 ppm.²⁰ However, another paper suggested that precious metals impregnated on alumina had better sulfur resistance than ASA.⁹ From a commercial standpoint, ASA has limited use in most petroleum refineries because it has low tolerance to basic compounds, such as ammonia, which are common during HDN.⁴

ZEOLITES

Zeolites are a family of crystalline aluminosilicates with more than 1,000 synthetic varieties.⁵³ Zeolites are one of the most commonly employed industrial supports because of their high surface area and adjustable acidity.⁴⁵ Zeolites can also act as catalysts themselves with their ability to perform some reactions without a metal. Zeolites (like ASA) have very high Brønsted acidity because of bridged hydroxyl groups between Si and Al atoms, and like ASA, the number of acid sites is proportional to the Si/Al molar ratio. However, zeolites differ from ASA because zeolites contain a crystalline framework, unlike the amorphous structure of ASA.

Zeolites come in many shapes and sizes, and the pore size is crucial in determining what catalysts are appropriate for a reaction. Diaromatic molecules, like naphthalene, are too large to fit inside the pores of medium-pore zeolites, like ZSM-5.⁵⁴ The kinetic diameter of naphthalene is 6.2 Å, and the pores of ZSM-5 only measure 5.3 x 5.6 Å, so the reaction would be severely diffusion limited.^{38,53} However, large-pore zeolites like faujasite (zeolite Y, 7.4 x 7.4 Å) and β-zeolite can be used for polycyclic molecules.⁵⁴

Since zeolites can contain high concentrations of Brønsted acid sites, they have a tendency to crack molecules.⁵⁵ These cracking reactions often lead to excessive coking on the catalytic surface, which causes the active sites to deactivate.^{44,56} The strength and number of acid sites can be decreased by

modifying the surface with addition of an alkali metal to ion-exchange on some of the sites, or by physically combining the zeolite a support with little Brønsted acidity, like alumina.⁹ Reducing the Brønsted acidity of the support yields higher amounts of hydrogenated products while limiting the number of hydrocracked products.

Zeolites have also been shown to increase the sulfur tolerance of Pt and Pd catalysts. Because the zeolitic support pulls electron density out of surface metallic species, it decreases the strength of Pt-S bonds on the catalysts surface. This helps sulfur escape from the catalyst surface, and is therefore not converted into a permanent poison.⁵⁷

OTHER SUPPORTS

There have been numerous other supports used in hydrogenation catalysts, including carbon, zirconia (ZrO₂), magnesia (MgO) and titania (TiO₂) to name a few. These supports are uncommon for hydrogenation of aromatics in petroleum upgrading, and as a result, there is little information on their usefulness. Carbon and magnesia are not used because they are neutral and basic supports, respectively, and do not assist metal sites in hydrogenation. And although zirconia and titania are acidic and are useful in bifunctional catalysts, their high cost and lower abundance limits their usability, although they have shown some promise as alternative supports for HDS reactions.¹⁴

METAL CATALYSTS

There are many factors to consider when designing a catalyst. The first and foremost of these is the activity of the metal. If the chosen metal cannot perform a reaction, then regardless of how efficient the catalytic system is, the reaction will not occur. The second consideration is the price of the materials. Although some metals are much cheaper, a lower activity is sometimes more detrimental than the material price. This is especially the case because industrial catalysts are expected to endure months or

years of continuous use (depending on the system conditions and presence of catalytic poisons). The 2006 and 2019 prices of some common transition metals are displayed in Figure 12.

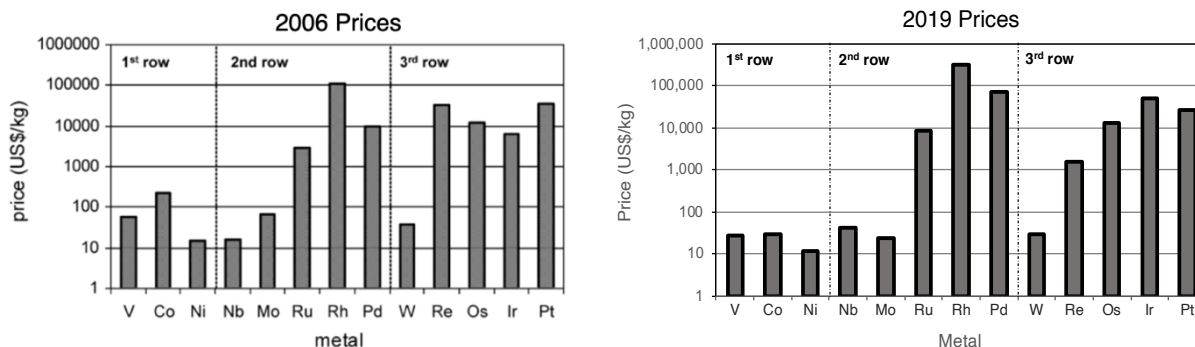


Figure 12. Price of several transition metals used in hydrogenation catalysts using 2006 (left) and 2019 prices (right).⁵⁸ 2006 prices reproduced from Eijsbouts *et al.* (2007).⁴³

Although most of the prices have remained consistent between 2006 and 2019, a few have dramatically changed. The price of rhenium has decreased, while the price of iridium and palladium have both significantly increased. Most of the expensive metals are precious metals, and with low natural abundances, it makes sense they cost more. Compare their prices to non-precious metals like nickel and cobalt, and you see a large difference. Non-precious metals remain very low in price compared to some precious metals that are used in hydrogenation catalysts. In this section, I will discuss the three main types of catalysts that are used in hydrogenation reactions, as well as benefits and drawbacks of each one.

PRECIOUS METAL CATALYSTS

A vast majority of precious metal catalysts are based on platinum or palladium, but there are other metals that also can perform these reactions. Huang and Kong (1996) studied hydrogenation of naphthalene with various metals supported on γ -Al₂O₃ and found the activity followed the trend Pt > Pd > Rh > Ru > Ir.⁵⁹ They found that after platinum and palladium, there was a large decrease in activity, which

explains why the latter three are uncommon in hydrogenation catalysts. Since most catalysts contain Pt or Pd, in this section I focus on their use and implementation.

Platinum was one of the first metals found to perform hydrogenation reactions. Studies have shown that when compared on a variety of supports, platinum has a greater turnover frequency (TOF) than palladium.⁶⁰ However, there are many factors that determine the metal activity, such as: metal dispersion, crystallite size, support interaction, and the metal incorporation method.⁴⁷

Palladium has also been used as an aromatic hydrogenation catalyst, albeit less often than platinum. One reason this may be is because in the presence of aromatics, palladium preferentially saturates olefins before aromatics.²⁹ Weitkamp (1968) also found that palladium hydrogenated naphthalene directly to tetralin with 99.7% selectivity, whereas platinum formed more decalin, the fully-hydrogenated form. Therefore, if a catalyst is meant to produce fully saturated products, it will likely be made of platinum, but for less-saturated products, palladium is the metal of choice.

Additionally, a bimetallic combination of Pt and Pd was found to possess superior characteristics than each of the metals individually.⁵⁵ They were found to be more efficient at hydrogenation reactions, and when paired with a zeolite support, they had a higher sulfur tolerance.²⁰

Despite their higher TOF and activity, precious metal catalysts have limited use because of their poor sulfur tolerance and high price. Although bimetallic PtPd alloys can have sulfur tolerance up to 50 ppm, there is still a significant amount of sulfur that must be removed from feedstocks (like crude oil) to reach that level of sulfur (which is often not economical). Additionally, as Figure 12 shows, the cost of hydrogenation metals Pt and Pd remain very high (\$40,000 and \$80,000 per kg respectively as of 2019), and for the catalyst to be economically feasible, only a small amount of metal may be deposited onto the

catalyst. As a result, there were catalysts developed that were more efficient at higher sulfur content (*c.f.*,

Sulfided Catalysts) and catalysts that were less costly (*c.f.*, Non-Precious Metal Catalysts), which are discussed in further detail in the next sections.

SULFIDED CATALYSTS

Sulfided catalysts, also known as transition metal sulfide (TMS) catalysts, are ones that are used specifically for feedstocks that contain large quantities (100-6000 ppm) of sulfur. For this reason, these are the main catalysts used in petroleum applications. Sulfided catalysts simultaneously perform not only hydrodesulfurization (HDS), but also hydrogenation.

Sulfided catalysts usually contain a Group VIB metal (Cr, Mo, W) coupled with a metal from the iron group (Fe, Co, Ni).⁴ Of these, Cr and Fe are rarely used, while Co, Ni, and Mo are widely used. In these catalysts, there is always at least one metal from each group. The reason for the coupling is because the Group VIB metal provides the metal needed for the active site, while Co and Ni are used as promoters for the reaction.

The active sites on sulfided catalysts are complex, but a brief summary is presented here. It has been proposed that active sites on sulfided catalysts are found at coordinatively unsaturated points where exposed Mo atoms exist with sulfur vacancies.⁵⁷ These vacancies are active for hydrogenation only if they are at the edge or corner sites of MoS₂ structures, not at basal sites.

Co- or Ni-promoted catalysts can enhance the rate of reaction by two different mechanisms that have been postulated. The first method (known as the contact synergy model) assumes that the promoter and active site each exist as separate crystallites, but the Co or Ni metal provides hydrogen atoms to the MoS₂ site, which activates them, similar to a hydrogen-spillover mechanism.⁶¹ The second postulated

mechanism states that Co or Ni atoms on the corner sites are used to donate electrons to adjacent Mo atoms. These added electrons weaken the Mo-S bond and create sulfur vacancies, which are the active sites in hydrogenation reactions.⁶²

However, not all combinations of metals are equally efficient, and they also have different sulfur tolerances and HYD capacity. For instance, the hydrogenation capacity of the catalysts follows the trend: NiW > NiMo > CoMo > CoW.⁴ However, CoMo has the highest sulfur tolerance and HDS activity of any catalyst followed by NiMo. The catalyst that is most efficient at a desired reaction depends entirely on the feed to a reactor. Feedstocks with very high sulfur content usually require CoMo, while applications where aromatic saturation is most important usually require NiMo.⁹

Sulfided catalysts are usually supported on a gamma-alumina carrier. This carrier contains a large surface area (200 to 300 m² g⁻¹) and provides moderate acidity for the reaction. Typically 13-20 wt% MoO₃ is added along with about 3 wt% of CoO and NiO.⁴ By adding both Co and Ni, the catalyst is able to perform at the optimal conditions for each metal. These catalysts are typically formed into extrudates between 1 and 4 mm long and with a length/diameter ratio of 2 to 4.⁴

One of the disadvantages of sulfided catalysts is that they have low TOF and thus only efficiently generate partially-hydrogenated products.²⁰ When a feed containing aromatics was fed into a two-stage reactor (NiMo in first stage, NiW in second stage), only moderate (25-50%) aromatic saturation occurred, which was due to lower activity.⁵⁷ This is contrary to most precious metal catalysts, which generally produce fully-hydrogenated species.

Another issue with sulfided catalysts is that they require a feed containing an appreciable amount of sulfur (at a minimum of about 50 ppm). This is because sulfur is routinely expelled from the catalytic surface, creating sulfur vacancies. Over time, as more and more sulfur vacancies are formed, the dwindling

amount of remaining sulfur on the surface becomes more difficult to remove and with a feedstock lacking the sulfur needed to replenish the catalyst, the activity would rapidly decrease, and the catalyst would need to be re-sulfided to become activated again. For this reason, sulfur is required in the feed to maintain a constant amount of sulfur that can replenish the sulfur lost when the sulfur vacancies are lost.

Because TDO oil is formed from cellulosic feedstocks, it inherently contains very little sulfur, making it a potentially attractive feedstock for ultra-low sulfur distillate (ULSD) fuel. However, to use a sulfided catalyst to hydrogenate TDO oil, sulfur would need to be added to the feedstock. This is not the best option because the final product would contain sulfur, and the fuel might not meet ULSD specifications. However, there are also other catalysts that are less expensive and do not require sulfur in their feed that can efficiently hydrogenate cellulosic fuels, such as TDO oil.

NON-PRECIOUS METAL CATALYSTS

Catalysts containing non-precious metals occupy a niche position for some reactions. They are much more affordable than precious metal catalysts and they do not require sulfur in the feed, but they do generally exhibit lower TOF's than precious metals and cannot tolerate high levels of sulfur (although they have higher tolerance than some precious metal catalysts). The only metal that falls into and is substantially used in this category is nickel.

Nickel is attractive for aromatic hydrogenation because it is active at low temperatures and has a moderately high activity.³¹ Its activity also dramatically increases as the hydrogen partial pressures increases, making reactions at high pressure advantageous.⁶³ Combining Ni with a precious metal catalyst can also have advantages, and Castaño *et al.* (2007) found that the incorporation of 1 wt% Pd onto Ni tempered catalyst deactivation and further increased activity.⁵¹

The biggest drawback with non-precious metal catalysts is their lower activity towards hydrogenation. Although they will activate aromatic hydrogenation reactions, they need more active sites to achieve the same conversion as their precious metal counterparts. In this thesis, the vast majority of catalysts produced were supported Ni catalysts.

CATALYST DEACTIVATION

Deactivation is a topic of interest when designing any sort of catalyst, because there are multiple methods of catalytic deactivation. While some types of deactivation are temporary, others are permanent. Determining what types of poisons are present in a feedstock is crucial to determining which type or types of deactivation will likely be relevant. The four main classes of catalyst deactivation are sintering, coking (fouling), poisoning, and erosion (leaching). A short description of each type of deactivation follows.

Sintering is a thermal process by which a catalyst loses surface area because of exposure to high temperatures. This loss in surface area is usually two-fold, with a loss in support surface area as well as a loss in metal surface area. The support surface area may be lost because of changes in the crystalline structure of the support or because of pore clogging that occurs as pores narrow or close.⁶⁴ Since the surface of metal particles are where most catalytic reactions take place, it is important to retain as much metallic surface area as possible. When temperatures approach the Tammann temperature (roughly 40% of the melting point of a metal), individual metal nanoparticles agglomerate into larger crystals.⁶⁵ Additionally, Ostwald ripening occurs when small nanoparticles dissolve from the catalytic surface and are redeposited in larger clusters. Either way, these large crystals have less surface area than the smaller ones, which leads to a smaller area for catalytic reactions to occur and thus lower activity.

Another common type of catalyst deactivation is known as coking or fouling. This deactivation occurs when carbonaceous deposits, known as coke, form on the surface of a catalyst. The coke is formed through a complex interaction between the metal and hydrocarbon, and coke is built up over time and blocks access to metal sites, which can completely clog pores. However, coke is not considered a poison, but rather a temporary inhibitor.⁶⁴ Catalysts coated with coke can usually be regenerated by burning the carbon off the catalyst. Additionally, coke production can be minimized by running reactions at high pressures and using excess hydrogen.

Another type of deactivation is called poisoning, which occurs when molecules irreversibly chemisorb onto a catalytic surface and poison the active sites. Because the chemisorption is irreversible, catalyst poisons cannot easily be removed from the surface. The active sites that are poisoned are permanently lost, so minimizing this type of deactivation is crucial to retaining activity and long catalyst lifespans.

The last type of deactivation I discuss is erosion, which is a mechanical process. As fluid (liquid or gas) flows through a reactor, it can wear away metal nanoparticles on the outside of a catalyst. This process is similar to how water from the Colorado River eroded layers of sandstone over millions of years, creating the Grand Canyon (although this is a much smaller scale).

Together, these four types of deactivation are common in catalytic systems, but in hydrogenation applications, coking and poisoning are the major ones observed. Coking is commonplace in many reactions, and coke is easily formed on fresh catalysts when a feedstock with aromatics is flowed over it.⁹ Rautanen *et al.* (2002) studied a Ni/Al₂O₃ catalyst and noted that significant deactivation occurred even without the presence of impurities, which indicated that coking was the major deactivation mechanism, not poisoning.³¹ They also went on to determine that the hydrogen pressure did not have a significant

effect on deactivation and that the coke formation was only mildly influenced by temperature. In another study, Park *et al.* (2013) studied a spent catalyst from 1-methylnaphthalene hydrogenation on a solid-state NMR, and their ^{13}C spectrum is displayed in Figure 13.⁵⁰

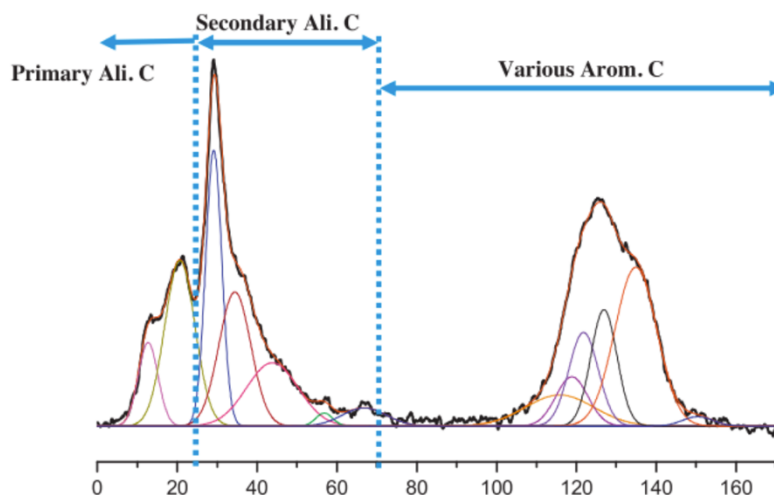


Figure 13. ^{13}C solid-state NMR spectrum of used alumina-USY catalyst. Reproduced from Park *et al.* (2013).⁵⁰

Figure 13 indicates that the coke on the catalyst contained a significant amount of aliphatic and aromatic carbons, indicating that 1-methylnaphthalene was not likely the major component in the coke. Rather, it appears that the coke is somewhat similar to a methyltetralin structure, possessing both aromatic carbons as well as primary and secondary aliphatic carbons. This conclusion fits with the result of Rautanen *et al.* (2002), who showed that tetralin dissociation was the major cause of coke buildup, whereas naphthalene dissociation was negligible.³¹ Although coking is usually the major cause of catalyst deactivation, poisoning is the other type of deactivation to watch out for.

Catalyst poisoning is commonplace in many reactions because there are a myriad of poisons that can destroy an active site. The most commonplace one in petroleum applications is sulfur, which binds to metal sites and deactivates them. Because the sulfur (and to a lesser extent nitrogen) levels of crude oil

are so high, sulfided catalysts must be used, otherwise a non-sulfided catalyst would be rapidly deactivated. But because of sulfided catalysts' low activity, efforts have been made to increase the sulfur tolerance of other catalysts. For instance, using a strongly acidic support can sufficiently modify the electronic structure of a metal to increase its sulfur tolerance. There also have been studies that showed that adding other elements, such as gold, to a catalyst can have a big impact on increasing the sulfur tolerance.⁶⁶

Because the ultimate goal of this thesis project is to hydrogenate TDO oil, it is important to think about the catalyst poisons that could be present in that feedstock. Because TDO oil is formed from renewable sources, there is a possibility that biomass impurities such as potassium, sodium, and other alkali metals may be present in TDO oil.⁶⁷ Chemicals used in the TDO process could also remain in the oil layer, such as sulfuric acid and calcium hydroxide. These can all act as catalyst poisons by binding to active sites and deactivating them. Regardless of the experiment, there will always be catalyst deactivation, but the goal should be to design a process that minimizes the deactivation that occurs.

CHAPTER 3

SYNTHESIS AND DESIGN OF HYDROGENATION CATALYSTS

MATERIALS AND METHODS

CATALYST CHARACTERIZATION

NITROGEN ADSORPTION/DESORPTION

Nitrogen physisorption was performed on a Micromeritics ASAP 2020, which is displayed in Figure 14. The multistep procedure involved carefully weighing out the sample, degassing the tube, and running sample analysis. Long, narrow bulb tubes were used to hold the samples. The mass of the tube and frit (the cap on the tube) were weighed out and then the sample was added. Generally, about 0.1 g of sample was weighed out, with less mass used for samples with high surface areas ($>200 \text{ m}^2 \text{ g}^{-1}$) and more mass used for lower surface area catalysts ($<100 \text{ m}^2 \text{ g}^{-1}$).



Figure 14. Micromeritics ASAP 2020 instrument used for nitrogen physisorption.

After the samples were weighed out, they were placed in the instrument for degassing. During the evacuation phase, the sample was heated to 90°C at $10^\circ\text{C}/\text{min}$ while evacuating to 100 mmHg. Afterwards, the sample was heated to 350°C at $10^\circ\text{C}/\text{min}$ and was kept constant for 4 hours. After the

sample cooled to room temperature, it was weighed out again and placed in the analyzer port. During the analysis phase, a Brunauer-Emmett-Teller (BET) isotherm was taken at 77 K. A sample isotherm is displayed in Figure 15 showing the adsorption and desorption curves.

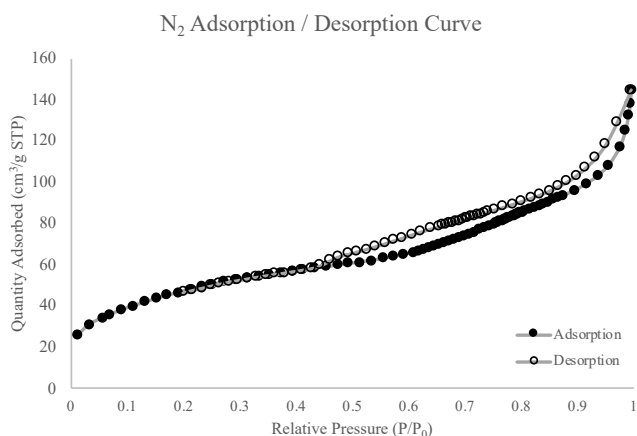


Figure 15. Nitrogen adsorption and desorption curves for Alfa Aesar catalyst.

Specific surface areas ($\text{m}^2 \text{g}^{-1}$) reported in this thesis are measurements of the BET surface area. Pore volumes ($\text{cm}^3 \text{g}^{-1}$) were measured as a cumulative sum of the total pore volume of all pores smaller than 4 microns. Average pore size (\AA) was measured as the average adsorption pore width.

THERMOGRAVIMETRIC ANALYSIS (TGA)

Thermogravimetric Analysis (TGA) was performed using a TGA Q500 instrument, shown in Figure 16. Using a very precise balance, a small amount of sample is heated in the presence of oxygen while measuring the change in mass. Looking at the mass loss curve, the sample undergoes periods of mass loss that correlate to various materials being ejected from the surface.

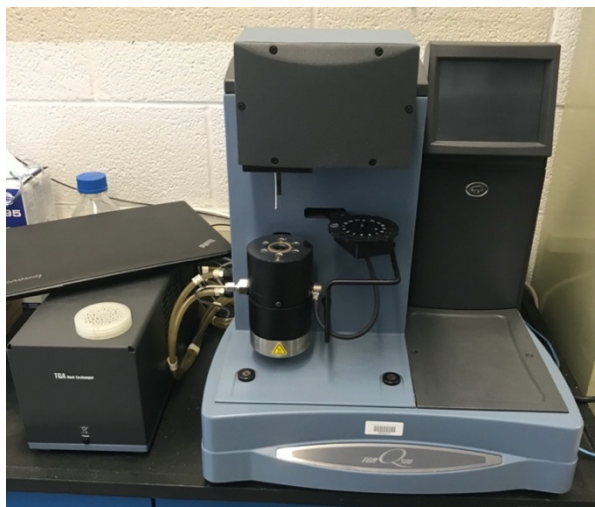


Figure 16. TGA Q500 used for this research.

Using the TGA Q500, samples of about 15 mg were loaded onto platinum trays and placed onto the sample holder via the autosampler. The furnace was then lifted over the sample and the temperature ramp was started. The temperature was increased at a rate of $10^{\circ}\text{C}/\text{min}$ from room temperature to 800°C , while the mass loss was studied. A sample TGA curve is displayed in Figure 17.

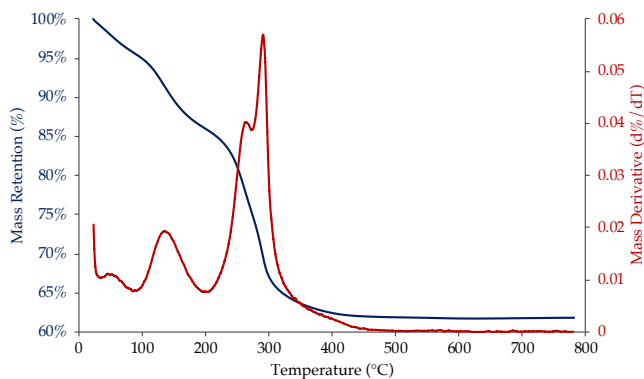


Figure 17. TGA curve of uncalcined 100Ni catalyst.

As Figure 17 shows, the mass retention is shown in blue and decreases during the heating ramp. The change in mass per unit time (first derivative) is displayed in red and clearly shows points where the

mass loss was highest. For instance, in this sample, the largest mass loss by far is around 300°C, with mass lost between 25 and 450°C.

X-RAY DIFFRACTION (XRD)

X-ray diffraction (XRD) analysis was performed on a Panalytical X-Pert Pro. Samples were prepared by placing about 0.1 g of calcined catalyst onto a glass plate. The plate was inserted into the instrument, and the sample was scanned from 20 to 80° using a scan step size of 0.05°. The instrument used a Cu K α X-ray anode with a parabolic mirror, 10 mm mask, and slit of 0.5°. As the sample was being scanned, a 255-channel PIXCEL detector was used to generate the resulting XRD spectra.

TRANSMISSION ELECTRON MICROSCOPY (TEM)

Transmission electron microscopy (TEM) is a microscopy technique in which a beam of electrons is passed through a specimen, forming an image. Samples were placed inside a vacuum chamber and the image was formed by the electron interaction, which was viewed by the user. The TEM used in this experiment was a Phillips CM-10 TEM, as Figure 18 shows.



Figure 18. Phillips CM-10 TEM.

Samples were prepared for use on the TEM by placing samples onto a copper coated grid. Excess solids were tapped off the surface, and the remaining materials were inserted into the instrument. The TEM operated at 100 kV and had a point resolution of 0.5 nm. Sample images were taken using the built-in Orius SC200 CCD camera.

CATALYST SYNTHESIS

Table 4 presents an overview of the catalysts which were synthesized for this thesis, and the synthesis methods are detailed in Appendix A. This current section includes abbreviated versions of how the catalysts were synthesized and why the preparation methods were used. Catalysts produced in this study were produced via incipient wetness impregnation (IWI), coprecipitation, or a combination of both.

Table 4. Synthesis methods for producing each type of catalyst.

Synthesis Method	Ref. ^a	Notes
Incipient Wetness Impregnation	A - D	Direct impregnation onto support
Coprecipitation	E - P	Solutions mixed at 25°C
	Q - V	Solutions mixed at 90°C
Multiple Synthesis	W - Z	Solutions mixed at 90°C to form coprecipitated support, then direct impregnation onto support

^a Corresponds to the location of the references in Appendix A.

INCIPIENT WETNESS IMPREGNATION CATALYSTS

Of all catalyst synthesis methods, incipient wetness impregnation (IWI) is the most commonly used. The impregnation of porous supports is simple, has limited waste byproducts, and gives reproducible results between batches.⁴⁷

The first step in synthesizing a catalyst via IWI was to determine the incipient wetness point of the support. Water was added dropwise to the support until it looked like a paste and had a texture like wet sand. Then, the amount of water was used to determine the volume of water that fit inside the pores of the support. Next, a metal solution was prepared by dissolving a metal precursor (nickel nitrate hexahydrate) in a solution of water (which had an equivalent volume as the pores of the support).

When the metal solution was slowly dropped onto the support, capillary action drew the solution into the pores of the catalysts. The support was stirred to break up chunks and to distribute the solution evenly across the support. After the dropwise addition of the metal solution was completed, the wetted support was dried to remove the solvent (in this case water) from the pores, leaving behind particles of the metal precursor. The catalyst was then heated (*i.e.*, >350°C) in oxygen to oxidize (calcine) the precursor and leave the metal oxide (NiO) deposited on the catalyst, which was safe to store and handle. Whenever it was time to perform a reaction, the calcined catalyst was inserted into the reactor and heated with hydrogen (reduced) at high temperatures.

Since most chemical reactions take place on metal sites on the surface of a catalyst, it might seem ideal to apply as much metal as possible to the surface. However, above a certain metal loading, the extra metal particles agglomerate, where smaller particles combine together, and the resulting catalyst has a decreased surface area and metal dispersion.⁵¹ Additionally, some of the precious metals used in hydrogenation catalysts are expensive (remember Figure 12), so there is also a trade-off between the cost of the catalyst and the desired activity.

COPRECIPITATION CATALYSTS

Coprecipitation is another method of synthesizing catalysts. The solids are produced from a solution, and a precipitating agent or a change in pH is used to precipitate the catalyst out of solution.⁶⁸

Unlike incipient wetness catalysts, coprecipitated catalysts can contain metal contents much larger than 20 wt%. However, there is a trade-off because IWI catalysts only disperse metal particles onto the surface and pores of the catalyst, but in coprecipitated catalysts, the positioning of the metal atoms is unknown. Some metal atoms would be present in the bulk of the catalyst (and thus would be unable to participate in the reaction), but there would also be many metal particles on the surface, which would be advantageous because they have stronger interactions between the metal and the support.⁶⁹

Detailed synthesis methods for all coprecipitated catalysts are in Appendix A. In this thesis, coprecipitated catalysts were formed from two solutions: one comprised of sodium carbonate and the other containing aluminum chloride with nickel nitrate. When the two solutions were combined together, the precipitating agent (sodium carbonate) caused the catalyst to precipitate out of the solution.

According to solubility rules, all carbonates are insoluble except for ones bound to a Group 1A cation (like Na^+). Ni and other transition metals were supplied in their nitrate or chloride form, which are all water-soluble. The same is true for the source of aluminum (AlCl_3). When these compounds dissolve in water, they dissociate into their cationic and anionic species. One solution contained Na_2CO_3 and the other solution contained Ni^{2+} and Al^{3+} , both of which were dissolved in water. However, when each of these solutions were combined, they underwent a double displacement reaction that formed NiCO_3 , $\text{Al}_2(\text{CO}_3)_3$, NaNO_3 , and NaCl . The first two products are water-insoluble, and so they precipitate out of solution together. The latter two remain in the solution and are washed off the catalyst during vacuum filtration.

Although we mentioned that $\text{Al}_2(\text{CO}_3)_3$ is formed via a double displacement reaction, other chemists question its stability as a species.⁷⁰ They believe that the carbonate species is so alkaline that it only produces gaseous CO_2 and water-insoluble $\text{Al}(\text{OH})_3$ instead of aluminum chloride. Although I cannot confirm which material was precipitated to produce the final catalysts, I know that the formed species is

merely a precursor to the catalyst. After the material was filtered, washed, and dried, it was calcined, which formed a powder of interlocking crystals of NiO and Al₂O₃ from the water-insoluble products. The coprecipitated catalysts were formulated as Ni/Al₂O₃.

Two different methods were used to synthesize the coprecipitated catalysts. The main difference was the temperature at which the carbonate and metal solutions were combined. Initially, the bimetallic coprecipitated catalysts (like NiCr) and some monometallic Ni catalysts were prepared by mixing solutions at room temperature (25°C). However, after multiple trials, we discovered that the catalyst characteristics could be dramatically enhanced by increasing the mixing temperature to 90°C. These results are discussed in further detail later, and more detailed synthesis descriptions are in Appendix A.

MULTIPLE SYNTHESIS METHODS

Catalysts synthesized by multiple methods were prepared by successive treatments of coprecipitation followed by IWI. This procedure was done to ensure that a precious metal would only be deposited on the surface and pores of the catalyst, while simultaneously containing active sites from the coprecipitated catalysts. Economically, this is also a good choice because a relatively inexpensive metal like Ni was used in the coprecipitated portion of the catalyst, while a more expensive metal, like Pt or Pd, would be dispersed across the catalyst surface and pores.

One large batch of 60 wt% Ni/Al₂O₃ (60Ni) coprecipitated support was used for preparing each of the precious metal catalysts to ensure consistency among the catalysts. The coprecipitated catalysts were prepared in the same manner as the 60Ni catalyst prepared at 90°C. From there, a 1 wt% solution of a precious metal (Pd, Pt, Ir, Ru) was impregnated onto the catalyst. Detailed synthesis methods for each of the catalysts can be found in Appendix A.

COMMERCIAL CATALYST

A nickel on silica-alumina catalyst purchased from Alfa Aesar was compared to each of the catalysts synthesized in this study. The Alfa Aesar catalyst (Part # 031276; Nickel on silica-alumina) used in this thesis has a proprietary composition, but it was sold as containing $66 \pm 5\%$ Ni. The same bottle of Alfa Aesar catalyst was used throughout the entirety of the experiments, and the batch of catalyst that was used contained 62 wt% Ni as well as a surface area of $173 \text{ m}^2 \text{ g}^{-1}$, a pore volume of $0.22 \text{ cm}^3 \text{ g}^{-1}$, and a pore size of 52 Å. This catalyst is hereafter referred to as Alfa Aesar.

RESULTS AND DISCUSSION

Prior to being calcined and reduced, the catalysts in this thesis were inactive. The calcination process converted the metal precursors into their respective metal oxide form upon the addition of oxygen (from air). From there, reduction with hydrogen reduced most (depending on the metal reducibility) of the metal oxide particles into their reduced form (ex. Ni^0 , Pt^0 , Pd^0 , etc.).

After each of the catalyst precursors were synthesized, they were dried overnight in an oven at 100°C . The resulting precursors were crushed and sieved down to 350-212 microns. The samples were calcined in a muffle furnace at 450°C for 4 hours using a heating ramp of $2^\circ\text{C}/\text{min}$. Catalysts were then reduced *in situ* under flowing hydrogen (Matheson, Grade 5) at 400°C for 4 hours using a heating ramp of $2^\circ\text{C}/\text{min}$.

To find the temperature required to calcine the catalysts, TGA was used to determine the temperature at which mass loss was limited. It was important to avoid overheating the samples, which could cause sintering (leading to a lower surface area), even though the calcination temperature used was lower than the Tammann temperature. The temperature at which sintering becomes highly likely for Ni is around 580°C .⁶⁵ The TGA curve for coprecipitated $60\text{Ni}/\text{Al}_2\text{O}_3$ is shown in Figure 19.

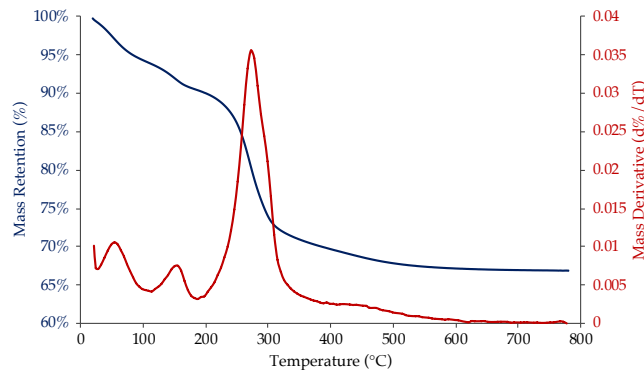


Figure 19. TGA curve of uncalcined 60Ni catalyst.

Figure 19 shows the TGA curve of an oven-dried 60Ni catalyst, which contains a mixture of nickel and aluminum carbonate. As the temperature is increased, the temperature where the nickel and aluminum carbonate species were oxidized to form NiO and Al_2O_3 was evaluated. The heating ramp shows the largest mass loss around 300°C, and by about 400°C, there appears to be minimal mass loss. For this reason, we chose 450°C for catalyst calcination.

Ma *et al.* (2013)⁷¹ showed that bulk NiO catalysts (such as the coprecipitated catalysts synthesized in this study) reduce fully at 370°C, but other studies have shown that higher reduction temperatures were necessary for supported Ni catalysts if there was NiAl_2O_4 spinel present.⁷²⁻⁷⁴ To determine if nickel aluminate was present, the catalyst was analyzed by XRD.

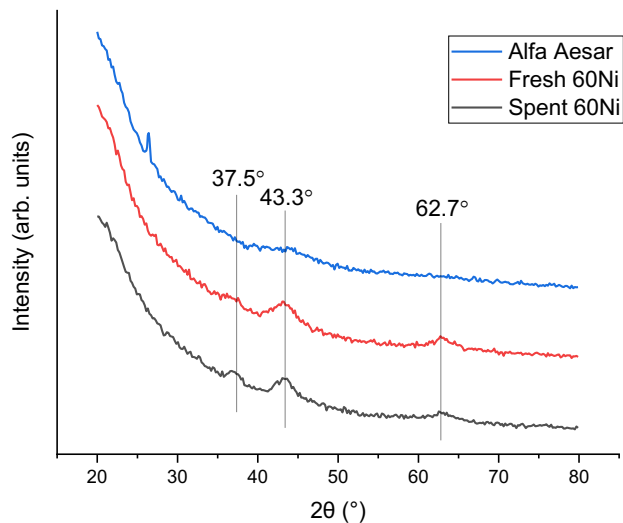


Figure 20. XRD curves for Alfa Aesar catalyst as well as fresh and spent 60Ni catalyst.

Figure 20 presents the XRD spectrum for the Alfa Aesar catalyst along with spectra for fresh and reacted-and-regenerated 60Ni catalysts. The XRD spectra for fresh and used 60Ni display similar peaks, but the peaks appear to be narrower in the fresh sample, indicating smaller crystallite particles. The three main reflections on the coprecipitated 60Ni catalysts at 37.3°, 43.3°, and 62.9° correspond to [1 1 1], [2 0 0], and [2 2 0] NiO planes, not spinel.^{65,75} The Alfa Aesar catalyst has a minor peak at 43.3°, but none of the other peaks for NiO. It also displays a sharp peak at 26.4°, which could be an α -SiO₂ [0 1 1] plane,⁷⁶ because the Alfa Aesar catalyst contains diatomaceous earth, which is comprised mainly of silica. These peaks also had similar relative intensities to the ones reported by Richardson *et al.* (2003). Barrio *et al.* (2003) also noted that after calcining at 450°C, there was limited diffusion of Ni into the support, and therefore there was a low likelihood that spinel-like structures existed, which matched with the results of the XRD curves displayed in Figure 20.⁷⁷

Because the TGA results in Figure 19 showed that almost all of the catalyst mass was lost by 350°C, calcining the samples at 450°C was enough to oxidize essentially all of the metal surface. Although we do

not have temperature programmed reduction (TPR) data for our catalysts, other groups have found that 400°C was enough to reduce nickel if no nickel aluminate spinel was formed.⁷¹ The XRD curve in Figure 20 displayed only peaks for NiO and none for NiAl₂O₄. This meant that all the coprecipitated Ni/Al₂O₃ catalysts were sufficiently reduced to metallic Ni for hydrogenation at 400°C. It has not been determined whether there was spinel formation on the incipient wetness impregnation Ni/Al₂O₃ catalyst or if the other catalysts were fully reduced.

CHAPTER 4

HYDROGENATION OF 2-METHYLNAPHTHALENE IN A TRICKLE BED REACTOR

INTRODUCTION

Polyaromatic molecules, such as those found in TDO oil, have low cetane numbers, due to their high aromatic content. Even after deep hydrogenation, certain combustion characteristics, such as specific volume, hydrogen content, and cetane number may still be below required specifications.^{20,78} One approach to solve these problems is through naphthenic ring opening. An ideal catalytic process would include complete hydrogenation and maximizing ring opening while minimizing cracking reactions (which reduce the molecular weight and cetane number of the products).^{5,44,79} This current work focuses on designing hydrogenation catalysts.

Although there has been plenty of research on monoaromatic compounds, there has been less focused on diaromatic or polyaromatic species. These compounds are more difficult to fully saturate because they require separate hydrogenation steps, and although saturating the first ring is somewhat easy, hydrogenating the second ring is much more difficult.^{30,31} Additionally, substituted diaromatic molecules like 2-methylnaphthalene (2-MN) are even more difficult to hydrogenate than unsubstituted ones, because of the steric hindrance of the methyl group.³⁶ Because 2-MN is the most common molecule present in TDO oil, as Figure 8 shows, we decided to study it as a model compound in our experiments.

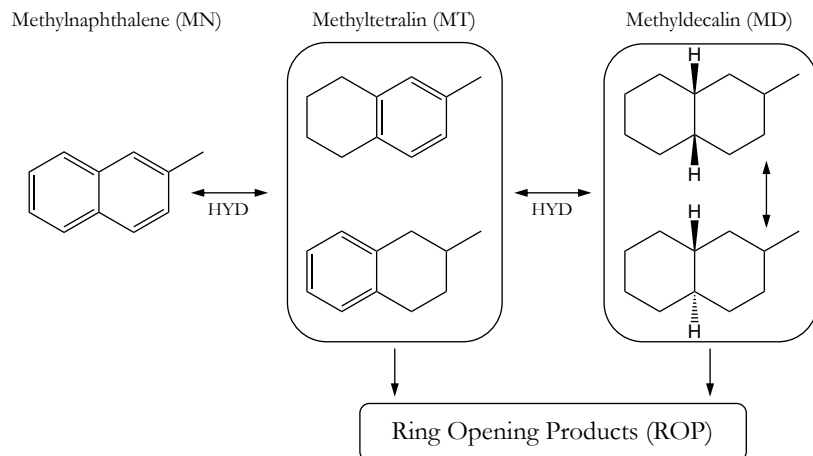


Figure 21. Reaction network for hydrogenation and ring opening of 2-methylnaphthalene.

Figure 21 shows the reaction network for hydrogenation of 2-methylnaphthalene. There are two major products, partially hydrogenated methyltetralins (MT), and fully hydrogenated methyldecalins (MD). There is stereochemistry in MD along the fused carbon-carbon bond as well as at the methyl group position. In this thesis, molecules are either designated as *cis*- or *trans*-MD depending on the central stereocenter (the one shown in Figure 21). Although methyloctalin is also formed as a stable intermediate, other studies have shown that it was only a very minor product.^{29,31,41} Because of resonance stabilization, the hydrogenation of tetralin-like molecules is difficult, and reaction rates for the hydrogenation of naphthalene to tetralin is at least an order of magnitude faster than tetralin to decalin.^{54,60,80} A more complete hydrogenation and ring opening scheme for methylnaphthalene is displayed in Figure 22, which shows reactions possible on both metal and acid sites of a bifunctional catalyst.

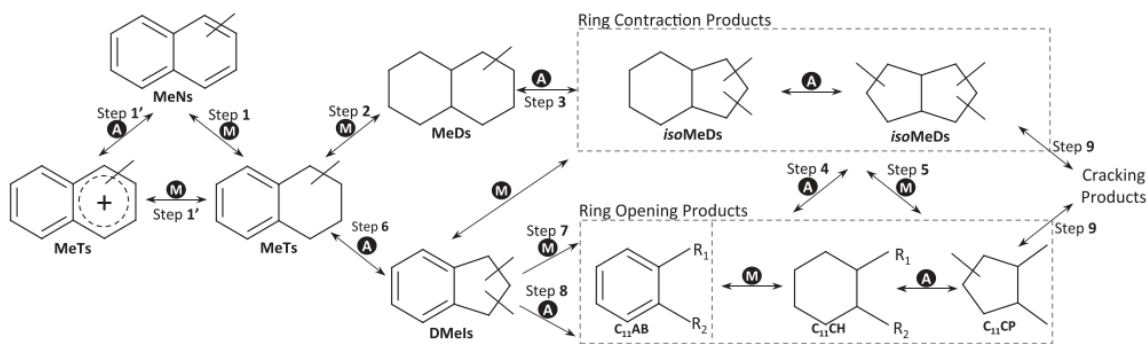


Figure 22. A more complete reaction mechanism for hydroconversion of methyl naphthalene showing hydrogenation, isomerization, ring contraction, and ring opening reactions. Reproduced from Jaroszewska *et al.* (2015).⁴⁷

The *cis*- and *trans*- stereoisomers of decalin have different chemical properties. First, the cetane numbers are different, and *cis*-decalin has a cetane number of 42, whereas the *trans*- form has a value of 32.⁸¹ *Cis*-decalin also has a slightly higher heat of combustion value (38.3 versus 37.2 MJ/m³).^{29,82} But perhaps most importantly, ring opening of *cis*-decalin is much more likely to occur over precious metals than *trans*-decalin.^{5,35} While *cis*-decalin preferentially performs ring opening reactions, *trans*-decalin tends to crack, producing lower molecular weight fragments with lower cetane numbers.⁵ Thus, a goal in designing a hydrogenation catalyst for diesel fuel is to preferentially produce *cis*- isomers. However, *trans*-decalin has a higher thermal stability and inhibits deposition of solid particles in aviation fuel, which makes it the stereoisomer of choice for jet fuel.^{74,83}

Hydrogenation of aromatic molecules can be difficult because they bind strongly to metal and acid sites on a catalyst. This is evidenced by the strong equilibrium constants of molecules with unsaturated rings (atm⁻¹): naphthalene (70), tetralin (50), *trans*-decalin (10), and *cis*-decalin (8).³⁰ Although aromatic molecules bind strongly to the surface, their saturated counterparts desorb quickly from a catalyst. In a study on benzene hydrogenation, van Meerten *et al.* (1976) found that cyclohexane rapidly desorbed from the catalyst surface and formed no inhibition for benzene adsorption.³² Therefore, we do

not believe that decalin will inhibit the catalytic sites, although it has been proposed that the products of tetralin dissociation can lead to catalyst inhibition.³¹

The goal of this project is to first determine the activation energy of 2-MN over various supported Ni catalysts. This work looks to develop catalysts that can effectively hydrogenate 2-MN and to compare the results with a commercial Ni catalyst. The final goal of this project is to determine the *cis/trans* ratio of various catalysts and to design a suitable catalyst that selectively produces *cis*-MD.

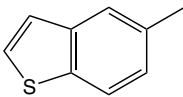
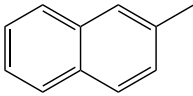
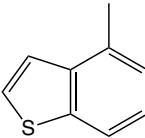
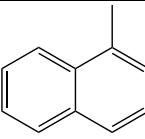
MATERIALS AND METHODS

FEEDSTOCK PURIFICATION

Since most naphthalene and methylnaphthalene reagents are derived from coal tar, they often contain sulfur impurities.²⁹ In the 2-methylnaphthalene (Alfa Aesar, 97%), there were two sulfur impurities (4- and 5-methylbenzothiophene), which correlated to a sulfur concentration of about 25 ppm. Sulfur binds very strongly to metal surfaces and deactivates the sites by poisoning them. To avoid deactivating the catalysts, we removed about 90% of the sulfur from the reactant by recrystallization.

A supersaturated solution of 2-MN was prepared in *n*-decane (Alfa Aesar, 99%) after heating the solution to 80°C. The solution was stirred continuously for 2 hours and was then transferred to an Erlenmeyer flask and was slowly cooled back to room temperature, where crystals of 2-MN slowly formed. The milky-colored crystals were tested on a gas chromatograph-mass spectrometer (GCMS) and were shown to have a dramatic reduction in the sulfur-laden peaks. Crystallization was effective because of the difference in the melting/freezing points of the impurities, which are shown in Table 5.

Table 5. Structure and melting points of 2-MN and impurities.

Compound Name	Structure	Melting/Freezing Point
5-methylbenzothiophene		20.5°C ⁸⁴
2-methylnaphthalene		34.4°C ⁸⁵
4-methylbenzothiophene		N/A
1-methylnaphthalene		-30.4°C ⁸⁶

Because of the differences in melting points that Table 5 shows, if the solution was kept above 25°C, in theory, only the 2-MN would precipitate, whereas the sulfur impurities would remain as a liquid and could easily be separated from the crystallized product. Although the melting/freezing point of the second sulfur impurity was not found in the literature, it was assumed to be below room temperature by comparing the melting points of 2-MN and 1-MN and knowing the β -position relative to the α -position melting point. After recrystallizing the 2-MN, the sulfur concentration was decreased to less than 2 ppm. This purified material was used as reactor feed, which was comprised of 10 wt% 2-MN dissolved in *n*-decane.

CATALYTIC REACTION TESTING

Catalytic studies were carried out in a high-pressure down-flow trickle-bed reactor as depicted in Figure 23. Reactor tubes were made from ¼" or ½" stainless steel tubing depending on the amount of

catalyst used in the study. The reactor tube was loaded with carborundum (Pfaltz & Bauer, 99%), calcined catalyst, and quartz wool to aid in liquid distribution and reduce void volume in the reactor. Catalytic testing was performed at $T = 200 - 350^{\circ}\text{C}$, $P = 1000 \text{ psi}$, $\text{WHSV} = 0.1 - 0.5 \text{ hr}^{-1}$, and $\text{H}_2/2\text{-MN} = 20 - 40$. All samples were taken after the system reached steady state, and the reactor was given time to adjust to new reactor conditions before taking samples.

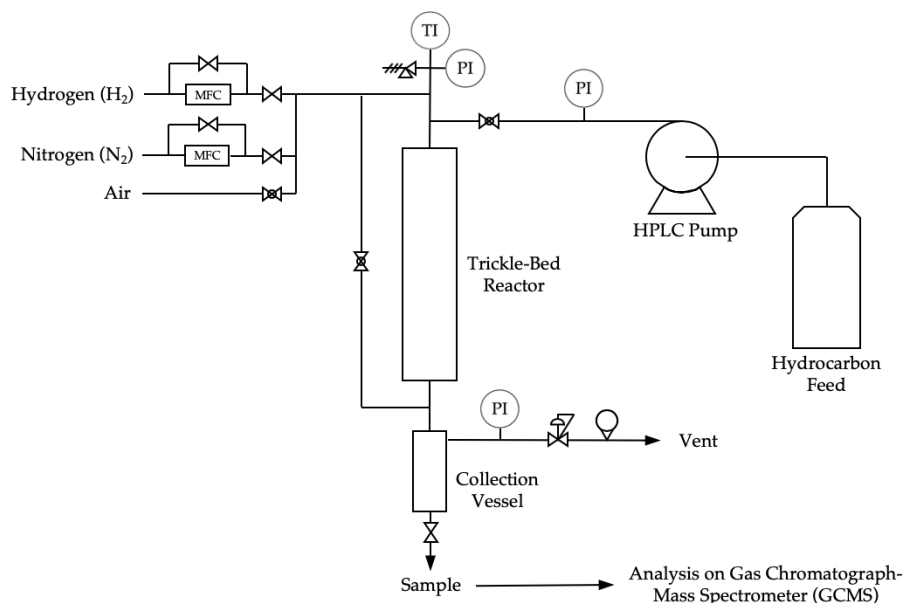


Figure 23. Reactor schematic for hydroprocessing studies.

SAMPLE ANALYSIS

All liquid samples were collected and analyzed on a GCMS (Shimadzu GCMS-QP2010) using a Restek Rxi-5ms column (30 m x 0.25 mmID x 0.25 μm). Biphenyl was used as an internal standard and peaks were identified using the resulting mass spectrum, comparisons with the internal NIST database, and use of the retention indices. Reaction products were grouped into five categories: ROP (ring opening products), MD (methyldecalins), MT (methyltetralins), MN (methylnaphthalenes), and DAP (dealkylated products - decalin and tetralin).

Over the course of each reaction, the steady-state mass balance closed within 98%, so it was assumed that there was minimal cracking of 2-MN or the solvent *n*-decane to light hydrocarbons. Additionally, there was limited isomerization of 2-MN to 1-MN. Conversion of 2-MN was defined as:

$$X = \frac{n_{2MN,in} - n_{2MN,out}}{n_{2MN,in}} \quad (3)$$

where X is the fractional conversion, $n_{2MN,in}$ is the number of moles of 2-MN flowing into the reactor, and $n_{2MN,out}$ is the number of moles of 2-MN collected as products. This conversion was calculated from a decrease in the 2-MN signal on the GCMS. The product selectivity (S_i) and *cis*-MD selectivity (S_{cis}) were defined as:

$$S_i = \frac{n_i}{n_{products}} \quad (4)$$

$$S_{cis} = \frac{n_{MD,cis}}{n_{MD}} \quad (5)$$

where n_i is the number of moles of species i , $n_{products}$ is the number of moles of products collected, $n_{MD,cis}$ is the number of moles of *cis*-MD and n_{MD} is the total number of moles of MD. Although there are two points of stereochemistry in MD, we ignored the stereochemistry of the methyl group because combustion characteristics were much more dependent on the shape of the saturated ring than the axial or equatorial position of the methyl group.²⁹

To verify that the data were reproducible, multiple experiments were conducted for each temperature and catalyst for the activation energy determination. The standard error was calculated for each initial reaction rate, and they were combined to estimate the error for each data point. Duplicate trials were also conducted to determine the *cis*-MD selectivity for each catalyst at 350°C, and the error bars represent the standard error between trials.

RESULTS AND DISCUSSION

DETERMINATION OF 2-MN ACTIVATION ENERGY

The activation energy for the initial hydrogenation of 2-MN was determined for catalysts of various acidities prepared by incipient wetness impregnation. The physical characteristics of the catalysts, such as surface area, are presented in Table 6. (The reference letters displayed in the following tables are used to view the synthesis methods of each catalyst in Appendix A.) The reactor was operated at conditions resulting in conversion less than 10% so that the rate constant and activation energy could be calculated using the amount of catalyst and amount of conversion (a so-called “differential reactor”). Because the catalysts rapidly deactivated over the course of the reaction (probably due to methyltetralin dissociation and inhibition on the catalyst surface),⁹ initial reaction rates were used to estimate catalyst performance. Apparent first-order activation energies (E_a) were estimated by plotting rates at multiple temperatures, T , and determining the slope of

$$\ln k = -\frac{E_a}{R} \left(\frac{1}{T} \right) + \ln A \quad (6)$$

where k is the initial reaction rate, R is the gas constant, and A is the pre-exponential factor. A modified Arrhenius plot is displayed in Figure 24, which shows the initial reaction rate values for each catalyst. Using a rearranged version of the Arrhenius equation, the apparent activation energies are plotted for each catalyst, and the results are displayed in Figure 25.

Table 6. Nitrogen physisorption measurements of incipient wetness impregnation catalysts and a commercial Ni catalyst.

Catalyst	Ref.	S_{ABET} ($\text{m}^2 \text{g}^{-1}$)	V_p ($\text{cm}^3 \text{g}^{-1}$)	d_p (\AA)
Ni/SiO ₂	A	400	0.48	48
Ni/Al ₂ O ₃	B	151	0.32	84
Ni/SiAl	C	308	0.43	56
Ni/ASA	D	218	0.31	68
Alfa Aesar	-	173	0.22	52

Note: Catalysts contain 20 wt% Ni except for Alfa Aesar catalyst (62 wt% Ni).

Note: S_{ABET} , surface area; V_p , pore volume; d_p average pore size.

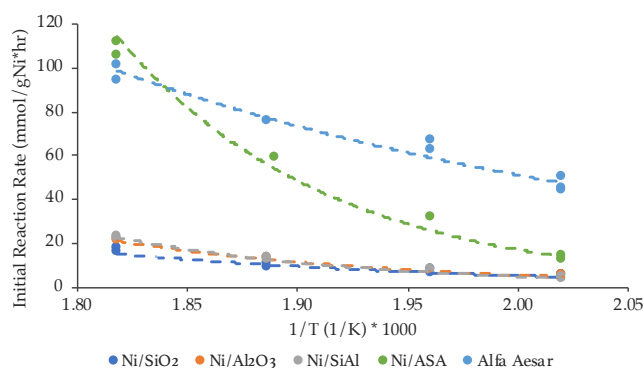


Figure 24. Arrhenius analysis to determine the activation energy of various supported Ni catalysts.

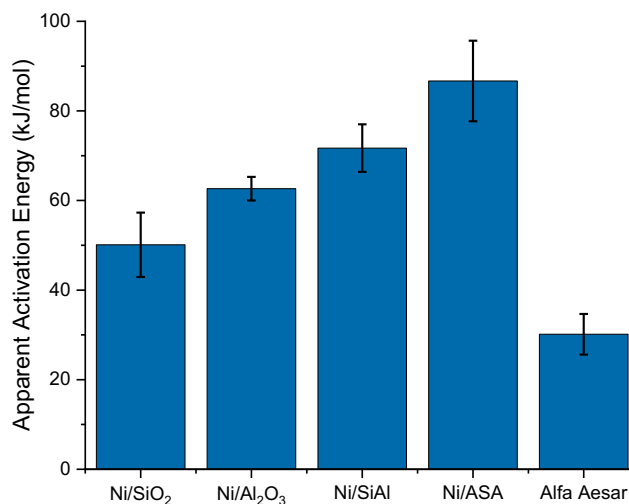


Figure 25. Apparent activation energies of the Ni catalysts in Figure 24.

Figure 25 shows an interesting trend for the activation energy; the activation energy was lowest for the Alfa Aesar catalyst and highest for the amorphous silica-alumina (ASA) catalyst. For the catalysts we synthesized, it appeared that the activation energy increased as the surface acidity increased. It is widely accepted that strength of acid sites follows the trend $\text{SiO}_2 < \text{Al}_2\text{O}_3 < \text{ASA}$. We found that this trend was similar to the activation energy, as the catalyst with the fewest and weakest strength acid sites (Ni/SiO_2) showed the lowest activation energy, whereas the catalyst with strongest acid sites (Ni/ASA) showed the highest activation energy. At very low conversions, the major products formed from 2-MN were 2-MT and 6-MT, partially hydrogenated products that can be produced from acid-assisted metal sites on a catalyst.^{44,47,87} Given our results, we believe that the acid-assisted hydrogenation reaction must have a higher energy barrier than a reaction solely on a metal site, which would be the reaction that occurs on a neutral support. However, when Lin and Vannice (1993) studied benzene hydrogenation with supported catalysts, they found the activation energy was independent of the support acidity.³³ Despite impregnating platinum on SiO_2 , Al_2O_3 , TiO_2 , and ASA, each of the activation energy values were similar (42 – 54 kJ/mol). The difference in activation energy between supported platinum and supported nickel catalysts could be explained because of different mechanisms or the difference in model compounds. However, more studies would need to be conducted to elucidate this difference.

One trend that we do not understand from Figure 25 is why the activation energy of Ni/SiAl (a physical mixture of silica and alumina – not to be confused with ASA) was higher than the trends for $\text{Ni}/\text{Al}_2\text{O}_3$ and Ni/SiO_2 . There is a very small chance this could be an anomaly, since the lower error bars of Ni/SiAl are close to the upper error bars of $\text{Ni}/\text{Al}_2\text{O}_3$. Otherwise, there is little evidence that explains why a physical mixture of two supports would have a value that is not between each of the individual

components. Future experiments could focus on titrating the catalysts or doing pyridine adsorption to determine the strength and number of Brønsted and Lewis acid sites on the Ni/SiAl catalyst and comparing that to the acid sites found on Ni/Al₂O₃ and Ni/SiO₂.

HYDROGENATION OVER COPRECIPITATED CATALYSTS

We hypothesized that the catalysts prepared by incipient wetness impregnation possessed low initial reaction rates and deactivated quickly because they possessed a limited number of metallic sites and were quickly deactivated by coking. Monometallic Ni/Al₂O₃ and Co/Al₂O₃ catalysts as well as bimetallic catalysts were used in this initial study. The monometallic catalysts were comprised of 60 wt% metal (60Ni or 60Co), whereas the bimetallic catalysts contained 60 wt% Ni with 4 wt% of another metal (NiM where M is second metal identity). The *cis/trans*-methyldecalin (MD) selectivities of some of the catalysts are displayed in Table 7.

Table 7. *Cis/trans*-MD selectivity of various monometallic and bimetallic coprecipitated catalysts.

Catalyst	Ref.	<i>cis</i> -MD Selectivity (%)			
		200°C	250°C	300°C	350°C
60Ni	E	77	61	15	13
60Co	F	<i>n.t.</i>	69	63	<i>n.d.</i>
NiCr	G	81	68	34	25
NiMn	H	53	38	16	12
NiFe	I	69	63	36	4
NiCo	J	58	42	40	42
NiCu	K	46	38	12	11
NiZn	L	58	48	41	<i>n.d.</i>

Note: *n.d.*, not detected; *n.t.* not tested.

The results in Table 7 show a variety of selectivities for monometallic and bimetallic catalysts that were synthesized at 25°C. It is important to note that the selectivities from Table 7 were only measured once, so these trials were not duplicated. One significant trend is that the *cis/trans* selectivity decreases as the temperature increases, meaning that more *trans*-MD is formed at higher temperatures. This trend was observed for most catalysts, and some catalysts gave a wide variety of selectivities as a function of temperature (NiCr, NiFe), whereas other ratios remained relatively similar (NiCo).

While most of the catalysts had a lower *cis/trans* ratio than 60Ni (the catalyst to compare to), there were two metals that might have a synergistic effect with Ni for hydrogenating 2-MN. The NiCr and NiFe both appeared to show good selectivity towards *cis*-MD and might be potential promoters to a Ni catalyst. One catalyst that produced mostly *trans*-MD at all temperatures was CuNi. Copper is known for having a low hydrogenation activity, and when alloyed with Pd, it was found to be a bad promoter metal for naphthalene hydrogenation.⁵⁵ We are unsure if the metals in each of the catalysts were alloyed together or had no interactions, but it is possible that we formed alloys because we coprecipitated the metals.⁸⁸

Although the previous catalysts were only prepared using 60 wt% Ni (and some with a bimetallic mixture), we were interested in evaluating the effect that changing the amount of metal on the catalyst had on the physisorption properties as well as the selectivity. Monometallic Ni catalysts were synthesized with Ni contents between 20 wt% (20Ni) and 100 wt% Ni (100Ni). These catalysts were synthesized at 25°C, and physisorption measurements of each catalyst is displayed in Table 8.

Table 8. Nitrogen physisorption measurements of coprecipitated Ni catalysts synthesized at 25°C.

Catalyst	Ref.	SA _{BET} (m ² g ⁻¹)	V _p (cm ³ g ⁻¹)	d _p (Å)
20Ni	M	142	0.49	139
40Ni	N	114	0.26	90
60Ni	E	88	0.24	108
80Ni	O	68	0.21	124
100Ni	P	30	0.11	145

The catalysts from Table 8 show a decrease in surface area as the Ni content increases. This is expected, since alumina is typically added to catalysts to increase the surface area, although most metals (at low loadings) are impregnated on γ -Al₂O₃, not precipitated with it.

During the catalyst synthesis, we discovered that heating the metal and carbonate solutions as they were added together enhanced the surface area and pore volume of the catalysts. (Detailed synthesis methods are found in Appendix A.) Instead of stirring the solution at room temperature (25°C), stirring it near the boiling point of water (~90°C) changed the catalyst characteristics (despite everything else remaining the same). Physisorption measurements of the 90°C coprecipitated catalysts are displayed in Table 9. The results show that there was a huge difference in the surface area and pore volume of the catalysts as the Ni content was varied, and a comparison of the surface area and pore volume of the catalysts from Table 8 and Table 9 are displayed in Figure 26.

Table 9. Nitrogen physisorption measurements of coprecipitated Ni catalysts synthesized at 90°C.

Catalyst	Ref.	SA _{BET} (m ² g ⁻¹)	V _p (cm ³ g ⁻¹)	d _p (Å)
Alumina	Q	80	0.50	248
20Ni	R	401	1.18	118
40Ni	S	331	1.12	107
60Ni	T	258	0.96	149
80Ni	U	100	0.29	165
100Ni	V	39	0.22	227
Alfa Aesar	-	173	0.22	52
60Ni ^a	-	199	0.85	171

^a Catalyst after reaction and regeneration.

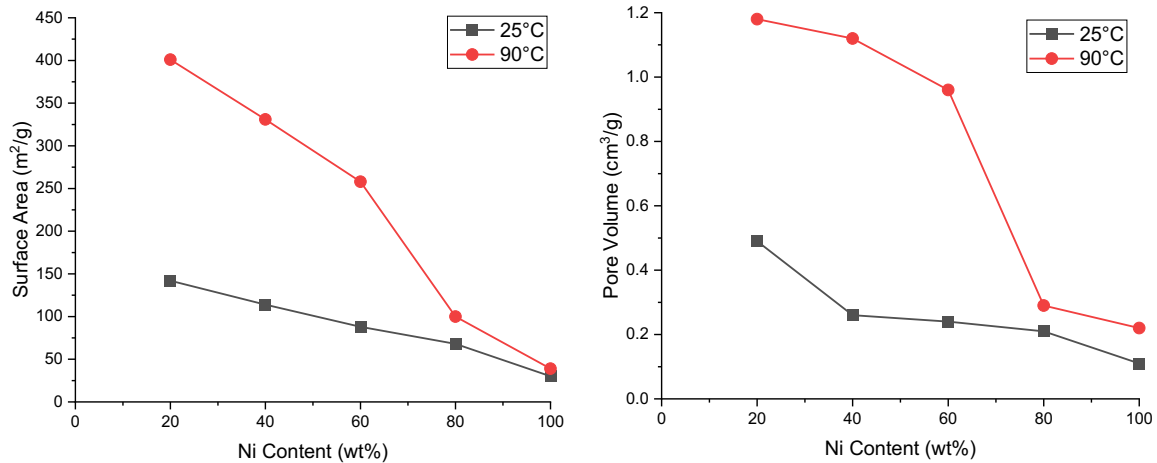


Figure 26. BET surface area and pore volume measurements of coprecipitated Ni/Al₂O₃ catalysts at various Ni content.

Also of interest in these graphs was that at high Ni content, the characteristics between the methods were fairly similar, but below 80% Ni, the properties diverge, and seem to further deviate as the Ni content decreases. One possible explanation for this is because the extra heat allowed the Ni and Al

species to migrate, creating a more complex framework. This could show why there is little deviations at high Ni loadings, because there is not a sufficient amount of alumina for the Ni species to migrate into.

Another important point is the difference between the 20Ni and 0Ni (alumina) shown in Table 9. The 20Ni catalyst had a surface area of $401 \text{ m}^2 \text{ g}^{-1}$ and a pore volume of $1.18 \text{ cm}^3 \text{ g}^{-1}$, but the 0Ni catalyst only had a surface area of $80 \text{ m}^2 \text{ g}^{-1}$ and a pore volume of $0.50 \text{ cm}^3 \text{ g}^{-1}$. That was a dramatic difference between the two catalysts, although it was not surprising that the 0Ni catalyst had a low surface area. Since there was no special preparation, we believe that we synthesized amorphous alumina, which is known to have a lower surface area than other alumina species. But nonetheless, the difference that the incorporation of 20 wt% Ni had was surprisingly large, and this difference was probably due to the incorporation of Ni into the alumina framework, which has been reported elsewhere to increase the surface area.⁶⁹

Over the course of a reaction, the catalyst is inhibited by aromatic adsorption and some catalyst sites are poisoned by the sulfur in the feedstock. To remove the deposited coke on the catalyst, the spent material was heated using the same calcination ramp as preparing catalysts (*i.e.*, heating to 450°C for 4 hours using a ramp of $2^\circ\text{C}/\text{min}$). However, the poisoned sites on the catalyst were not able to be regenerated, and over the course of the reaction, some pore closing and other mechanical deactivation occurred, which all would lead to inferior physisorption measurements than fresh catalyst.

Interestingly enough, the regenerated 60Ni catalyst only showed a decrease in surface area by about 25%, while the pore volume and pore size were only slightly changed from their original values. This is consistent with the small difference between the XRD data for fresh and spent 60Ni catalysts in Figure 20, indicating that most of the crystalline structure was retained after regenerating the spent catalyst.

Although the surface areas of the catalysts differ with the synthesis method, the selectivities were similar except for the 100Ni catalyst, and Table 10 compares conversion and selectivity data of the two highest Ni loading catalysts at two different reaction temperatures.

Table 10. Conversion and selectivity of 80Ni and 100Ni catalysts (both synthesized at 90°C).

Catalyst	Temp. (K)	Conv. (%)	Product Selectivity (%)				
			ROP	MD	MT	MN	DAP
80Ni	473	99.9	1.6	66.5	31.3	0.1	0.4
	623	97.7	6.3	68.4	6.3	2.3	16.4
100Ni	473	0.6	<i>n.d.</i>	<i>n.d.</i>	0.6	99.4	<i>n.d.</i>
	623	21.3	<i>n.d.</i>	<i>n.d.</i>	21.3	78.7	<i>n.d.</i>

Reaction conditions: P = 6.9 MPa, WHSV = 0.2 hr⁻¹, H₂/2-MN = 20.

Note: ROP (ring opening products), MD (methyldecalin), MT (methyltetralin), MN (methylnaphthalene), DAP (dealkylated products), *n.d.*, not detected.

Table 10 shows the conversion and selectivity data for 80Ni and 100Ni catalysts (both synthesized at 90°C). There was a dramatic difference in the conversion and selectivity of each of these catalysts despite identical reaction conditions. The 80Ni catalyst showed selectivity towards fully hydrogenated products at both temperatures listed, but the 100Ni catalyst barely had any conversion. And when it did have slight conversion at the higher temperature, it only formed methyltetralins, the initial hydrogenation step over the catalyst.

This difference in reactivity could be explained by the surface area of each catalyst, but as Table 9 shows, the difference in surface area between the two catalysts is not dramatic. Instead, we believe that the difference in reactivity is caused by the hydrogenation process. We believe that acid-assisted hydrogenation (found on 80Ni) is easier to perform than hydrogenation on solely a metal site (found on 100Ni). This difference in reactivity was explained by Lin and Vannice (1993), who showed the reaction

included aromatics adsorbing on acid sites near a metal-acid interface and reacting with spillover hydrogen atoms from Ni particles.³³

Although the conversion and selectivity data for the catalysts 20Ni, 40Ni, and 60Ni were very similar to 80Ni (and are thus not displayed in Table 10 for brevity), there was a slight deviation in their *cis/trans* ratio. In Figure 27, the *cis*-MD selectivity of the different catalysts at 6.9 MPa is shown at various reaction temperatures.

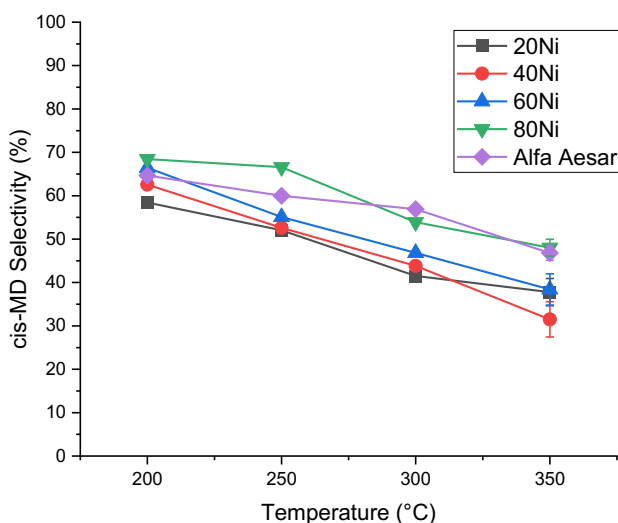


Figure 27. *Cis*-MD selectivity of coprecipitated Ni catalysts and a commercial Ni catalyst.

Figure 27 shows the *cis*-MD selectivity of the products that were formed on different catalysts. The graph appears to show that the ratio is slightly dependent on the amount of Ni in the catalyst, but the reaction temperature appears to be more important. This result has been verified by Huang and Kang (1996) as well as Rautanen *et al.* (2001), who showed that the *cis/trans* ratio was dependent on the catalyst activity and slightly dependent on the reaction temperature.^{41,59} Our results also show that the Alfa Aesar catalyst has a similar *cis*-MD selectivity as most of the coprecipitated catalysts designed in this

thesis. Given the similar selectivity and Ni content between the 60Ni and Alfa Aesar catalyst (62 wt% Ni), we analyzed samples on a TEM to look at their nanostructures, which are displayed in Figure 28.

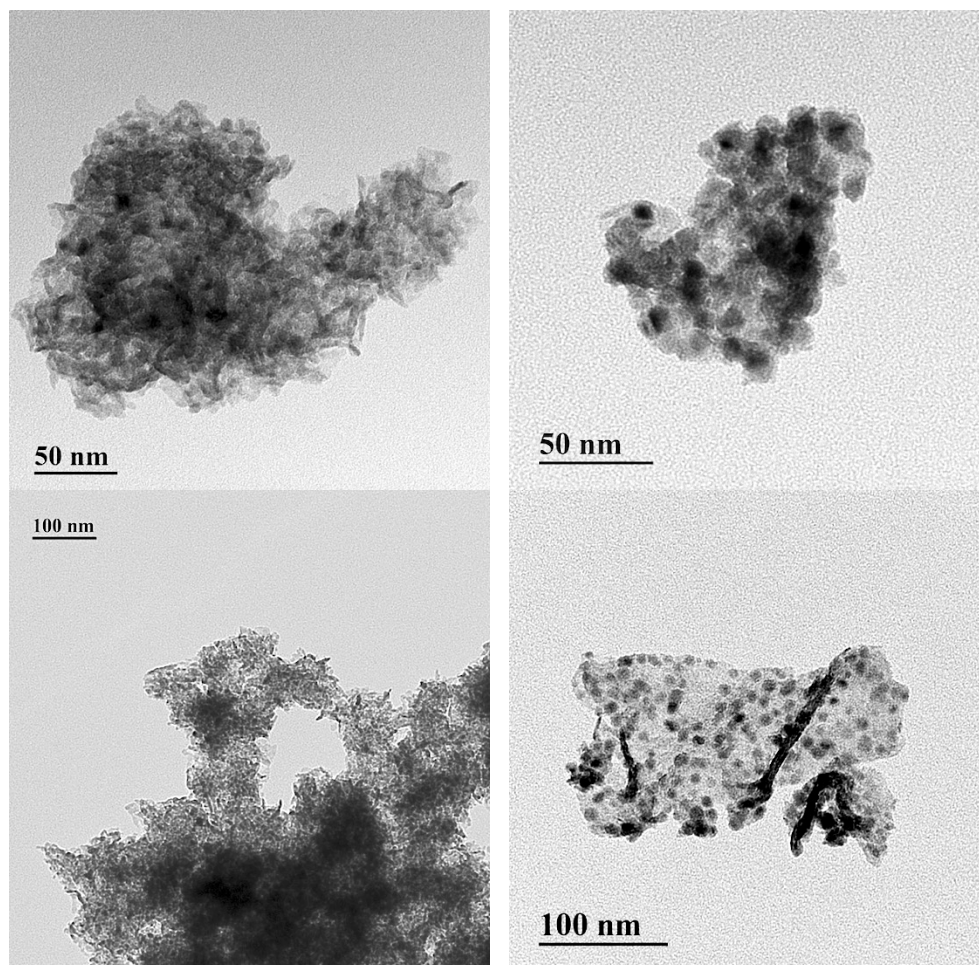


Figure 28. TEM images of coprecipitated 60Ni catalyst (left) and Alfa Aesar commercial Ni catalyst (right).

The TEM micrographs in Figure 28 show many differences between the materials. The coprecipitated 60Ni catalyst on the left shows the presence of rod-like structures covering the entirety of the catalyst. These are in sharp contrast to the nodule-like structures shown on the right for the commercial Alfa Aesar catalyst.

These different structures probably account for the difference in physisorption characteristics from Table 9. The 60Ni catalyst had a BET surface area of $258 \text{ m}^2 \text{ g}^{-1}$, a pore volume of $0.96 \text{ cm}^3 \text{ g}^{-1}$, and an

average pore size of 149 Å, compared to the commercial catalyst, which had a surface area of 173 m² g⁻¹, a pore volume of 0.22 cm³ g⁻¹, and a pore size of 52 Å. The larger pore size makes the 60Ni catalyst more ideal for hydrogenating large polyaromatic molecules, like those found in TDO oil. Additionally, the much larger pore volume makes the 60Ni catalyst ideal for the impregnation of another metal onto the catalyst.

HYDROGENATION OVER IMPREGNATED COPRECIPITATION CATALYSTS

To enhance the *cis*-MD selectivity of the catalysts, we incorporated 1 wt% of several precious metals onto a 60Ni catalyst using incipient wetness impregnation. We assumed that the catalysts had comparable physisorption properties as the 60Ni sample in Table 9 because only a small amount of metal was incorporated onto the surface, which would make a marginal change in the surface area and pore volume. The *cis*-MD selectivity was tested for each bimetallic catalyst at 6.9 MPa, and the results are displayed in Figure 29.

Table 11. Reference letters of each catalyst catalogued in Appendix A.

Catalyst	Ref.
PdNi	W
PtNi	X
IrNi	Y
RuNi	Z

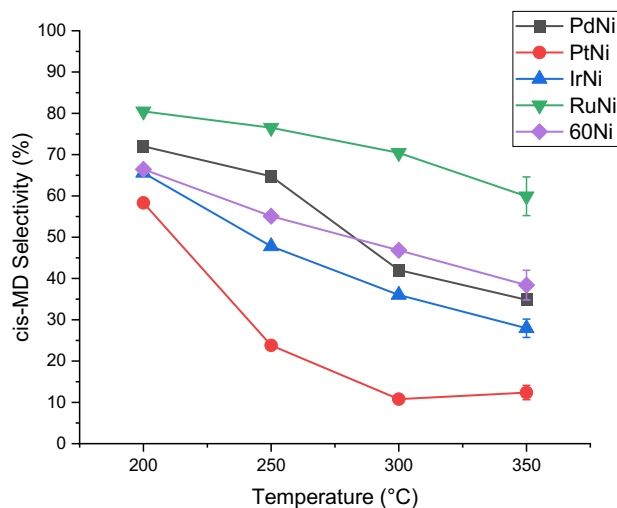


Figure 29. *Cis*-MD selectivity of various bimetallic coprecipitated Ni catalysts. For comparison purposes, the selectivity of monometallic 60Ni is displayed.

Figure 29 shows that the impregnation of a second metal onto the catalyst pores dramatically changed the *cis*-MD selectivity. The catalyst containing platinum (PtNi) produced more *trans*-MD, but the catalyst containing ruthenium (RuNi) increased the formation of *cis*-MD. The catalysts containing palladium (PdNi) and iridium (IrNi) had similar selectivities as the monometallic 60Ni catalyst. These results show that the incorporation of a precious metal onto the catalyst surface can noticeably shift the *cis/trans* ratio towards the stereoisomer of preference.

To our knowledge, there have not been any studies of bimetallic Ni catalysts that analyzed the stereochemistry of the product decalin species. However, there have been studies on monometallic Pt that showed a tendency to produce *trans*- stereoisomers. Huang and Kang (1996) studied naphthalene hydrogenation and Jaroszewska *et al.* (2013) studied 1-methylnaphthalene hydrogenation over Pt catalysts, and each showed that *trans*- isomers were selectively produced.^{59,89} Unfortunately, there is very limited literature on hydrogenation of naphthalene or tetralin with Ru-based catalysts, so we are unsure if this *cis*- selectivity should have been expected or not.

In a review of naphthalene hydrogenation, Weitkamp (1968) proposed a series of steps for the hydrogenation of tetralin to the *cis*- and *trans*- forms of decalin, which is shown in Figure 30.²⁹ Ignoring the presence of hexalin (hexahydronaphthalene), which is extremely unstable and has not been reported in almost any study, tetralin is hydrogenated through one of the octalins to produce decalin. The $\Delta^{9,10}$ -octalin intermediate is more thermodynamically favorable, and only reacts to form *cis*-decalin. That is contrary to $\Delta^{1,9}$ -octalin, which can be hydrogenated to form both *cis*- and *trans*-decalin, although *trans*-decalin is more thermodynamically stable.

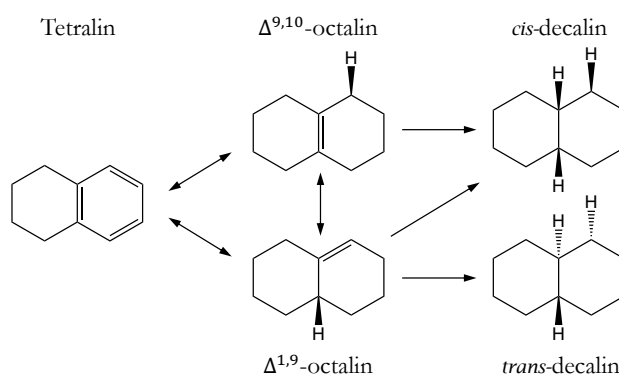


Figure 30. Possible reaction network for hydrogenation of tetralin through an octalin intermediate proposed by Weitkamp (1968).²⁹ (Chirality of hydrogen atom at 1-position is meant for illustrative purposes to show addition of hydrogen, not stereochemistry.)

Weitkamp also went one step further and showed that Ru catalysts on a variety of supports produced large amounts of $\Delta^{9,10}$ -octalin, much higher than Ir, Pd, and Pt catalysts.²⁹ In the present study, we found that at low temperatures, the RuNi catalyst produced $\Delta^{9,10}$ -methyloctalin almost 20-fold more than $\Delta^{1,9}$ -methyloctalin. Because the RuNi catalyst produced the thermodynamically favorable methyloctalin intermediate, it is likely that that initial hydrogenation of tetralin is fast compared to the hydrogenation of methyloctalin. Therefore, the thermodynamically favorable $\Delta^{9,10}$ -methyloctalin species accumulated because the final hydrogenation step was slower. And because $\Delta^{9,10}$ -methyloctalin can only

be hydrogenated to form *cis*-MD, this is a plausible reason that the RuNi catalyst selectively produced *cis*-MD.

On the other hand, the PtNi catalyst produced almost no methyloctalin intermediate, and the ratio between the $\Delta^{9,10}$ - and $\Delta^{1,9}$ -methyloctalin isomers was almost unity. This likely means that there was no accumulation of methyloctalin, because there was no buildup of $\Delta^{9,10}$ -methyloctalin. Additionally, it has been demonstrated that the hydrogenation rate of $\Delta^{1,9}$ -octalin on Pt is 25 times faster than the $\Delta^{9,10}$ -octalin form.⁹⁰ This means that the methyloctalin intermediate reacted to form a MD species before it had time to equilibrate to $\Delta^{9,10}$ -methyloctalin. And Weitkamp also noticed that $\Delta^{1,9}$ -methyloctalin produced a mixture of *cis*- and *trans*-MD, but much more of the latter.²⁹ We believe that the rapid hydrogenation of methyloctalin combined with a lack of $\Delta^{9,10}$ -methyloctalin buildup is the reason that the PtNi catalyst selectively produced *trans*-MD.

CHAPTER 5

CONCLUSIONS AND RECOMMENDATIONS

CONCLUSIONS

One of the biggest issues preventing the use of TDO oil as a blending agent in diesel fuel is the low cetane number that TDO oil possesses. Although there have been attempts to hydrogenate TDO oil using a commercial nickel catalyst,²¹ the cetane number was still below the required specifications. This present work developed catalysts to efficiently hydrogenate TDO oil to increase the cetane number. A laboratory-scale trickle bed reactor was used to perform hydrogenation reactions, and 2-methylnaphthalene was chosen as a model compound because of its presence in TDO oil as well as the difficulty in fully saturating diaromatic molecules. Using the conversion and product selectivities, catalysts were chosen that yielded desired molecules and stereoisomers.

This research began by analyzing the activation energies of impregnated nickel catalysts. The results showed that catalysts with Brønsted acid supports had the highest apparent activation energy, while catalysts with almost no acid sites had lower energy barriers. We attributed this to different reaction mechanisms, as monofunctional (only metal sites) catalysts had a lower energy barrier for hydrogenating the model compound than acid-assisted bifunctional (metal and acid sites) catalysts. However, the commercial Alfa Aesar catalyst had a lower activation energy than all the impregnated catalysts we synthesized, and our catalysts were rapidly deactivated from coke deposition. To resolve these issues, we produced coprecipitated catalysts, which contained larger amounts of nickel. The catalysts had higher initial reaction rates and maintained their selectivity for longer periods than the impregnated catalysts.

The coprecipitated catalysts contained varying amounts of nickel, and it was found that adjusting the mixing temperature of the solution from 25°C to 90°C dramatically enhanced the surface area and

pore volume of the resulting catalysts. These improved coprecipitated catalysts showed promise for producing *cis*- isomers (the desired stereoisomer) at low temperatures, but while hydrogenating at high temperatures, mostly *trans*- molecules were formed. The amount of nickel was found to be slightly important to the stereoisomerism of the product, and catalysts synthesized with more nickel tended to produce more *cis*- isomers. A coprecipitated and commercial catalyst were examined using TEM, and they were shown to possess different structures, although their product selectivities were similar.

Some coprecipitated catalysts were impregnated with a precious metal to further enhance the stereoselectivity. Although the impregnation of either palladium or iridium to nickel catalysts did not significantly change the selectivity, incorporation of two other metals did change the product distribution. It was found that adding platinum to a nickel (PtNi) catalyst dramatically increased the amount of *trans*- isomers, while adding ruthenium to the nickel (RuNi) catalyst pushed selectivity towards *cis*- molecules. We hypothesized that this difference in selectivity was caused by the methyloctalin intermediate that dictated which final stereoisomer would be favored.

The results of this research are important for designing hydrogenation catalysts that can be used to hydrogenate TDO oil. Using the results of this study, the catalyst best suited for producing diesel fuel was the ruthenium-nickel catalyst (Ref. Z) because it produced fully saturated products with desired *cis*- stereochemistry. Thus, this catalyst would likely hydrogenate the molecules from TDO oil with the highest cetane numbers.

RECOMMENDATIONS FOR FUTURE STUDIES

In this study, we posed several questions that could be evaluated in future studies. Firstly, finding an explanation for the different activation energy of Ni/SiAl would be noteworthy, which could involve testing the acid sites using pyridine adsorption to determine the number and strength of Lewis and

Brønsted acid sites of that catalyst compared with Ni/SiO₂, Ni/Al₂O₃, and Ni/ASA. Temperature programmed reduction (TPR) could also be performed on the catalysts to ensure that the nickel catalysts were fully reduced at 400°C before being used for hydrogenation.

Additionally, further TEM studies could be conducted to compare the coprecipitated catalysts synthesized at 25°C and 90°C. Because of the large difference in surface area and pore volume at the different temperatures, we believe the TEM micrographs would look very different from each other. This could provide insight into the surface area enhancement and explain why the increased temperature produced better catalyst characteristics. Further TEM studies with energy-dispersive X-ray analysis (EDX) could also be used to determine the Ni and Al concentration of the rod-like and nodule-like structures in the 60Ni and Alfa Aesar catalysts displayed in Figure 28.

Most of the reactions in this thesis were operated at a 20:1 hydrogen to 2-methylnaphthalene (2-MN) molar ratio, which is four times the amount of hydrogen required to fully saturate 2-MN (which requires 5 H₂). This ratio could be adjusted to minimize the hydrogen flow rate while getting the required aromatic saturation. Additionally, these reactions were performed solely at 1000 psi, and studying the effect of pressure on these reactions could prove important. Optimizing both parameters would be crucial to minimize reagent costs because hydrogen is expensive, and aromatic saturation requires a substantial amount of it.

Future experiments could also be performed using TDO oil as the feedstock for this reaction to evaluate its feasibility. Using the most promising catalysts, the hydrogenation could take place in a ¾" trickle bed reactor to hydrogenate about 1 L of material. If successful, the catalyst could be used in a larger reactor to produce a larger amount of fuel, like 20 L. At that point, it would be important to investigate the cost of preparing the catalysts for scaling-up. Fortunately, the catalysts designed in these experiments

were produced with nickel, which is much cheaper than some other precious metals. The cost of producing the catalysts and the expected catalyst lifetime would also need to be accounted for if the TDO oil upgrading process is performed at a larger scale.

Even with the best catalyst produced in this experiment, the cetane number of hydrogenated TDO oil would likely still be below specifications. We believe that the best process to further increase the cetane number is through selective ring opening of naphthenic molecules. If a ring opening catalyst could be developed that converted cycloparaffins into linear or mildly branched paraffins, then the fuel might meet the cetane number requirements. For this reason, we believe that the TDO oil upgrading steps will require a dual-reactor setup, consisting of a hydrogenation catalyst followed by a ring-opening catalyst. If successful, this process would be able to produce renewable diesel fuel and would help reduce our reliance on fossil fuels.

REFERENCES

- (1) U.S. Energy Information Administration. *Annual Energy Outlook 2020*; Washington, DC, 2020.
- (2) ExxonMobil. *Exxon Mobil 2019 Outlook for Energy: A Perspective to 2040*; 2019. <https://doi.org/10.1017/CBO9781107415324.004>.
- (3) Sivena, A. Hydrocracking Reaction Pathways of 1-Methylnaphthalene in a Continuous Fixed-Bed Reactor, Imperial College London, 2015.
- (4) Speight, J. G. *The Chemistry and Technology of Petroleum*, 4th ed.; CRC Press, 2007.
- (5) Du, H.; Fairbridge, C.; Yang, H.; Ring, Z. The Chemistry of Selective Ring-Opening Catalysts. *Appl. Catal. A Gen.* **2005**, *294* (1), 1–21. <https://doi.org/10.1016/j.apcata.2005.06.033>.
- (6) Arias, P. L.; Cambra, J. F.; Güemez, B.; Barrio, V. L.; Navarro, R.; Pawelec, B.; Fierro, J. L. G. Methyl-Naphthalene Hydrogenation on Pt/HY-Al₂O₃ Catalysts. An Approach to Hydrogenation of Polyaromatic Hydrocarbon Mixtures. *Fuel Process. Technol.* **2000**, *64* (1), 117–133. [https://doi.org/10.1016/S0378-3820\(99\)00125-3](https://doi.org/10.1016/S0378-3820(99)00125-3).
- (7) Glotov, A.; Stytsenko, V.; Artemova, M.; Kotelev, M.; Ivanov, E.; Gushchin, P.; Vinokurov, V. Hydroconversion of Aromatic Hydrocarbons over Bimetallic Catalysts. *Catalysts* **2019**, *9* (4). <https://doi.org/10.3390/catal9040384>.
- (8) Choi, Y.; Lee, J.; Shin, J.; Lee, S.; Kim, D.; Lee, J. K. Selective Hydroconversion of Naphthalenes into Light Alkyl-Aromatic Hydrocarbons. *Appl. Catal. A Gen.* **2015**, *492*, 140–150. <https://doi.org/10.1016/j.apcata.2014.12.001>.
- (9) Ding, L.; Zheng, Y.; Zhang, Z.; Ring, Z.; Chen, J. HDS, HDN, HDA, and Hydrocracking of Model Compounds over Mo-Ni Catalysts with Various Acidities. *Appl. Catal. A Gen.* **2007**, *319*, 25–37. <https://doi.org/10.1016/j.apcata.2006.11.016>.
- (10) Laredo, G. C.; Vega Merino, P. M.; Hernández, P. S. Light Cycle Oil Upgrading to High Quality Fuels and Petrochemicals: A Review. *Ind. Eng. Chem. Res.* **2018**, *57* (22), 7315–7321. <https://doi.org/10.1021/acs.iecr.8b00248>.
- (11) Mosio-Mosiewski, J.; Morawski, I. Study on Single-Stage Hydrocracking of Vacuum Residue in the Suspension of Ni-Mo Catalyst. *Appl. Catal. A Gen.* **2005**, *283* (1–2), 147–155. <https://doi.org/10.1016/j.apcata.2005.01.001>.
- (12) *Controls and Prohibitions on Diesel Fuel Quality*; United States Congress, 2001.
- (13) Schulz, H.; Böhringer, W.; Ousmanov, F.; Waller, P. Refractory Sulfur Compounds in Gas Oils. *Fuel Process. Technol.* **1999**, *61* (1), 5–41. [https://doi.org/10.1016/S0378-3820\(99\)00028-4](https://doi.org/10.1016/S0378-3820(99)00028-4).

- (14) Azizi, N.; Ali, S. A.; Alhooshani, K.; Kim, T.; Lee, Y.; Park, J. II; Miyawaki, J.; Yoon, S. H.; Mochida, I. Hydrotreating of Light Cycle Oil over NiMo and CoMo Catalysts with Different Supports. *Fuel Process. Technol.* **2013**, *109*, 172–178. <https://doi.org/10.1016/j.fuproc.2012.11.001>.
- (15) Moreau, C.; Aubert, C.; Durand, R.; Zmimita, N.; Geneste, P. Structure-Activity Relationships in Hydroprocessing of Aromatic and Heteroaromatic Model Compounds over Sulphided NiO-MoO₃/ γ -Al₂O₃ and NiO-WO₃/ γ -Al₂O₃ Catalysts; Chemical Evidence for the Existence of Two Types of Catalytic Sites. *Catal. Today* **1988**, *4* (1), 117–131. [https://doi.org/10.1016/0920-5861\(88\)87049-4](https://doi.org/10.1016/0920-5861(88)87049-4).
- (16) Rédey, Á.; Nasser, H.; Golubeva, I. Alternative Sources for Biomass Energy. In *The International Conference on Renewable Energy, Damascus, Syria*; 2011.
- (17) Do, P. T. M.; Crossley, S.; Santikunaporn, M.; Resasco, D. E. Catalytic Strategies for Improving Specific Fuel Properties. *Catalysis* **2008**, No. 405, 33–64. <https://doi.org/10.1039/b602366p>.
- (18) Santana, R. C.; Do, P. T.; Santikunaporn, M.; Alvarez, W. E.; Taylor, J. D.; Sughrue, E. L.; Resasco, D. E. Evaluation of Different Reaction Strategies for the Improvement of Cetane Number in Diesel Fuels. *Fuel* **2006**, *85* (5–6), 643–656. <https://doi.org/10.1016/j.fuel.2005.08.028>.
- (19) *Standards for Motor Vehicle Fuels*; California Air Resources Board: California, 2014.
- (20) Cooper, B. H.; Donniss, B. B. L. Aromatic Saturation of Distillates: An Overview. *Appl. Catal. A Gen.* **1996**, *137* (2), 203–223. [https://doi.org/10.1016/0926-860X\(95\)00258-8](https://doi.org/10.1016/0926-860X(95)00258-8).
- (21) Eaton, S. J.; Beis, S. H.; Karunarathne, S. A.; Pendse, H. P.; Wheeler, M. C. Hydroprocessing of Biorenewable Thermal Deoxygenation Oils. *Energy and Fuels* **2015**, *29* (5), 3224–3232. <https://doi.org/10.1021/acs.energyfuels.5b00396>.
- (22) Schwartz, T. J.; Van Heiningen, A. R. P.; Wheeler, M. C. Energy Densification of Levulinic Acid by Thermal Deoxygenation. *Green Chem.* **2010**, *12* (8), 1353–1356. <https://doi.org/10.1039/c005067a>.
- (23) Case, P. A.; Van Heiningen, A. R. P.; Wheeler, M. C. Liquid Hydrocarbon Fuels from Cellulosic Feedstocks via Thermal Deoxygenation of Levulinic Acid and Formic Acid Salt Mixtures. *Green Chem.* **2012**, *14* (1), 85–89. <https://doi.org/10.1039/c1gc15914c>.
- (24) Wheeler, M. C.; van Walsum, G. P.; Schwartz, T. J.; Van Heiningen, A. Energy Densification of Biomass-Derived Organic Acids. US 8,362,306 B2, 2013.
- (25) Holtzapple, M. T.; Davison, R. R.; Ross, M. K.; Aldrett-Lee, S.; Nagwani, M.; Lee, C. M.; Lee, C.; Adelson, S.; Kaar, W.; Gaskin, D.; et al. Biomass Conversion to Mixed Alcohol Fuels Using the MixAlco Process. *Appl. Biochem. Biotechnol.* **1999**, *77–79*, 609–631. <https://doi.org/10.1385/abab:79:1-3:609>.
- (26) Chang, N. S.; Aldrett, S.; Holtzapple, M. T.; Davison, R. R. Kinetic Studies of Ketone Hydrogenation over Raney Nickel Catalyst. *Chem. Eng. Sci.* **2000**, *55* (23), 5721–5732. [https://doi.org/10.1016/S0009-2509\(00\)00222-0](https://doi.org/10.1016/S0009-2509(00)00222-0).

- (27) Eaton, S. J.; Beis, S. H.; Bunting, B. G.; Fitzpatrick, S. W.; Van Walsum, G. P.; Pendse, H. P.; Wheeler, M. C. Characterization and Combustion of Crude Thermal Deoxygenation Oils Derived from Hydrolyzed Woody Biomass. *Energy and Fuels* **2013**, *27* (9), 5246–5252. <https://doi.org/10.1021/ef4007033>.
- (28) McVicker, G. B.; Daage, M.; Touvelle, M. S.; Hudson, C. W.; Klein, D. P.; Baird, W. C.; Cook, B. R.; Chen, J. G.; Hantzer, S.; Vaughan, D. E. W.; et al. Selective Ring Opening of Naphthenic Molecules. *J. Catal.* **2002**, *210* (1), 137–148. <https://doi.org/10.1006/jcat.2002.3685>.
- (29) Weitkamp, A. W. Stereochemistry and Mechanism of Hydrogenation of Naphthalenes on Transition Metal Catalysts and Conformational Analysis of the Products. *Adv. Catal.* **1968**, *18* (C), 1–110. [https://doi.org/10.1016/S0360-0564\(08\)60428-9](https://doi.org/10.1016/S0360-0564(08)60428-9).
- (30) Beltramone, A. R.; Resasco, D. E.; Alvarez, W. E.; Choudhary, T. V. Simultaneous Hydrogenation of Multiring Aromatic Compounds over NiMo Catalyst. *Ind. Eng. Chem. Res.* **2008**, *47* (19), 7161–7166. <https://doi.org/10.1021/ie8004258>.
- (31) Rautanen, P. A.; Lylykangas, M. S.; Aittamaa, J. R.; Krause, A. O. I. Liquid-Phase Hydrogenation of Naphthalene and Tetralin on Ni/Al₂O₃: Kinetic Modeling. *Ind. Eng. Chem. Res.* **2002**, *41* (24), 5966–5975. <https://doi.org/10.1021/ie020395q>.
- (32) van Meerten, R. Z. C.; Verhaak, A. C. M.; Coenen, J. W. E. Gas Phase Benzene Hydrogenation on a Nickel-Silica Catalyst. *J. Catal.* **1976**, *225*, 217–225.
- (33) Lin, S. D.; Vannice, M. A. Hydrogenation of Aromatic Hydrocarbons over Supported Pt Catalysts: I. Benzene Hydrogenation. *Journal of Catalysis*. 1993, pp 539–553. <https://doi.org/10.1006/jcat.1993.1297>.
- (34) Park, J. Il; Lee, J. K.; Miyawaki, J.; Kim, Y. K.; Yoon, S. H.; Mochida, I. Hydro-Conversion of 1-Methyl Naphthalene into (Alkyl)Benzenes over Alumina-Coated USY Zeolite-Supported NiMoS Catalysts. *Fuel* **2011**, *90* (1), 182–189. <https://doi.org/10.1016/j.fuel.2010.09.002>.
- (35) Jacquin, M.; Jones, D. J.; Rozière, J.; Albertazzi, S.; Vaccari, A.; Lenarda, M.; Storaro, L.; Ganzerla, R. Novel Supported Rh, Pt, Ir and Ru Mesoporous Aluminosilicates as Catalysts for the Hydrogenation of Naphthalene. *Appl. Catal. A Gen.* **2003**, *251* (1), 131–141. [https://doi.org/10.1016/S0926-860X\(03\)00314-4](https://doi.org/10.1016/S0926-860X(03)00314-4).
- (36) Miki, Y.; Sugimoto, Y. Hydrocracking of Polycyclic Aromatic Compounds. 1. Methyl naphthalenes. *Fuel Process. Technol.* **1995**, *43* (2), 137–146. [https://doi.org/10.1016/0378-3820\(95\)00005-R](https://doi.org/10.1016/0378-3820(95)00005-R).
- (37) Karakhanov, E.; Maximov, A.; Kardasheva, Y.; Vinnikova, M.; Kulikov, L. Hydrotreating of Light Cycle Oil over Supported on Porous Aromatic Framework Catalysts. *Catalysts* **2018**, *8* (9). <https://doi.org/10.3390/catal8090397>.

- (38) He, T.; Wang, Y.; Miao, P.; Li, J.; Wu, J.; Fang, Y. Hydrogenation of Naphthalene over Noble Metal Supported on Mesoporous Zeolite in the Absence and Presence of Sulfur. *Fuel* **2013**, *106*, 365–371. <https://doi.org/10.1016/j.fuel.2012.12.025>.
- (39) Cooper, B. H.; Stanislaus, A.; Hannerup, P. N. *ACS Fuel Chem Div. Prepr.* **1992**, *37*, 41.
- (40) Albertazzi, S.; Rodríguez-Castellón, E.; Livi, M.; Jiménez-López, A.; Vaccari, A. Hydrogenation and Hydrogenolysis/Ring-Opening of Naphthalene on Pd/Pt Supported on Zirconium-Doped Mesoporous Silica Catalysts. *J. Catal.* **2004**, *228* (1), 218–224. <https://doi.org/10.1016/j.jcat.2004.07.023>.
- (41) Rautanen, P. A.; Aittamaa, J. R.; Krause, A. O. I. Liquid Phase Hydrogenation of Tetralin on Ni/Al₂O₃. *Chem. Eng. Sci.* **2001**, *56* (4), 1247–1254. [https://doi.org/10.1016/S0009-2509\(00\)00346-8](https://doi.org/10.1016/S0009-2509(00)00346-8).
- (42) Schmidt, A.; Bowers, G.; Song, C. Shape-Selective Hydrogenation of Naphthalene over Zeolite-Supported Pt and Pd Catalysts. *Catal. Today* **1996**, *31* (1–2), 45–56.
- (43) Eijsbouts, S.; Mayo, S. W.; Fujita, K. Unsupported Transition Metal Sulfide Catalysts: From Fundamentals to Industrial Application. *Appl. Catal. A Gen.* **2007**, *322* (SUPPL.), 58–66. <https://doi.org/10.1016/j.apcata.2007.01.008>.
- (44) Arribas, M. A.; Martínez, A. The Influence of Zeolite Acidity for the Coupled Hydrogenation and Ring Opening of 1-Methylnaphthalene on Pt/USY Catalysts. *Appl. Catal. A Gen.* **2002**, *230* (1–2), 203–217. [https://doi.org/10.1016/S0926-860X\(01\)01015-8](https://doi.org/10.1016/S0926-860X(01)01015-8).
- (45) Majka, M.; Tomaszewicz, G.; Mianowski, A. Experimental Study on the Coal Tar Hydrocracking Process over Different Catalysts. *J. Energy Inst.* **2018**, *91* (6), 1164–1176. <https://doi.org/10.1016/j.joei.2017.06.007>.
- (46) Mouli, K. C.; Choudhary, O.; Soni, K.; Dalai, A. K. Improvement of Cetane Number of LGO by Ring Opening of Naphthenes on Pt/Al-SBA-15 Catalysts. *Catal. Today* **2012**, *198* (1), 69–76. <https://doi.org/10.1016/j.cattod.2012.01.027>.
- (47) Jaroszevska, K.; Masalska, A.; Grzechowiak, J. R.; Grams, J. Hydroconversion of 1-Methylnaphthalene over Pt/AlSBA-15–Al₂O₃ Composite Catalysts. *Appl. Catal. A Gen.* **2015**, *505*, 116–130. <https://doi.org/10.1016/j.apcata.2015.07.021>.
- (48) Trueba, M.; Trasatti, S. P. γ -Alumina as a Support for Catalysts: A Review of Fundamental Aspects. *Eur. J. Inorg. Chem.* **2005**, No. 17, 3393–3403. <https://doi.org/10.1002/ejic.200500348>.
- (49) Daniell, W.; Schubert, U.; Glöckler, R.; Meyer, A.; Noweck, K.; Knözinger, H. Enhanced Surface Acidity in Mixed Alumina–Silicas. *Appl. Catal. A Gen.* **2000**, *196*, 247–260. [https://doi.org/10.1016/S0926-860X\(99\)00474-3](https://doi.org/10.1016/S0926-860X(99)00474-3).
- (50) Park, J. II; Ali, S. A.; Alhooshani, K.; Azizi, N.; Miyawaki, J.; Kim, T.; Lee, Y.; Kim, H. S.; Yoon, S. H.; Mochida, I. Mild Hydrocracking of 1-Methyl Naphthalene (1-MN) over Alumina Modified Zeolite. *J. Ind. Eng. Chem.* **2013**, *19* (2), 627–632. <https://doi.org/10.1016/j.jiec.2012.09.014>.

- (51) Castaño, P.; Pawelec, B.; Fierro, J. L. G.; Arandes, J. M.; Bilbao, J. Enhancement of Pyrolysis Gasoline Hydrogenation over Pd-Promoted Ni/SiO₂-Al₂O₃ Catalysts. *Fuel* **2007**, *86* (15), 2262–2274. <https://doi.org/10.1016/j.fuel.2007.01.020>.
- (52) Timken, H. K. Method for Preparing a Highly Homogenous Amorphous Silica-Alumina Composition. US 6,872,685 B2, 2005.
- (53) Baerlocher, C.; Meier, W. M.; Olson, D. H. *Atlas of Zeolite Framework Types*, 5th Editio.; Elsevier, 2001.
- (54) Corma, A.; Martínez, A.; Martínez-Soria, V. Catalytic Performance of the New Delaminated ITQ-2 Zeolite for Mild Hydrocracking and Aromatic Hydrogenation Processes. *J. Catal.* **2001**, *200* (2), 259–269. <https://doi.org/10.1006/jcat.2001.3219>.
- (55) Barrio, V. L.; Arias, P. L.; Cambra, J. F.; Güemez, M. B.; Pawelec, B.; Fierro, J. L. G. Hydrodesulfurization and Hydrogenation of Model Compounds on Silica-Alumina Supported Bimetallic Systems. *Fuel* **2003**, *82* (5), 501–509. [https://doi.org/10.1016/S0016-2361\(02\)00322-8](https://doi.org/10.1016/S0016-2361(02)00322-8).
- (56) Wang, L.; Shen, B.; Fang, F.; Wang, F.; Tian, R.; Zhang, Z.; Cui, L. Upgrading of Light Cycle Oil via Coupled Hydrogenation and Ring-Opening over NiW/Al₂O₃-USY Catalysts. *Catal. Today* **2010**, *158* (3–4), 343–347. <https://doi.org/10.1016/j.cattod.2010.04.018>.
- (57) Stanislaus, A.; Barry, H. C. Aromatic Hydrogenation Catalysis: A Review. *Catal. Rev.* **1994**, *36* (1), 75–123. <https://doi.org/10.1080/01614949408013921>.
- (58) Daily Metal Spot Prices <https://www.dailymetalprice.com/metalprices.php?c=mo&u=oz&d=20> (accessed Apr 10, 2020).
- (59) Huang, T. C.; Kang, B. C. Hydrogenation of Naphthalene with Platinum-Aluminium Borate Catalysts. *Chem. Eng. J. Biochem. Eng. J.* **1996**, *63* (1), 27–36. [https://doi.org/10.1016/0923-0467\(95\)03070-0](https://doi.org/10.1016/0923-0467(95)03070-0).
- (60) Pawelec, B.; Mariscal, R.; Navarro, R. M.; Van Bokhorst, S.; Rojas, S.; Fierro, J. L. G. Hydrogenation of Aromatics over Supported Pt-Pd Catalysts. *Appl. Catal. A Gen.* **2002**, *225* (1–2), 223–237. [https://doi.org/10.1016/S0926-860X\(01\)00868-7](https://doi.org/10.1016/S0926-860X(01)00868-7).
- (61) Karroua, M.; Grange, P.; Delmon, B. Existence of Synergy between “CoMoS” and Co₉S₈. New Proof of Remote Control in Hydrodesulfurization. *Appl. Catal.* **1989**, *50* (1), 0–5. [https://doi.org/10.1016/S0166-9834\(00\)80849-0](https://doi.org/10.1016/S0166-9834(00)80849-0).
- (62) Mortensen, P. M.; Grunwaldt, J. D.; Jensen, P. A.; Knudsen, K. G.; Jensen, A. D. A Review of Catalytic Upgrading of Bio-Oil to Engine Fuels. *Appl. Catal. A Gen.* **2011**, *407* (1–2), 1–19. <https://doi.org/10.1016/j.apcata.2011.08.046>.
- (63) Atsumi, R.; Kobayashi, K.; Xieli, C.; Nanba, T.; Matsumoto, H.; Matsuda, K.; Tsujimura, T. Effects of Steam on Toluene Hydrogenation over a Ni Catalyst. *Appl. Catal. A Gen.* **2020**, *590* (November 2019), 117374. <https://doi.org/10.1016/j.apcata.2019.117374>.

- (64) Argyle, M. D.; Bartholomew, C. H. Heterogeneous Catalyst Deactivation and Regeneration: A Review. *Catalysts* **2015**, *5* (1), 145–269. <https://doi.org/10.3390/catal5010145>.
- (65) Zhang, Y.; Wang, W.; Wang, Z.; Zhou, X.; Wang, Z.; Liu, C. J. Steam Reforming of Methane over Ni/SiO₂ Catalyst with Enhanced Coke Resistance at Low Steam to Methane Ratio. *Catal. Today* **2015**, *256* (Part 1), 130–136. <https://doi.org/10.1016/j.cattod.2015.01.016>.
- (66) Venezia, A. M.; La Parola, V.; Pawelec, B.; Fierro, J. L. G. Hydrogenation of Aromatics over Au-Pd/SiO₂-Al₂O₃ Catalysts; Support Acidity Effect. *Appl. Catal. A Gen.* **2004**, *264* (1), 43–51. <https://doi.org/10.1016/j.apcata.2003.12.025>.
- (67) Huber, G. W.; Iborra, S.; Corma, A. Synthesis of Transportation Fuels from Biomass: Chemistry, Catalysts, and Engineering. *Chem. Rev.* **2006**, *106* (9), 4044–4098. <https://doi.org/10.1021/cr068360d>.
- (68) Munnik, P.; de Jongh, P. E.; de Jong, K. P. Recent Developments in the Synthesis of Supported Catalysts. *Chem. Rev.* **2015**, *115* (14), 6687–6718. <https://doi.org/10.1021/cr500486u>.
- (69) Aksoylu, A. E.; Önsan, Z. I. Hydrogenation of Carbon Oxides Using Coprecipitated and Impregnated Ni/Al₂O₃ Catalysts. *Appl. Catal. A Gen.* **1997**, *164* (1–2), 1–11.
- (70) Bernard, M. *Comparative Inorganic Chemistry*; Elsevier, 2013.
- (71) Ma, Q.; Wang, D.; Wu, M.; Zhao, T.; Yoneyama, Y.; Tsubaki, N. Effect of Catalytic Site Position: Nickel Nanocatalyst Selectively Loaded inside or Outside Carbon Nanotubes for Methane Dry Reforming. *Fuel* **2013**, *108*, 430–438. <https://doi.org/10.1016/j.fuel.2012.12.028>.
- (72) Lucrédio, A. F.; Assaf, J. M.; Assaf, E. M. Methane Conversion Reactions on Ni Catalysts Promoted with Rh: Influence of Support. *Appl. Catal. A Gen.* **2011**, *400* (1–2), 156–165. <https://doi.org/10.1016/j.apcata.2011.04.035>.
- (73) Özdemir, H.; Faruk Öksüzömer, M. A.; Ali Gürkaynak, M. Preparation and Characterization of Ni Based Catalysts for the Catalytic Partial Oxidation of Methane: Effect of Support Basicity on H₂/CO Ratio and Carbon Deposition. *Int. J. Hydrogen Energy* **2010**, *35* (22), 12147–12160. <https://doi.org/10.1016/j.ijhydene.2010.08.091>.
- (74) Upare, D. P.; Song, B. J.; Lee, C. W. Hydrogenation of Tetralin over Supported Ni and Ir Catalysts. *J. Nanomater.* **2013**, *2013*. <https://doi.org/10.1155/2013/210894>.
- (75) Richardson, J. T.; Scates, R.; Twigg, M. V. X-Ray Diffraction Study of Nickel Oxide Reduction by Hydrogen. *Appl. Catal. A Gen.* **2003**, *246* (1), 137–150. [https://doi.org/10.1016/S0926-860X\(02\)00669-5](https://doi.org/10.1016/S0926-860X(02)00669-5).
- (76) Ulfa, S. M.; Prihartini, D.; Taufiq, A. Structural Characterization of Ni/ZrO₂/SiO₂ Nanocomposites Prepared by Wet Impregnation Route. *Mater. Sci. Eng.* **2019**, *515* (1). <https://doi.org/10.1088/1757-899X/515/1/012014>.

- (77) Barrio, V. L.; Arias, P. L.; Cambra, J. F.; Güemez, M. B.; Campos-Martin, J. M.; Pawelec, B.; Fierro, J. L. G. Evaluation of Silica-Alumina-Supported Nickel Catalysts in Dibenzothiophene Hydrodesulphurisation. *Appl. Catal. A Gen.* **2003**, *248* (1–2), 211–225. [https://doi.org/10.1016/S0926-860X\(03\)00158-3](https://doi.org/10.1016/S0926-860X(03)00158-3).
- (78) Ghosh, P.; Jaffe, S. B. Detailed Composition-Based Model for Predicting the Cetane Number of Diesel Fuels. *Ind. Eng. Chem. Res.* **2006**, *45* (1), 346–351. <https://doi.org/10.1021/ie0508132>.
- (79) Kustov, L. M.; Finashina, E. D.; Avaev, V. I.; Ershov, B. G. Decalin Ring Opening on Pt-Ru/SiO₂ Catalysts. *Fuel Process. Technol.* **2018**, *173*, 270–275. <https://doi.org/10.1016/j.fuproc.2018.02.007>.
- (80) Pang, M.; Liu, C.; Xia, W.; Muhler, M.; Liang, C. Activated Carbon Supported Molybdenum Carbides as Cheap and Highly Efficient Catalyst in the Selective Hydrogenation of Naphthalene to Tetralin. *Green Chem.* **2012**, *14* (5), 1272–1276. <https://doi.org/10.1039/c2gc35177c>.
- (81) Heyne, J. S.; Boehman, A. L.; Kirby, S. Autoignition Studies of Trans- and Cis-Decalin in an Ignition Quality Tester (IQT) and the Development of a High Thermal Stability Unifuel/Single Battlefield Fuel. *Energy and Fuels* **2009**, *23* (12), 5879–5885. <https://doi.org/10.1021/ef900715m>.
- (82) Huang, T. C.; Kang, B. C. Naphthalene Hydrogenation over Pt/Al₂O₃ Catalyst in a Trickle Bed Reactor. *Ind. Eng. Chem. Res.* **1995**, *34* (7), 2349–2357. <https://doi.org/10.1021/ie00046a017>.
- (83) Lai, W.-C.; Song, C. Conformational Isomerization of Cis-Decahydronaphthalene over Zeolite Catalysts. *Catal. Today* **1996**, *31* (1–2), 171–181.
- (84) DSSTox Substance ID - 5-Methylbenzo[b]thiophene
<https://comptox.epa.gov/dashboard/dsstoxdb/results?search=DTXSID3074523> (accessed Mar 9, 2020).
- (85) DSSTox Substance ID - 2-Methylnaphthalene
<https://comptox.epa.gov/dashboard/dsstoxdb/results?search=DTXSID4020878#details> (accessed Mar 9, 2020).
- (86) DSSTox Substance ID - 1-Methylnaphthalene
<https://comptox.epa.gov/dashboard/dsstoxdb/results?search=DTXSID9020877#details> (accessed Mar 9, 2020).
- (87) Huang, T. C.; Kang, B. C. Kinetic Study of Naphthalene Hydrogenation over Pt/Al₂O₃ Catalyst. *Ind. Eng. Chem. Res.* **1995**, *34* (4), 1140–1148. <https://doi.org/10.1021/ie00043a016>.
- (88) Qi, S. C.; Wei, X. Y.; Zong, Z. M.; Wang, Y. K. Application of Supported Metallic Catalysts in Catalytic Hydrogenation of Arenes. *RSC Adv.* **2013**, *3* (34), 14219–14232. <https://doi.org/10.1039/c3ra40848e>.

- (89) Jaroszevska, K.; Masalska, A.; Baęczkowska, K.; Grzechowiak, J. R. Conversion of Decalin and 1-Methylnaphthalene over AISBA-15 Supported Pt Catalysts. *Catal. Today* **2012**, *196* (1), 110–118. <https://doi.org/10.1016/j.cattod.2012.06.011>.
- (90) Smith, G. V.; Burwell, R. L. Reactions between Deuterium and Olefins in the Liquid Phase on Platinum Oxide Catalysts. *J. Am. Chem. Soc.* **1962**, *84* (6), 925–934. <https://doi.org/10.1021/ja00865a010>.

APPENDIX A

SYNTHESIS METHODS OF SUPPORTED HYDROGENATION CATALYSTS

INCIPIENT WETNESS IMPREGNATED CATALYSTS

A. Ni/SiO₂ (20 wt% Ni)

- 2.5281 g of Ni(NO₃)₂·6H₂O was dissolved in 1.7838 g of deionized water
- The nickel solution was added dropwise to 2.0238 g of silica and stirred to break up any chunks
- The catalyst was moved to the oven, where it was heated to 100°C overnight
- The catalyst chunks were broken up with a mortar and pestle and placed in a furnace that was heated by 2°C/min to a maximum temperature of 450°C, where the temperature held constant for 3 hours before cooling off to room temperature
- Resulting catalyst had a surface area of 400 m² g⁻¹, pore volume of 0.48 cm³ g⁻¹, and pore size of 48 Å



Figure 31. Stages of incipient wetness impregnation for a 20 wt% Ni/SiO₂ catalyst: 1) metal solution is added dropwise to the support 2) catalyst is dried in oven overnight at 100°C, 3) catalyst is crushed and prepared for calcination, 4) catalyst is calcined at 450°C for 3 hours.

B. Ni/γ-Al₂O₃ (20 wt% Ni)

- 3.7261 g of Ni(NO₃)₂·6H₂O was dissolved in 1.6986 g of deionized water
- The nickel solution was added dropwise to 3.0076 g of gamma-alumina and stirred to break up any chunks
- The catalyst was moved to the oven, where it was heated to 100°C overnight
- The catalyst chunks were broken up with a mortar and pestle and placed in a furnace that was heated by 2°C/min to a maximum temperature of 450°C, where the temperature held constant for 3 hours before cooling off to room temperature
- Resulting catalyst had a surface area of 151 m² g⁻¹, pore volume of 0.32 cm³ g⁻¹, and pore size of 84 Å

C. Ni/SiAl (20 wt% Ni)

- To make this support, both silica and alumina were added together in a 50:50 ratio, where 2.0068 g of alumina and 2.0084 g of silica were combined (Molecular Si:Al ratio = 0.884)
- 2.8952 g of $\text{Ni}(\text{NO}_3)_2 \cdot 6\text{H}_2\text{O}$ was dissolved in 2.0691 g of deionized water
- The nickel solution was added dropwise to 2.9128 g of the mixed support and stirred to break up any chunks
- The catalyst was moved to the oven, where it was heated to 100°C overnight
- The catalyst chunks were broken up with a mortar and pestle and placed in a furnace that was heated by 2°C/min to a maximum temperature of 450°C, where the temperature held constant for 3 hours before cooling off to room temperature
- Resulting catalyst had a surface area of 308 m² g⁻¹, pore volume of 0.43 cm³ g⁻¹, and pore size of 56 Å

D. Ni/ASA (20 wt% Ni)

- This procedure is largely based on US Patent # 6,872,685 B2 (2005)⁵²
- Solution 2 (6 wt% SiO₂) was prepared by dissolving 9.1855 g of sodium orthosilicate (Na₄SiO₄) in 40.8503 g of deionized water using a stir bar
- Solution 1 (6 wt% Al₂O₃) was prepared by dissolving 17.4810 g of Al₂(SO₄)₃·14H₂O in 30.4721 g of deionized water. The aluminum sulfate did not completely dissolve, so 2.717 g of concentrated H₂SO₄ was added to the solution until all of the aluminum sulfate pieces dissolved at a pH of about 0.5
- Solution 1 was stirred vigorously while solution 2 was added dropwise to solution 1 using a glass Pasteur pipette. White flakes formed as the drops were added. The flakes dissolved upon further stirring, and the pH of the solution was kept below 2.0 by adding more sulfuric acid. The final solution (solution 1+2) was translucent and had a pH of 1.2
- Solution 3 was prepared by adding 37.452 g of 32 wt% NH₃ solution to 116.489 g of deionized water
- Simultaneously, some of each solution (1+2 and 3) was added to a new 600 mL beaker and the gelation started instantly, as both clear solutions turned white and appeared to gel. The pH was monitored very closely to maintain it between 6.5 and 7.5. More of the solutions were added to ensure that the pH remained in the correct range while the stir bar ran at the maximum speed possible. Once both solutions were completely added, the gel was allowed to set for 2 hours while being continuously stirred. The solution was an opaque white gel-like solution and by the end, the pH was 6.75
- Solution 4 was prepared by dissolving 12.563 g of ammonium acetate in 251.107 g of deionized water. This solution was heated on a hot plate until it was about 50°C
- After the 2 hours had elapsed, the opaque gel solution was vacuum filtered. Solution 4 was added in 50 mL aliquots to the gel, then 500 mL of deionized water was used to wash the paste
- The filtrate was allowed to air dry for an hour then dried in an oven at 100°C overnight

- The support was then sieved to size and the powder was calcined overnight at 450°C using a ramp of 2°C/min. The resulting ASA was beige-white after calcination
- Resulting support had a surface area of 333 m² g⁻¹, pore volume of 0.56 cm³ g⁻¹, and pore size of 68 Å



Figure 32. Stages of synthesis of ASA support: 1) solution 2 is added to an acidic aluminum solution 2) upon addition of basic solution, the gel persists as a milky viscous liquid 3) the flakes are collected after vacuum filtration 4) the support was dried in an oven overnight and persisted as a white powder.

- 2.5626 g of Ni(NO₃)₂·6H₂O was dissolved in 1.8005 g of deionized water
- The nickel solution was added dropwise to 2.0691 g of amorphous silica alumina and stirred to break up any chunks of support
- The catalyst was moved to the oven, where it was heated to 100°C overnight
- The catalyst chunks were broken up with a mortar and pestle and placed in a furnace that was heated by 2°C/min to a maximum temperature of 450°C, where the temperature held constant for 3 hours before cooling off to room temperature
- Resulting catalyst had a surface area of 218 m² g⁻¹, pore volume of 0.31 cm³ g⁻¹, and pore size of 68 Å



Figure 33. Various stages of incipient wetness impregnation using nickel on amorphous silica-alumina (ASA).



Figure 34. Comparison of dried ASA support, calcined support, and synthesized 20 wt% Ni/ASA catalyst.

COPRECIPITATED CATALYSTS

E. 60Ni – (Method I)

- In a 250 mL beaker, 9.413 g of $\text{Ni}(\text{NO}_3)_2 \cdot 6\text{H}_2\text{O}$ and 2.998 g of $\text{AlCl}_3 \cdot 6\text{H}_2\text{O}$ were dissolved in 80 mL of deionized water
- In a 150 mL beaker, a carbonate solution containing 7.569 g of Na_2CO_3 was dissolved in 50 mL of deionized water
- A 600 mL beaker was filled with 150 mL of DI water
- The first two solutions were added dropwise into the 600 mL beaker, which was stirred vigorously at room temperature
- The resulting solution was filtered to separate the precipitate
- 2-100 mL aliquots of water were added to the filtrate
- 2-25 mL aliquots of methanol were added to the filtrate
- The filtrate cake was then transferred to a crucible and dried overnight at 100°C
- The catalyst was calcined in a muffle furnace at 450°C for 3 hours with a 2°C/min ramp
- Resulting catalyst had a surface area of $88 \text{ m}^2 \text{ g}^{-1}$, pore volume of $0.24 \text{ cm}^3 \text{ g}^{-1}$, and pore size of 108 Å



Figure 35. Images of coprecipitated 60Ni catalyst.

F. 60Co – (Method I)

- In a 250 mL beaker, 9.612 g of $\text{Co}(\text{NO}_3)_2 \cdot 6\text{H}_2\text{O}$ and 3.075 g of $\text{AlCl}_3 \cdot 6\text{H}_2\text{O}$ were dissolved in 80 mL of deionized water
- In a 150 mL beaker, a carbonate solution containing 6.31 g of Na_2CO_3 was dissolved in 50 mL of deionized water
- A 600 mL beaker was filled with 150 mL of DI water
- The first two solutions were added dropwise into the 600 mL beaker, which was stirred vigorously at room temperature
- The resulting solution was filtered to separate the precipitate
- 2-100 mL aliquots of water were added to the filtrate
- 2-25 mL aliquots of methanol were added to the filtrate
- The filtrate cake was then transferred to a crucible and dried overnight at 100°C
- The catalyst was calcined in a muffle furnace at 450°C for 3 hours with a $2^\circ\text{C}/\text{min}$ ramp



Figure 36. Images of coprecipitated 60Co catalyst.

G. NiCr – (Method I)

- In a 250 mL beaker, 9.891 g of $\text{Ni}(\text{NO}_3)_2 \cdot 6\text{H}_2\text{O}$, 2.838 g of $\text{AlCl}_3 \cdot 6\text{H}_2\text{O}$, and 0.691 g of $\text{CrCl}_2 \cdot 6\text{H}_2\text{O}$ were dissolved in 80 mL of deionized water
- In a 150 mL beaker, a carbonate solution containing 7.64 g of Na_2CO_3 was dissolved in 50 mL of deionized water
- A 600 mL beaker was filled with 150 mL of DI water
- The first two solutions were added dropwise into the 600 mL beaker, which was stirred vigorously at room temperature
- The resulting solution was filtered to separate the precipitate
- 2-100 mL aliquots of water were added to the filtrate
- 2-25 mL aliquots of methanol were added to the filtrate
- The filtrate cake was then transferred to a crucible and dried overnight at 100°C
- The catalyst was calcined in a muffle furnace at 450°C for 3 hours with a $2^\circ\text{C}/\text{min}$ ramp
- Final sample ratio was 59.9 – 4.1 – 36.0 (Ni – Cr – Al_2O_3)
- Resulting catalyst had a surface area of $98 \text{ m}^2 \text{ g}^{-1}$, pore volume of $0.20 \text{ cm}^3 \text{ g}^{-1}$, and pore size of 83 \AA



Figure 37. Images of coprecipitated NiCr catalyst.

H. NiMn – (Method I)

- In a 250 mL beaker, 12.195 g of $\text{Ni}(\text{NO}_3)_2 \cdot 6\text{H}_2\text{O}$, 2.846 g of $\text{AlCl}_3 \cdot 6\text{H}_2\text{O}$, and 0.365 g of MnSO_4 were dissolved in 80 mL of deionized water
- In a 150 mL beaker, a carbonate solution containing 7.545 g of Na_2CO_3 was dissolved in 50 mL of deionized water
- A 600 mL beaker was filled with 150 mL of DI water
- The first two solutions were added dropwise into the 600 mL beaker, which was stirred vigorously at room temperature
- The resulting solution was filtered to separate the precipitate
- 2-100 mL aliquots of water were added to the filtrate
- 2-25 mL aliquots of methanol were added to the filtrate
- The filtrate cake was then transferred to a crucible and dried overnight at 100°C
- The catalyst was calcined in a muffle furnace at 450°C for 3 hours with a $2^\circ\text{C}/\text{min}$ ramp
- Final sample ratio was 60.1 – 4.0 – 35.9



Figure 38. Images of coprecipitated NiMn catalyst.

I. NiFe – (Method I)

- In a 250 mL beaker, 12.532 g of $\text{Ni}(\text{NO}_3)_2 \cdot 6\text{H}_2\text{O}$, 2.949 g of $\text{AlCl}_3 \cdot 6\text{H}_2\text{O}$, and 0.412 g of FeCl_3 were dissolved in 80 mL of deionized water
- In a 150 mL beaker, a carbonate solution containing 7.086 g of Na_2CO_3 was dissolved in 50 mL of deionized water
- A 600 mL beaker was filled with 150 mL of DI water
- The first two solutions were added dropwise into the 600 mL beaker, which was stirred vigorously at room temperature
- The resulting solution was filtered to separate the precipitate
- 2-100 mL aliquots of water were added to the filtrate
- 2-25 mL aliquots of methanol were added to the filtrate
- The filtrate cake was then transferred to a crucible and dried overnight at 100°C
- The catalyst was calcined in a muffle furnace at 450°C for 3 hours with a $2^\circ\text{C}/\text{min}$ ramp
- Final sample ratio was 59.8 – 4.1 – 36.1



Figure 39. Images of coprecipitated NiFe catalyst.

J. NiCo – (Method I)

- In a 250 mL beaker, 9.461 g of $\text{Ni}(\text{NO}_3)_2 \cdot 6\text{H}_2\text{O}$, 2.736 g of $\text{AlCl}_3 \cdot 6\text{H}_2\text{O}$, and 0.646 g of $\text{Co}(\text{NO}_3)_2 \cdot 6\text{H}_2\text{O}$ were dissolved in 80 mL of deionized water
- In a 150 mL beaker, a carbonate solution containing 7.839 g of Na_2CO_3 was dissolved in 50 mL of deionized water
- A 600 mL beaker was filled with 150 mL of DI water
- The first two solutions were added dropwise into the 600 mL beaker, which was stirred vigorously at room temperature
- The resulting solution was filtered to separate the precipitate
- 2-100 mL aliquots of water were added to the filtrate
- 2-25 mL aliquots of methanol were added to the filtrate
- The filtrate cake was then transferred to a crucible and dried overnight at 100°C
- The catalyst was calcined in a muffle furnace at 450°C for 3 hours with a $2^\circ\text{C}/\text{min}$ ramp
- Final sample ratio was 59.8 – 4.1 – 36.2



Figure 40. Images of coprecipitated NiCo catalyst.

K. NiCu – (Method I)

- In a 250 mL beaker, 11.607 g of $\text{Ni}(\text{NO}_3)_2 \cdot 6\text{H}_2\text{O}$, 2.722 g of $\text{AlCl}_3 \cdot 6\text{H}_2\text{O}$, and 0.484 g of $\text{Cu}(\text{NO}_3)_2 \cdot 3\text{H}_2\text{O}$ were dissolved in 80 mL of deionized water
- In a 150 mL beaker, a carbonate solution containing 7.694 g of Na_2CO_3 was dissolved in 50 mL of deionized water
- A 600 mL beaker was filled with 150 mL of DI water
- The first two solutions were added dropwise into the 600 mL beaker, which was stirred vigorously at room temperature
- The resulting solution was filtered to separate the precipitate
- 2-100 mL aliquots of water were added to the filtrate
- 2-25 mL aliquots of methanol were added to the filtrate
- The filtrate cake was then transferred to a crucible and dried overnight at 100°C
- The catalyst was calcined in a muffle furnace at 450°C for 3 hours with a $2^\circ\text{C}/\text{min}$ ramp
- Final sample ratio was 60.0 – 4.0 – 36.0



Figure 41. Images of coprecipitated NiCu catalyst.

L. NiZn – (Method I)

- In a 250 mL beaker, 11.548 g of $\text{Ni}(\text{NO}_3)_2 \cdot 6\text{H}_2\text{O}$, 2.675 g of $\text{AlCl}_3 \cdot 6\text{H}_2\text{O}$, and 0.475 g of zinc acetate dihydrate were dissolved in 80 mL of deionized water
- In a 150 mL beaker, a carbonate solution containing 7.36 g of Na_2CO_3 was dissolved in 50 mL of deionized water
- A 600 mL beaker was filled with 150 mL of DI water
- The first two solutions were added dropwise into the 600 mL beaker, which was stirred vigorously at room temperature
- The resulting solution was filtered to separate the precipitate
- 2-100 mL aliquots of water were added to the filtrate
- 2-25 mL aliquots of methanol were added to the filtrate
- The filtrate cake was then transferred to a crucible and dried overnight at 100°C
- The catalyst was calcined in a muffle furnace at 450°C for 3 hours with a $2^\circ\text{C}/\text{min}$ ramp
- Final sample ratio was 59.8 – 4.5 – 35.8



Figure 42. Images of coprecipitated NiZn catalyst.

M. 20Ni – (Method I)

- In a 250 mL beaker, 3.138 g of $\text{Ni}(\text{NO}_3)_2 \cdot 6\text{H}_2\text{O}$ and 5.996 g of $\text{AlCl}_3 \cdot 6\text{H}_2\text{O}$ were dissolved in 80 mL of deionized water
- In a 150 mL beaker, a carbonate solution containing 7.652 g of Na_2CO_3 was dissolved in 50 mL of deionized water
- A 600 mL beaker was filled with 150 mL of DI water
- The first two solutions were added dropwise into the 600 mL beaker, which was stirred vigorously at room temperature
- The resulting solution was filtered to separate the precipitate
- 2-100 mL aliquots of water were added to the filtrate
- 2-25 mL aliquots of methanol were added to the filtrate
- The filtrate cake was then transferred to a crucible and dried overnight at 100°C
- The catalyst was calcined in a muffle furnace at 450°C for 3 hours with a $2^\circ\text{C}/\text{min}$ ramp
- Resulting catalyst had a surface area of $142 \text{ m}^2 \text{ g}^{-1}$, pore volume of $0.49 \text{ cm}^3 \text{ g}^{-1}$, and pore size of 139 \AA

N. 40Ni – (Method I)

- In a 250 mL beaker, 6.356 g of $\text{Ni}(\text{NO}_3)_2 \cdot 6\text{H}_2\text{O}$ and 4.540 g of $\text{AlCl}_3 \cdot 6\text{H}_2\text{O}$ were dissolved in 80 mL of deionized water
- In a 150 mL beaker, a carbonate solution containing 7.496 g of Na_2CO_3 was dissolved in 50 mL of deionized water
- A 600 mL beaker was filled with 150 mL of DI water
- The first two solutions were added dropwise into the 600 mL beaker, which was stirred vigorously at room temperature
- The resulting solution was filtered to separate the precipitate
- 2-100 mL aliquots of water were added to the filtrate
- 2-25 mL aliquots of methanol were added to the filtrate
- The filtrate cake was then transferred to a crucible and dried overnight at 100°C
- The catalyst was calcined in a muffle furnace at 450°C for 3 hours with a 2°C/min ramp
- Resulting catalyst had a surface area of 114 $\text{m}^2 \text{g}^{-1}$, pore volume of 0.26 $\text{cm}^3 \text{g}^{-1}$, and pore size of 90 Å

O. 80Ni – (Method I)

- In a 250 mL beaker, 13.459 g of $\text{Ni}(\text{NO}_3)_2 \cdot 6\text{H}_2\text{O}$ and 1.617 g of $\text{AlCl}_3 \cdot 6\text{H}_2\text{O}$ were dissolved in 80 mL of deionized water
- In a 150 mL beaker, a carbonate solution containing 7.821 g of Na_2CO_3 was dissolved in 50 mL of deionized water
- A 600 mL beaker was filled with 150 mL of DI water
- The first two solutions were added dropwise into the 600 mL beaker, which was stirred vigorously at room temperature
- The resulting solution was filtered to separate the precipitate
- 2-100 mL aliquots of water were added to the filtrate
- 2-25 mL aliquots of methanol were added to the filtrate
- The filtrate cake was then transferred to a crucible and dried overnight at 100°C
- The catalyst was calcined in a muffle furnace at 450°C for 3 hours with a 2°C/min ramp
- Resulting catalyst had a surface area of 68 $\text{m}^2 \text{g}^{-1}$, pore volume of 0.21 $\text{cm}^3 \text{g}^{-1}$, and pore size of 124 Å

P. 100Ni – (Method I)

- In a 250 mL beaker, 15.392 g of $\text{Ni}(\text{NO}_3)_2 \cdot 6\text{H}_2\text{O}$ was dissolved in 80 mL of deionized water
- In a 150 mL beaker, a carbonate solution containing 7.597 g of Na_2CO_3 was dissolved in 50 mL of deionized water
- A 600 mL beaker was filled with 150 mL of DI water
- The first two solutions were added dropwise into the 600 mL beaker, which was stirred vigorously at room temperature
- The resulting solution was filtered to separate the precipitate

- 2-100 mL aliquots of water were added to the filtrate
- 2-25 mL aliquots of methanol were added to the filtrate
- The filtrate cake was then transferred to a crucible and dried overnight at 100°C
- The catalyst was calcined in a muffle furnace at 450°C for 3 hours with a 2°C/min ramp
- Resulting catalyst had a surface area of 30 m² g⁻¹, pore volume of 0.11 cm³ g⁻¹, and pore size of 145 Å

Q. Amorphous Alumina – (Method II)

- In a 250 mL beaker, 10.024 g of AlCl₃·6H₂O was dissolved in 75 mL of deionized water
- In a 50 mL beaker, a carbonate solution containing 8.313 g of Na₂CO₃ was dissolved in 45 mL of deionized water
- A 600 mL beaker was filled with 150 mL of DI water
- The first two solutions were added dropwise into the 600 mL beaker, which was stirred vigorously at 90°C. While adding the solutions together, a gas emerged as the aluminum chloride solution was added
- The resulting solution was filtered to separate the precipitate
- 2-100 mL aliquots of water were added to the filtrate
- 2-25 mL aliquots of methanol were added to the filtrate
- The filtrate cake was then transferred to a crucible and dried overnight at 100°C
- The catalyst was calcined in a muffle furnace at 450°C for 3 hours with a 2°C/min ramp
- Resulting catalyst had a surface area of 80 m² g⁻¹, pore volume of 0.50 cm³ g⁻¹, and pore size of 248 Å

R. 20Ni – (Method II)

- In a 250 mL beaker, 3.151 g of Ni(NO₃)₂·6H₂O and 6.024 g of AlCl₃·6H₂O were dissolved in 75 mL of deionized water
- In a 50 mL beaker, a carbonate solution containing 7.627 g of Na₂CO₃ was dissolved in 45 mL of deionized water
- A 600 mL beaker was filled with 150 mL of DI water
- The first two solutions were added dropwise into the 600 mL beaker, which was stirred vigorously at 90°C
- The resulting solution was filtered to separate the precipitate
- 2-100 mL aliquots of water were added to the filtrate
- 2-25 mL aliquots of methanol were added to the filtrate
- The filtrate cake was then transferred to a crucible and dried overnight at 100°C
- The catalyst was calcined in a muffle furnace at 450°C for 3 hours with a 2°C/min ramp
- Resulting catalyst had a surface area of 401 m² g⁻¹, pore volume of 1.18 cm³ g⁻¹, and pore size of 118 Å

S. 40Ni – (Method II)

- In a 250 mL beaker, 6.687 g of $\text{Ni}(\text{NO}_3)_2 \cdot 6\text{H}_2\text{O}$ and 4.788 g of $\text{AlCl}_3 \cdot 6\text{H}_2\text{O}$ were dissolved in 75 mL of deionized water
- In a 50 mL beaker, a carbonate solution containing 7.615 g of Na_2CO_3 was dissolved in 45 mL of deionized water
- A 600 mL beaker was filled with 150 mL of DI water
- The first two solutions were added dropwise into the 600 mL beaker, which was stirred vigorously at 90°C
- The resulting solution was filtered to separate the precipitate
- 2-100 mL aliquots of water were added to the filtrate
- 2-25 mL aliquots of methanol were added to the filtrate
- The filtrate cake was then transferred to a crucible and dried overnight at 100°C
- The catalyst was calcined in a muffle furnace at 450°C for 3 hours with a 2°C/min ramp
- Resulting catalyst had a surface area of 331 $\text{m}^2 \text{g}^{-1}$, pore volume of 1.12 $\text{cm}^3 \text{g}^{-1}$, and pore size of 107 Å

T. 60Ni – (Method II)

- In a 250 mL beaker, 9.419 g of $\text{Ni}(\text{NO}_3)_2 \cdot 6\text{H}_2\text{O}$ and 2.992 g of $\text{AlCl}_3 \cdot 6\text{H}_2\text{O}$ were dissolved in 75 mL of deionized water
- In a 150 mL beaker, a carbonate solution containing 7.479 g of Na_2CO_3 was dissolved in 50 mL of deionized water
- A 600 mL beaker was filled with 150 mL of DI water
- The first two solutions were added dropwise into the 600 mL beaker, which was stirred vigorously at 90°C
- The resulting solution was filtered to separate the precipitate
- 2-100 mL aliquots of water were added to the filtrate
- 2-25 mL aliquots of methanol were added to the filtrate
- The filtrate cake was then transferred to a crucible and dried overnight at 100°C
- The catalyst was calcined in a muffle furnace at 450°C for 3 hours with a 2°C/min ramp
- Resulting catalyst had a surface area of 258 $\text{m}^2 \text{g}^{-1}$, pore volume of 0.96 $\text{cm}^3 \text{g}^{-1}$, and pore size of 149 Å

U. 80Ni – (Method II)

- In a 250 mL beaker, 13.391 g of $\text{Ni}(\text{NO}_3)_2 \cdot 6\text{H}_2\text{O}$ and 1.612 g of $\text{AlCl}_3 \cdot 6\text{H}_2\text{O}$ were dissolved in 75 mL of deionized water
- In a 50 mL beaker, a carbonate solution containing 7.486 g of Na_2CO_3 was dissolved in 45 mL of deionized water
- A 600 mL beaker was filled with 150 mL of DI water
- The first two solutions were added dropwise into the 600 mL beaker, which was stirred vigorously at 90°C

- The resulting solution was filtered to separate the precipitate
- 2-100 mL aliquots of water were added to the filtrate
- 2-25 mL aliquots of methanol were added to the filtrate
- The filtrate cake was then transferred to a crucible and dried overnight at 100°C
- The catalyst was calcined in a muffle furnace at 450°C for 3 hours with a 2°C/min ramp
- Resulting catalyst had a surface area of 100 m² g⁻¹, pore volume of 0.29 cm³ g⁻¹, and pore size of 165 Å

V. 100Ni – (Method II)

- In a 250 mL beaker, 12.992 g of Ni(NO₃)₂·6H₂O was dissolved in 75 mL of deionized water
- In a 50 mL beaker, a carbonate solution containing 7.630 g of Na₂CO₃ was dissolved in 45 mL of deionized water
- A 600 mL beaker was filled with 150 mL of DI water
- The first two solutions were added dropwise into the 600 mL beaker, which was stirred vigorously at 90°C
- The resulting solution was filtered to separate the precipitate
- 2-100 mL aliquots of water were added to the filtrate
- 2-25 mL aliquots of methanol were added to the filtrate
- The filtrate cake was then transferred to a crucible and dried overnight at 100°C
- The catalyst was calcined in a muffle furnace at 450°C for 3 hours with a 2°C/min ramp
- Resulting catalyst had a surface area of 39 m² g⁻¹, pore volume of 0.22 cm³ g⁻¹, and pore size of 227 Å

IMPREGNATED COPRECIPITATED CATALYSTS

Procedure for synthesis of 60Ni/Al₂O₃ support for subsequent impregnation

- In a 250 mL beaker, 36.112 g of Ni(NO₃)₂·6H₂O and 11.516 g of AlCl₃·6H₂O were dissolved in 100 mL of deionized water
- In a 150 mL beaker, a carbonate solution containing 30.017 g of Na₂CO₃ was dissolved in 100 mL of deionized water
- A 600 mL beaker was filled with 150 mL of DI water
- The first two solutions were added dropwise into the 600 mL beaker, which was stirred vigorously at 90°C
- The resulting solution was filtered to separate the precipitate
- 2-100 mL aliquots of water were added to the filtrate
- 2-25 mL aliquots of methanol were added to the filtrate
- The filtrate cake was then transferred to a crucible and dried overnight at 100°C
- The catalyst was calcined in a muffle furnace at 450°C for 3 hours with a 2°C/min ramp
- Resulting catalyst had a surface area of 258 m² g⁻¹, pore volume of 0.96 cm³ g⁻¹, and pore size of 149 Å

W. PdNi – (1 wt% Pd, 60 wt% Ni)

- When weighed out, the mass of the 60Ni “support” was 2.5003 g
- 0.0421 g of PdCl₂ was weighed out along with 3.9845 g of deionized water
- The palladium solution was added dropwise to the support and stirred to break up chunks of support.
- The wet catalyst was moved to the oven, where it was heated at 100°C overnight
- The catalyst chunks were broken up with a mortar and pestle and then placed in a furnace that was heated by 2°C/min to a maximum temperature of 450°C, where the temperature held constant for 3 hours before cooling off to room temperature

X. PtNi – (1 wt% Pt, 60 wt% Ni)

- When weighed out, the mass of the 60Ni “support” was 2.5021 g
- 0.0654 g of H₂PtCl₆·xH₂O (x was found to equal 5.3) was weighed out along with 4.0034 g of deionized water
- The platinum solution was added dropwise to the support and stirred to break up chunks of support.
- The wet catalyst was moved to the oven, where it was heated at 100°C overnight
- The catalyst chunks were broken up with a mortar and pestle and then placed in a furnace that was heated by 2°C/min to a maximum temperature of 450°C, where the temperature held constant for 3 hours before cooling off to room temperature

Y. IrNi – (1 wt% Ir, 60 wt% Ni)

- When weighed out, the mass of the 60Ni “support” was 2.5051 g
- 0.0439 g of IrCl₄ was weighed out along with 3.9973 g of deionized water
- The iridium solution was added dropwise to the support and stirred to break up chunks of support.
- The wet catalyst was moved to the oven, where it was heated at 100°C overnight
- The catalyst chunks were broken up with a mortar and pestle and then placed in a furnace that was heated by 2°C/min to a maximum temperature of 450°C, where the temperature held constant for 3 hours before cooling off to room temperature

Z. RuNi – (1 wt% Ru, 60 wt% Ni)

- When weighed out, the mass of the 60Ni “support” was 2.4975 g
- 0.0518 g of RuCl₃ was weighed out along with 4.0050 g of deionized water
- The ruthenium solution was added dropwise to the support and stirred to break up chunks of support.
- The wet catalyst was moved to the oven, where it was heated at 100°C overnight
- The catalyst chunks were broken up with a mortar and pestle and then placed in a furnace that was heated by 2°C/min to a maximum temperature of 450°C, where the temperature held constant for 3 hours before cooling off to room temperature

Alfa Aesar Catalyst

The Alfa Aesar catalyst (Part # 031276; Nickel on silica-alumina) used in this thesis has a proprietary composition, but it was sold as containing $66 \pm 5\%$ Ni. The same bottle of Alfa Aesar catalyst was used throughout the entirety of the experiments, and the batch of catalyst that was used contained 62 wt% Ni as well as a surface area of $173 \text{ m}^2 \text{ g}^{-1}$, a pore volume of $0.22 \text{ cm}^3 \text{ g}^{-1}$, and a pore size of 52 \AA .

When I inquired about the composition of the Alfa Aesar catalyst, I got an email response from Rafi Dekermendjian (rafi.dekermendjian@thermofisher.com), who said that the catalyst composition was proprietary, but he provided a vague description of the catalyst, saying it was essentially Ni on kieselguhr.

He also listed the following percentages:

- 40 – 50% NiO
- 30 – 40% Ni
- 10 – 20% Kieselguhr (amorphous silica)
- <10% Alumina
- <10% Proprietary Components

When the Alfa Aesar catalyst was studied under the TEM, it was clear that the catalyst contained kieselguhr, a fancy name for diatomaceous earth. Although the TEM images shown in Figure 28 show a more microscopic view of the catalyst, we also discovered there were large diatomites present in the catalyst mixture. Figure 43 shows one of these diatomites we discovered, and the surface was coated in large agglomerations of Ni particles.

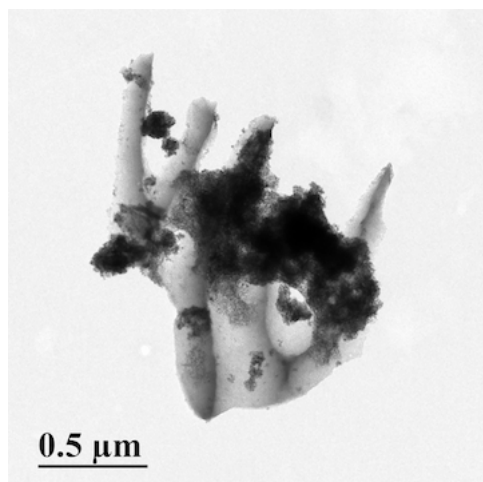


Figure 43. A TEM image of the Alfa Aesar catalyst showing a diatomite littered with Ni particles.

BIOGRAPHY OF THE AUTHOR

Matthew Jonathan Kline was born in Erie, Pennsylvania. A year later, his family moved to Monaca, Pennsylvania, in the suburbs of Pittsburgh. He graduated from Central Valley High School in 2014 and attended Seton Hill University. There, he played four years of collegiate (Division II) basketball and studied chemistry. After four years, he graduated with a Bachelor of Science degree in 2018.

A week after graduation, he hiked an 1,100-mile section of the Appalachian Trail (AT), stretching from southern Pennsylvania to Maine in a span of two months. A few weeks after summiting Mount Katahdin at the AT Northern Terminus, he started graduate school at the University of Maine. After finishing his first year of graduate school, he set out for the West Coast and hiked a stretch of the Pacific Crest Trail (PCT) in Oregon and California. After the weather conditions proved too dangerous, he was forced to make an early departure. Upon his return, he wrote and self-published a book about his experiences on the trail, *Memories with the Trees* (ISBN: 1706263643).

When he isn't working in the laboratory working on his research, he enjoys playing basketball, spending time exploring the vast Maine wilderness, or working on his various hobbies. After receiving his degree, Matthew will continue his research at the University of Maine, as he works his way towards receiving a Doctor of Philosophy in Chemical Engineering. Matthew is a candidate for the Master of Science degree in Chemical Engineering from the University of Maine in December 2020.